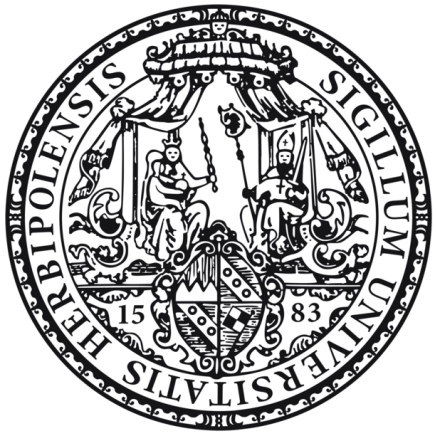

Targeting viral and host factors to optimize anti-measles virus therapy

Zielgerichtete Hemmung von Virus- und Wirtsfaktoren zur Optimierung der Anti-Masern-Virus-Therapie

Doctoral thesis for a doctoral degree
at the Graduate School of Life Sciences,
Julius-Maximilians-Universität Würzburg,
Section: Infection and Immunity
submitted by

Janice Chithelen

from

Kalyan, India

Würzburg 2022

Submitted on:

Office stamp

Members of the Thesis Committee

Chairperson: Prof. Dr. rer. nat. Carmen Villmann,
Institute for Clinical Neurobiology, Julius-Maximilians-Universität, Würzburg

Primary Supervisor: Prof. Dr. rer. nat. Jürgen Schneider-Schaulies,
Institute for Virology and Immunobiology, Julius-Maximilians-Universität, Würzburg

Supervisor (Second): Priv.-Doz. Dr. med. Niklas Beyersdorf,
Institute for Virology and Immunobiology, Julius-Maximilians-Universität, Würzburg

Supervisor (Third): Dr. rer. nat. Martin Fraunholz,
Biocenter of the University of Würzburg

Affidavit

I hereby confirm that my thesis entitled **'Targeting viral and host factors to optimize anti-measles virus therapy'** is the result of my own work. I did not receive any help or support from commercial consultants. All sources and / or materials applied are listed and specified in the thesis.

Furthermore, I confirm that this thesis has not yet been submitted as part of another examination process neither in identical nor in similar form.

_____

Würzburg, 2022 Janice Chithelen

Eidesstattliche Erklärung

Hiermit erkläre ich an Eides statt, die Dissertation '**Zielgerichtete Hemmung von Virus- und Wirtsfaktoren zur Optimierung der Anti-Masern-Virus-Therapie'** eigenständig, d.h. insbesondere selbständig und ohne Hilfe eines kommerziellen Promotionsberaters, angefertigt und keine anderen als die von mir angegebenen Quellen und Hilfsmittel verwendet zu haben.

Ich erkläre außerdem, dass die Dissertation weder in gleicher noch in ähnlicher Form bereits in einem anderen Prüfungsverfahren vorgelegen hat.

_____

Würzburg, 2022 Janice Chithelen

CONTENTS

Summary

Measles is an ancient disease with historical records as early as the 9th century. Extensive study as well as advances in scientific knowledge of virology have led to identification of the viral pathogen and subsequent development of an effective vaccine leading to global efforts towards measles elimination. In 2018, around 140,000 deaths were reported due to measles with incomplete vaccine coverage being one of the leading causes of resurgence. Measles is highly contagious and often regarded as a childhood illness. However, measles is associated with a number of complications and persistent infections like subacute sclerosing panencephalitis (SSPE), which have brought into focus the need for specific anti-viral therapies.

The aim of this study was to target host and viral factors to optimize anti-measles virus therapy. Our approach was to test a panel of compounds known to inhibit host cell functions or viral factors for their antiviral effect on measles replication. Primary human lymphocytes, persistently infected NT2 cells and post-mitotic neurons were used as *in vitro* model systems of acute, persistent and neuronal infection respectively to test the inhibitors. Using the inhibitors Ceranib-2 and SKI-II to target the sphingolipid metabolism enzymes acid ceramidase and sphingosine kinase in infected human primary lymphocytes, we observed a decreased protein translational capacity mediated by mTORC1, EIF4E and ribosomal protein S6 phosphorylation that probably contributes to the antiviral effect. In the persistently infected neural NT2 cells and post-mitotic neurons derived from LUHMES cells, we observed effective infection inhibition and viral clearance upon treatment with a small non-nucleoside inhibitor (ERDRP-0519) specifically targeting the *Morbillivirus* large polymerase. Other inhibitors such as Ribavirin and Favipiravir were less effective. To conclude, 1) we identified a mTOR associated protein translation axis associated with the sphingolipid metabolism, which affects measles virus replication and 2) *In vitro* persistently infected neuronal and post-mitotic neuron models were successfully used as a rapid method to test antivirals against measles virus.

Zusammenfassung

Masern sind eine uralte Krankheit, die bereits im 9. Jahrhundert historisch belegt ist. Umfangreiche Studien und Fortschritte in der Virologie haben die Identifizierung des viralen Erregers und anschließende Entwicklung eines wirksamen Impfstoffs ermöglicht, was zu weltweiten Bemühungen um die Eliminierung der Masern geführt hat. Im Jahr 2018 wurden rund 140.000 Todesfälle aufgrund von Masern gemeldet, wobei die unvollständige Durchimpfungsrate eine der Hauptursachen für das Wiederauftreten der Krankheit ist. Masern sind hoch ansteckend und werden oft als Kinderkrankheit betrachtet. Die Erkrankung ist jedoch assoziiert mit einer Reihe Komplikationen und persistierenden Infektionen wie die subakute sklerosierende Panenzephalitis (SSPE), was den Bedarf nach spezifischen antiviralen Therapien in den Focus gebracht hat.

Ziel dieser Studie war es, zelluläre und virale Faktoren ins Visier zu nehmen, um die Therapie gegen das Masernvirus zu optimieren. Unser Ansatz bestand darin, eine Reihe von Substanzen, die bekanntermaßen Wirtsfunktionen oder virale Faktoren hemmen, auf ihre antivirale Wirkung auf die Masernreplikation zu testen. Primäre menschliche Lymphozyten, persistierend infizierte NT2-Zellen und post-mitotische Neuronen wurden als in-vitro-Modellsysteme für akute, persistierende und neuronale Infektionen verwendet, um die Inhibitoren zu testen. Durch den Einsatz der Inhibitoren Ceranib-2 und SKI-II, die auf die Enzyme saure Ceramidase und Sphingosinkinase des Sphingolipid-Stoffwechsels abzielen, konnten wir in infizierten menschlichen primären Lymphozyten eine verringerte Protein-Translationskapazität vermittelt durch mTORC1, EIF4E und ribosomales Protein S6-Phosphorylierung beobachten, die wahrscheinlich zur antiviralen Wirkung beiträgt. In den persistierend infizierten neuronalen NT2-Zellen und aus LUHMES-Zellen differenzierten post-mitotischen Neuronen beobachteten wir eine effektive Elimination des Virus oder Infektionshemmung bei Behandlung mit einem nicht-nukleosidischen Inhibitor (ERDRP-0519), der spezifisch auf die Polymerase des Morbillivirus abzielt. Andere Inhibitoren wie Ribavirin und Favipiravir waren weniger effektiv. Zusammenfassend lässt sich sagen, dass wir 1) wir eine mTOR-assoziierte Protein-Translationsachse identifiziert haben, die mit dem Sphingolipid-Stoffwechsel in Verbindung steht und die Masernvirus-Replikation beeinflusst, und 2) In-vitro-Modelle für persistierend infizierte neuronale und post-mitotische Neuronen erfolgreich als schnelle Methode zum Testen von Virostatika gegen Masernvirus angewandt haben.

Abbreviations

List of all the relevant and frequently used abbreviations:

Abbreviation	Meaning
°C	Degree Celsius
µg	Microgram
µM	Micro meter
17-AAG	17-N-allylamino-17-demethoxygeldanamycin
A.D.	anno domini
aa	amino acid
aCDase	Acid ceramidase
ADAR	Adenosine deaminase acting on RNA
APC	Antigen presenting cells
APC	Allophycocyanin
ATP	Adenosine triphosphate
BSA	Bovine serum albumin
cAMP	Cyclic adenosine monophosphate
CDC	Center for disease control
CDV	Canine distemper virus
Cer-2	Ceranib-2
CNS	Central nervous system
CO_2	Carbon dioxide
DC	Dendritic cells
dH_2O	Distilled water
DMSO	Dimethyl sulfoxide
EGFP	Enhanced green fluorescent protein
EIF4E	Eukaryotic translation initiation factor 4E
ER	endoplasmic reticulum
ERK	Extracellular signal related kinase
FACS	Fluorescence activated single cell sorting
FGF	Fibroblast growth factor
FITC	Fluorescein isothiocynate
FMDV	Food and Mouth disease virus
g	Gram
GAPDH	Glyceraldehyde-3-phosphate dehydrogenase
h	Hour
hpi	Hour post infection
HIV	Human immunodeficiency virus
HR A/B/C	Heptad region A/B/C
HRP	Horse radish peroxidase
Hsp 90	Heat shock protein 90
IFN	Interferon
IgG	Immunoglobulin G
IKK	Inhibitor of kB (I kB) kinase
IU	International units
kb	Kilobase
kDa	Kilo Dalton
L	Liter
LARP	La related protein 1
LUHMES	Lund human mesencephalic neuronal cells

M	Molar
mA	Milli ampere
MAPK	Mitogen associated protein kinase
MDA	Melanoma differentiation associated protein
MFI	Mean fluorescence intensity
min	Minute
ml	Milliliter
mM	Milli molar
MNK1	MAP kinase-interacting Ser/Thr-protein kinase
MOI	Multiplicity of infection
mRNA	Messenger RNA
mTOR	Mammalian target of Rapamycin
MV	measles Virus
NF-kB	Nuclear factor kappa beta
ng	Nanogram
NLRP3	NOD-like receptor pyrin domain containing
nm	Nanometer
ORF	open reading frame
PBL	Peripheral blood lymphocytes
PBMC	Peripheral blood mononuclear cells
PCR	Polymerase chain reaction
PFA	Paraformaldehyde
PFU	Plaque forming unit
pH	Potential of hydrogen
PHA	Phyto hemagglutinin
PI	Propidium iodide
pi-NT2	Persistently infected NT2
PVLR	Polio virus receptor like
R_0	Reproduction number
RdRp	RNA dependent RNA polymerase
Rh GDNF	Recombinant human glial derived neurotropic factor
RIPA	Radio immunoprecipitation assay buffer
RNA	ribonucleic acid
RNP	Ribonucleoprotein
rpm	Revolutions per minute
RPV	rinderpest Virus
S1P	Sphingosine 1 phosphate
SARS CoV	Severe acute respiratory syndrome Coronavirus
SCR	Short consensus repeat
SDS	Sodium dodecyl sulphate
siRNA	Small interfering RNA
SLAM	Signalling lymphocyte activation molecule
SphK	Sphingosine kinase
SSPE	Subacute scelerosing panencephalitis
STAT	Signal transducer and activation of transcription
TLR	Toll like receptor
TNF	Tumor necrosis factor
TOP	Terminal oligopyrimidine tract
TRAF	Tumor necrosis factor receptor associated factor
WHO	World Health organization

List of Figures

List of Tables

INTRODUCTION

1.1 Virus

The term 'virus' was originated from Latin which means poison and to describe 'filterable toxins' or infectious disease causing agents that were smaller than bacteria. Pioneering theoretical and experimental work by Dmitri Ivanovsky and Martinus Beijerinck in the late 19th century initiated the foundation of 'Virology'. Since then, research in virology expanded with discovery of numerous viruses infecting plants, humans, livestock, insects' prokaryotes and fungi. Development of vaccines made it possible to eradicate and/or prevent life threatening diseases like polio, smallpox, measles and the very recent Covid-19. Since the late 21st century, upgraded molecular techniques further led to discovery of viral elements like active endogenous retroviral genes or 'viral fossils' within the human genome. Moreover, the discovery of existence of viruses (phages) infecting pathogenic bacteria e.g. Vibrio cholerae thereby contributing to its virulence (Waldor et al., 1996) or those that infect ocean microbial life thereby affecting large scale nutrient cycling or weather events has further shed light on the influential role of viral species in the Earth's biosphere (Trainic et al., 2018). Mathematical calculations estimate the number of virus particles on earth to be around 10^{31} – a number which is apparently more than the estimated stars in the universe (Mushegian, 2020). Thus, lacking the cellular structure, a virus can be defined as an acellular obligate intracellular parasite that possess its own genetic material encoding for proteins essential for its assembly, replication and further infection which it does by using host cellular machinery and biomolecules.

1.2 Measles – Historical Records and Emergence

Recognition of measles as a disease distinct from other prominent viral exanthematous diseases like smallpox or chicken pox have been identified from description of medical texts by scholars Abu-Bakr (6th A.D.) and Rhazes (10th A.D). Nevertheless, many ancient texts / literatures across the globe may have documented measles like illnesses in the earlier times (Fig. 1.1). Experimental evidence of an infectious agent being involved was demonstrated by an English surgeon Francis Home in 1758, while Hektoen in 1905, using bacteria free blood as inoculum recorded a non-bacterial agent was involved (Hektoen, 1905). During a measles epidemic on the Faroe Islands Peter

Panum not only noted the transmission and natural history of disease but also that infection induced a life-long immunity. Clemens von Pirquet in 1911 first reported 'immunosuppression' where tuberculin skin response was transiently impaired during acute measles infection. Finally, in 1954, the Measles virus (MV) was isolated in tissue culture by Enders and Peebles. Subsequently, vaccine developments led to a drastic decrease in measles and measles associated complications. Rinderpest virus (RPV), now eradicated is the closest relative to MV. Thus, the virus may have jumped into human species at a time when humans and cattle/livestock began co-existing. A recent study reports that MV-RPV further diverged later with MV emerging around 2500 years ago and endemically established itself in large populations. Coincidence of rise of large cities around the same time provided high human density enough to maintain the MV transmission (Düx et al., 2020).

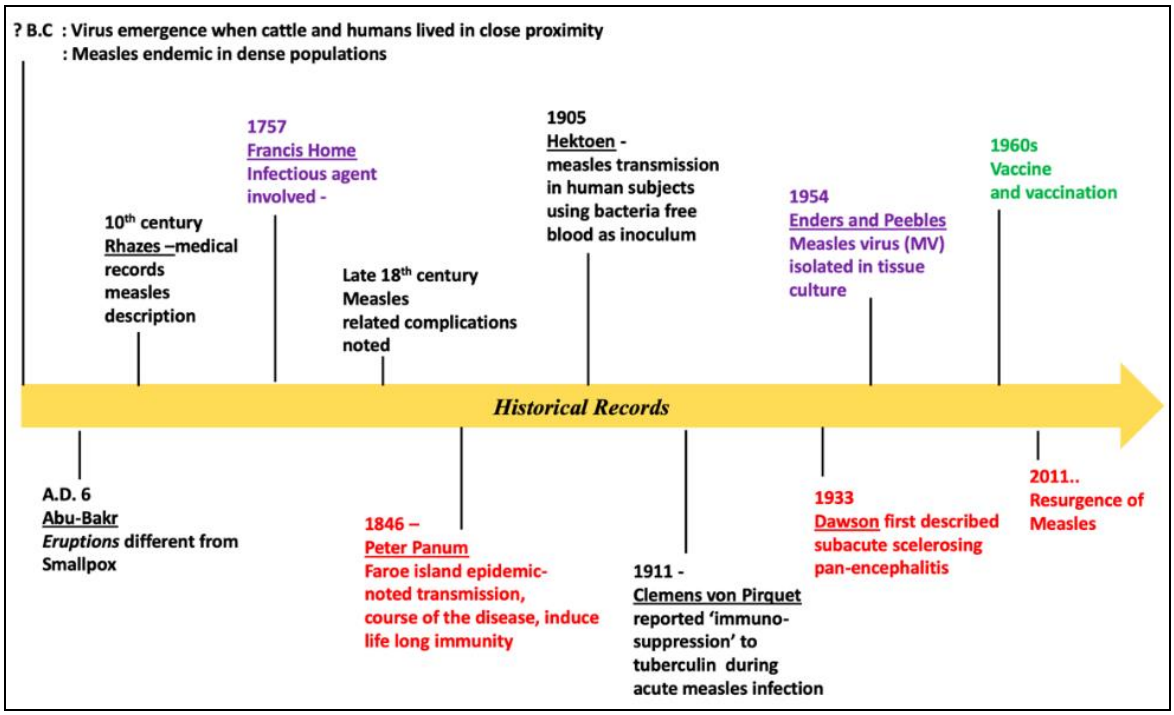

Fig. 1.1: Recognition of measles based on available historical records (*arrow timeline not to scale)

1.3 Taxonomy of Measles Virus

As per the International Committee of Taxonomy of Viruses (ICTV), MV is classified as :

Rank	Rank Name	Defining features of Rank
Realm	*Riboviria*	Viruses using RNA dependent polymerase for replication
Phylum	*Negarnaviricota*	Negative sense single-stranded RNA genome (-ssRNA)
Class	*Monjiviricetes*	Infect fungi, plants, vertebrates and invertebrates
Order	*Mononegavirales*	Possess linear, typical non-segmented genome
Family	*Paramyxoviridae*	Vertebrates serve as natural hosts (*myxo*-affinity for mucin)
Sub-family	*Orthoparamyxovirinae*	Possess 6-8 transcriptional elements in genome
Genus	*Morbillivirus*	Lack neuraminidase activity, possess P/C/V transcription unit, narrow host range due to receptor specificity
Species	*Measles morbillivirus*	

Table 1.1 : Classification of Measles virus. (Rima et al., 2019 ICTV Consortium)

1.4 Morphology and Genome Organization

MV is an enveloped negative sense RNA virus. It has pleomorphic forms but mostly spherical virions with a diameter of 300-500 nm. Structurally (Fig.1.2), it consists of surface proteins haemagglutinin (H) and fusion (F) that mediate attachment to cellular receptor with subsequent fusion and entry within the cell. The envelope is host cell derived lipid and lined by the viral matrix (M) protein. The viral genome is encapsidated as a ribonucleoprotein (RNP) complex consisting of viral RNA, nucleoprotein (N), large (L) polymerase and phosphoprotein (P).

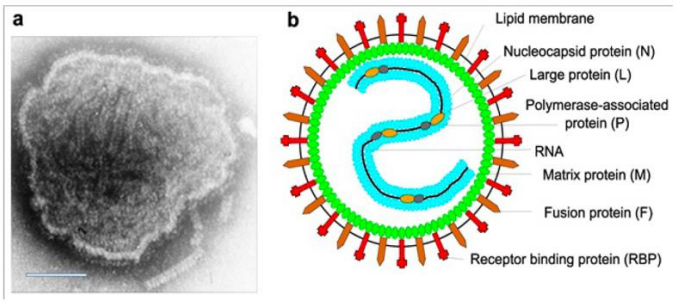

Fig 1.2: Measles morbillivirus structure (a) Negative-contrast electron micrograph of MV particle. Scale bar = 100 nm. (b) Schematic diagram of MV particle in cross section. (Image adapted from Rima et. al., 2019 ICTV Consortium)

The MV linear non-segmented negative sense RNA genome is around 15-16 kb in size which codes for 6 essential proteins and 2 accessory proteins V and C within the P

gene (Fig. 1.3). Each gene sequence is flanked by a Gene Start (GS) and Gene End (GE) sequence and separated by an intergenic sequence. The RNP consists of around 2,649 N, ~300 P, and ~20 to 50 L proteins. Nucleotide length in genomes of *Paramyxoviridae* tend to follow the 'Rule of 6' so as to ensure efficient replication since every N protein binds to 6 nucleotides. This estimated stoichiometry may provide the optimal accessibility of the template RNA to the vRdRp since the N-P complex is also a substrate of the vRdRP (Plumet et al., 2005). The -ssRNA genome serves as template for mRNA transcription and also anti-genome synthesis during replication. The genome is also flanked by leader and trailer (Tr) sequences at the 3' and 5' end (Fig. 1.3).

Fig. 1.3: Schematic layout of MV genome

1.5 Viral Replication Cycle – at Cellular Level

The success of virus infection and subsequent replication within the cell depends on factors like susceptibility and permissiveness of the cell. A cell is susceptible when it has the specific functional receptor that binds to the virus and enables its entry while a permissive cell has the favorable intracellular factors for the virus to replicate. Thus, in a cell that is both susceptible and permissive, the replication cycle for MV involves: 1) Typically, the viral surface protein H attaches to specific cellular receptor. This triggers a conformational change in the nearby viral F surface protein – the F structure opens up and extends to latch on via the fusion peptide to the cellular membrane thereby bringing the viral and cellular membrane closer and enabling fusion of the two membranes. 2) Upon membrane fusion, the viral genome encased as a ribonucleoprotein (RNP) complex is now released within the cell cytoplasm. The RNP is a complex of the viral negative sense genome wrapped with N, P and L proteins. The viral N-RNA is the substrate for viral RdRp which begins transcription using the negative sense genome as template to synthesize mRNA transcripts of viral genes. Morbilliviruses typically follow a transcription gradient where by the most upstream N gene is transcribed and translated abundantly while the last gene L transcribed the least based on the genome sequence 3'-N-P(V/C)-M-F-H-L-5'. Host cell machinery is used for production of proteins from the viral

mRNA transcripts. As the newly synthesized viral proteins accumulate, free N-P complexes serve as an important parameter for shifting the predominance from transcription to replication. During genome replication phase, the vRdRp ignores the GS, GE, editing sites and intergenic signals and synthesizes full length positive sense antigenomes which serve as templates for negative sense genome synthesis. While the N-P proteins associate to form new RNP complexes for the progeny, the matrix M protein that is involved in particle integrity accumulates at the inner side of the plasma membrane. Meanwhile translation of surface glycoproteins F and H occur at the rough endoplasmic membrane, with dimerization and assembly taking place within the endoplasmic reticulum (ER) and trans-Golgi network respectively and finally transported to cell surface. Viral assembly at plasma membrane and subsequent budding of progeny is mainly regulated by M protein. Once assembly is complete, the progeny virions are released by budding from the cell (Ferren et al., 2019, Rima et al., 2009, Plemper et al., 2001, Iwasaki et al., 2009). A diagrammatic summary of the above described viral replication process is represented by figure (Fig. 1.4)

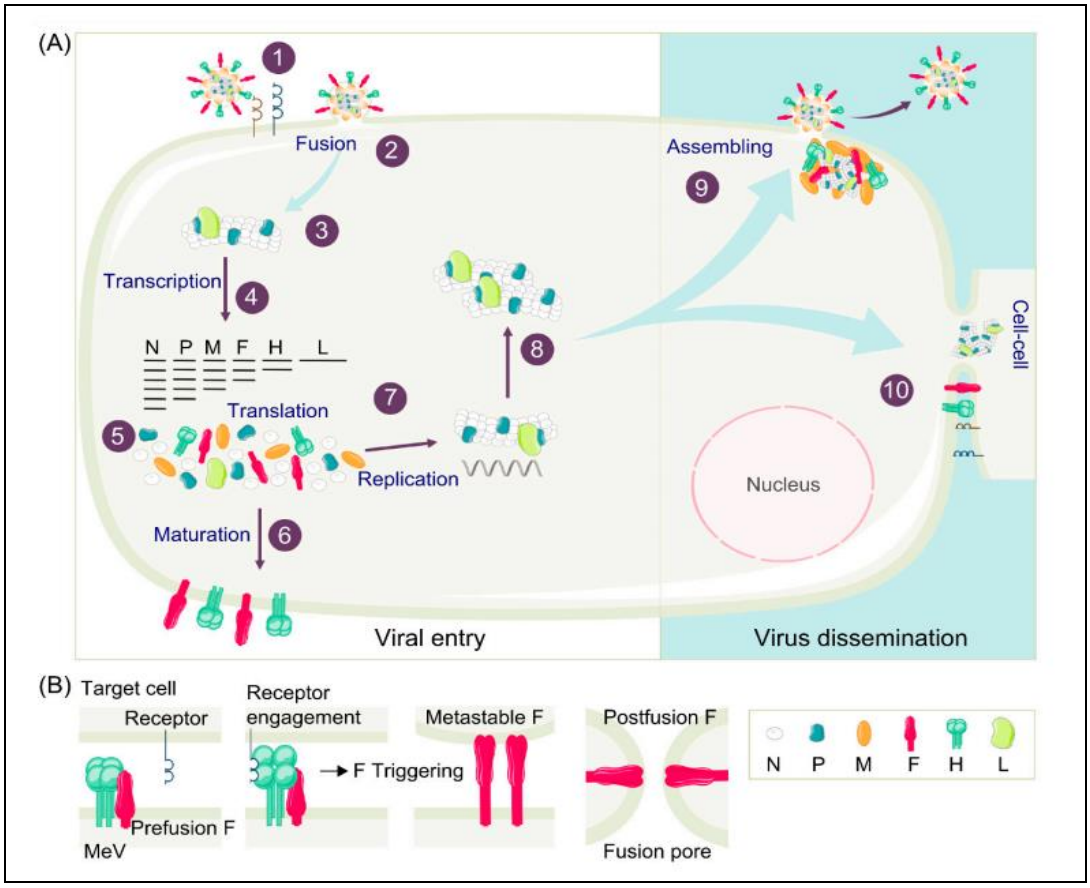

Fig. 1.4: Schematic of replication cycle of Measles virus (Figure adapted from - Ferren M. et al., 2019)

1.6 Viral Proteins

The following table summarizes the annotated MV genome:

Nucleotide number[a]	mRNA	ORF length	Number of codons
1-52	Leader	-	-
56-1744	N	108-1682	525
1748-3402	P/V/C	1807-3327 (P) 1807-2702 + 1 G (V) 1829 – 2386 (C)	507 231+69=300 186
3406-4872	M	3438-4442 (M)	335
4876-7247	F	5458-7107 (F)	550
7251-9208	H	7271-9121 (H)	617
9212-18,854	L	9234-15,782	2183
15,858-15,894	Trailer	-	-

Table 1.2: Annotation of Measles virus genome. [a]Nucleotides are numbered in positive sense. (Data adapted from Rima et al., 2009)

Nucleocapsid (N)

The nucleoprotein (N) is the first protein to be encoded in the genome and synthesized abundantly due to transcription gradient. The N protein binds to the viral RNA so as to assemble it into a helical nucleocapsid. The encased viral RNA is now protected from degradation by cellular nucleases thereby contributing to its stability and second, it forms as the substrate for the viral polymerase complex which consists of N, P and the L protein (Rima et al., 2009). The N is a phosphorylated protein built up of 525 aa Structurally it consists of two parts: N_{core} and a flexible N_{tail}. A motif within the intrinsically disordered domain of the N_{tail} binds to the C-terminal domain of the P protein. As per 'Rule of 6', the N protein binds to 6 bases of the viral RNA irrespective to sequences. The interaction of the flexible N_{tail} with the X-domain of the phosphoprotein is supposed to mediate contact of the L protein (complex) with the template RNA (Rima et al., 2011, Guseva et al., 2019). *In vitro* expression system found that phosphorylation of Serine at sites 479 and 510 of the N protein activated viral transcription and replication.

Phosphoprotein (P)

The phosphoprotein (P) is a 507 aa length protein of which 380 residues are disordered i.e. they lack a stable structure thereby making it flexible. Structurally it consists of a long tail, a tetrameric domain consisting of four parallel helices and a folded X-domain containing C-terminal., It occurs as a tetramer and the polymerase L bind to P via the tetrameric domain (Guseva et al., 2019). Apart from anchoring and forming a part of the vRNP complex, the phosphoprotein may also have other modulatory functions (Rima et al., 2011). Mutation study of conserved 'HELL' (Histidine-Glutamic acid-Leucine-Leucine) residues within the a-helix of the phosphoprotein have led to suppression of measles transcription and replication. Reported activation of cellular ubiquitin modifying enzyme A20 gene in monocytic cells by MV phosphoprotein led to suppression of antiviral responses involving nuclear transcription factor (NF-kB) and other Toll-like receptor (TLR) mediated responses in the infected cells.

Accessory proteins V/C

V protein

Accessory proteins V and C are denoted as virulence factors of MV, of which the V protein has reported to demonstrate most versatility in this regard. The V protein is built up of 300 aa Structurally, it's N terminal sequence overlaps with P protein but it has a unique C-terminal domain (CTD) which is generated by RNA editing (+1 reading frame) and contains a conserved cysteine rich region (also containing Zinc binding site) (Ramachandran et al., 2008). This Cysteine (Cys) rich region of the V protein interacts with numerous components of the immune signaling – for example blockage of Interferon α/β signaling via interaction with Jak/STAT1, STAT2, MDA5, TLR7 and/or IKK α. In monocytic cells, also suppressed inflammatory interleukin-1β secretion via interaction with inflammasome NLRP3 (Komune et al., 2011). *In vivo* studies using V deleted mutants in mice model brain infections, less efficient replication and viral spread was observed thereby improving mortality (Patterson et al., 2000)

C protein

The accessory C protein is comprised of 186 aa and translated from the second ORF within the P/V/C coding gene. A conserved 22 aa. sequence of unknown function has also been identified. The role of C protein has been linked to dampening host innate and interferon immune response and that infectious viral production was retarded in studies

with C deletion mutants. One such reported C mediated function is suppression of protein kinase R (PKR) – a cellular antiviral protein which induces MAPK activation and interferon-beta induction. By suppressing PKR, it prevents antiviral MAPK and interferon-beta response mounted by the cell during the viral replication phase (Rima et al., 2011).

Matrix protein (M)

The viral envelope structure is supported by a layer of the matrix (M) protein which also interacts with the cytoplasmic tails of surface viral proteins F and H (Rima et al., 2011). It is a hydrophobic protein constituting of 335 aa. M also interacts with the N protein via the C-terminal of the nucleoprotein This N-M interaction is not only important for efficient production into infectious progeny particles via recruiting RNP complexes but also regulation of viral RNA synthesis. During viral assembly, the M protein begins to assemble on the cytoplasmic side of the plasma membrane (Iwasaki et al., 2009). At the assembly site, the M in tandem interaction with F and RNPs forms a flexible lattice so as to enable budding off from the plasma membrane (Ke et al., 2018). Increased cell associated virus and low cell free virus titers were observed in studies with recombinant MV expressing a mutated or no M protein (Rima et al., 2011, Iwasaki et al., 2009). Interestingly, presence or accumulation M can function as a viral transcription regulator since increased MV-genome and P-transcripts as well as increased syncytia formation were observed using siRNA (small interfering) mediated inhibition of M mRNA expression (Reuter et al., 2006)

Fusion protein (F)

The MV fusion protein (F) is a type 1 transmembrane glycoprotein with a cytoplasmic tail. It is functionally active as a homo-trimer. Synthesis as an inactive precursor F0 and subsequent trimerization occurs in the endoplasmic reticulum. As the precursor F0 transports along the *trans*-Golgi network it is cleaved by furin into F1 and F2 subunits linked by disulfide bonds. Within the ER it also interacts with the H protein and this H-F complex travels along the secretory pathway to the cell surface.

Structurally, the F proteins consists of conserved cytoplasmic and transmembrane domains forming the stalk, three heptad regions HRA; HRB and HRC and an N-terminal hydrophobic region (known as fusion peptide) which is exposed when F0 is cleaved. It belongs to type I viral fusion proteins due to predominance of alpha helices in their structure and existence of two states: an inactive pre-fusion state which undergoes

structural rearrangements into a post fusion state upon receptor mediated trigger from H protein. In the post fusion state, due to structural rearrangement, the now exposed fusion peptide inserts within the target cell membrane to initiate fusion (Plattet et al., 2016). The fusion is a pH dependent process.

Hemagglutinin (H)

The H functions as an attachment glycoprotein that directly interacts with the cellular receptor. Structurally, these 617 aa proteins comprises of a C-terminal receptor binding head domain, a stalk, a transmembrane region (24 aa) and an N-terminal cytoplasmic tail (34 aa). It functions as a dimer of dimers (a tetramer) which render it a globular domain like appearance. It is highly glycosylated and glycosylation at asparagine residues at position 200 and 215 influences the dimer structure (Rima et al., 2011). The receptor-binding site, which lies on the head domain but not in the heavily glycosylated region also serves as the major neutralizing epitope against MV (Tahara et al., 2013).

Large protein (L)

The L protein consisting of 2183 aa is also denoted (together with P) as viral RNA dependent RNA polymerase (vRdRp). It forms a part of the RNP complex and performs catalytic functions like viral RNA transcription, capping and polyadenylation. Thus, it possesses domains for ATP binding, GTPase activity, transferase and polymerase. As the nascent RNA is generated, a GDP polyribonucleotidyl transferase (PRNTase activity) adds the cap structure, followed by ribose 2'O methylation and guanine-N-7 methylation and finally polyadenylation of the RNA. As the proteins are translated, the accumulated intracellular concentration of N protein signals the polymerase to switch to genome replication wherein all intragenomic transcription sequences are bypassed to generate whole viral genomic RNA (UniProt.org).

1.7 Genotypes and Serotype

Measles virus has only one serotype due to the high similarity in the surface antigens across the various MV genotypes. This antigenic stability confers a life-long protection after natural infection and vaccination with one vaccine strain. Vaccination generates neutralizing antibodies against both F and H, but the anti-H antibodies have been reported to have a much larger contribution to virus neutralization (Rik de Swart et al., 2005).

The genetic stability of MV could be attributed to a lower mutation rate of approximately 4 to $5*10^{-4}$ substitutions per base per year as compared to other RNA viruses like HIV, Influenza A virus, FMDV with a high mutation rates of $1.6*10^{-3}$ per base per year (Beaty et al., 2016). An exception is the highly mutated MV sequences in brains of SSPE patients. Excess hypermutations have mainly been found in the viral M, but also F and H genes. These hypermutations have been attributed to have generated by RNA editing mechanisms within the infected neurons as for example by the enzyme ADAR (adenosine deaminase acting on RNA).

According to the WHO criteria, the main MV genotype classification is based on 450 highly variable nucleotides at the carboxy terminus of the N gene (Beaty et al., 2016). Based on this system 24 genotypes have been recognized namely A, B1-B3, C1-C2, D1-D11, E, F, G1-G3 and H1-H2 of which B3, D3, D4, D6, D8, D9, G3 and H1 are in predominant circulation globally. While wild-type strains in clade A are considered to be extinct, the vaccines strains fall into this clade. Since there has been no proof of significance of clinical severity associated with the genotypes, the MV genotype classification is mainly used as an epidemiology tool to study sudden outbreaks or regional transmissions. With respect to persistent infection like SSPE, the genotype of MV detected in the brain was that of the genotype in circulation when the patient had the acute MV infection. Phylogenetic analysis is thus mainly based on sequenced from N-450 region and also can be from coding region of H gene. Other reports recommend genotyping based on other regions within the MV genome have also been suggested for e.g. the partial non-coding between M and F gene, the partial H gene and the partial L gene (Bodewes et al., 2021, WHO Manual, Chapter 7, 2018).

1.8 Cellular Receptors and Other Modes of Viral Entry

CD46

CD46 has been identified in 1993 as the first receptor for MV by two groups (Dörig et al., 1993, Naniche et al., 1993). CD46 or membrane cofactor protein MCP, is ubiquitously expressed on nucleated human cells. This glycosylated membrane associated protein ranging between 50-70 kDa functions as a complement regulator by binding to complement proteins C3b and C4b and inactivating them thereby preventing host cell lysis. It also functions as a co-stimulatory signal for $CD4^+$ T cell differentiation into T regulatory cells (Kemper et al., 2003). Other reports highlight the involvement of CD46 during fertilization of oocyte with spermatozoa (Proteinatlas Org.).

On the extracellular N-terminal side, CD46 contains four SCRs (short consensus repeats) or CCP (complement control modules) followed by glycosylated three STP (serine/threonine/proline) rich domains, a short sequence of unknown function finally followed by transmembrane region and cytoplasmic tail (Delpuet et al.,2014). MV binding was mapped to the first two CCP modules of CD46 (Cattaneo et al., 2004, Lin et al. 2016).

Besides MV, other pathogens like human herpes virus 6 (HHV-6), Adenovirus, Bovine viral diarrhea virus, *Streptococcus pyogenes* and pathogenic *Neisseria* have been reported to use CD46 as cellular receptor. Interestingly, all these binds to different structures on the ectodomain indicating the absence of a single consensus binding region (Cattaneo et al., 2004). Since the cytoplasmic tail of CD46 is postulated to initiate immune response related signaling pathways, it was speculated that the usage of this receptor may dampen the immune response.

It was observed that the infection of cells with all MV isolates available at this time (1993-1995) could be inhibited by high anti-CD46 antibody concentrations. In contrast, infection only with vaccine strains and some MV isolates led to the downregulation of CD46, whereas infection with other MV isolates did not lead to CD46 downregulation (Schneider-Schaulies et al., 1995). Later it was found that MV vaccine strains and laboratory-adapted strains (and practically all old isolates were Vero cell-adapted) interact with CD46 and lead to CD46 downregulation, whereas fresh wildtype isolates cultured only on lymphocytes do not induce CD46 downregulation. The infection of lymphocytes with these isolates also could not be inhibited by anti-CD46 antibodies (very high antibody concentrations probably mask the cells unspecifically). Specific amino acids of MV-H which interact with CD46 were mapped (Bartz et al., 1998 and 1996). These findings revealed that wild-type MV strains use a receptor different from CD46, and that cultivation of MV isolates on Vero cells led to adaptation and usage of CD46 as receptor.

CD150

CD150 was reported by Tatsuo et al., 2000 and Erlenhoefer et al., 2001 as the receptor for wild-type measles virus.

CD150 or SLAMF1 (Signaling Lymphocyte activation molecule family member 1) or IPO-3 is a heavily glycosylated single chain transmembrane protein which has a molecular weight of 75-95 kDa and belongs to the immunoglobulin superfamily. This has also been reported to possess a kinase activity. It is mainly expressed on thymocytes, T cell

subsets, B cells dendritic cells, NK cells and endothelial cells, with its expression further upregulated upon activation of these cells (Wang et al., 2001). Thus highest expression is observed in bone marrow and lymphoid tissue like spleen and also to an extent in the kidney and the urinary bladder (ProteinAtlas.org). Mouse and human CD150 have been reported to share homology with other genes like CD84, CD229, CD244, CD48 and 19A (Sidorenko et al.,1993). Recently, novel isoform arising from splicing of CD150 mRNA have been identified especially in context of human CNS tumor cells (Heath et al., 2021).

Structurally (Fig.5), CD150 consists of a variable (V-loop) domain and a constant (C2) immunoglobulin-like domain on the extracellular side followed by a transmembrane region and a cytoplasmic tail consisting of two ITSMs (immunoreceptor tyrosine-based switch motifs) which interact via phosphorylation of the tyrosine residues by proteins like Src kinases mediate the downstream signaling pathways for e.g. ERK and Akt. MV was found to interact with the V-loop domain of human CD150 which was both sufficient and necessary for viral entry (Sidorenko et al.,2003). Further extrapolation studies identified that other species of the *Morbillivirus* use CD150 (SLAM) of the respective host species for viral entry (Tatsuo et al., 2001). To summarize, MV binds via its surface H with the SCR1 and SCR2 region of CD46 or with the V-loop domain of SLAM (Hashiguchi et al., 2011).

Nectin-4

In 2010, Nectin-4 as the epithelial cell receptor for MV was again reported in two studies using microarray screen and siRNA knockdown studies (Noyce et al., 2011, Mühlebach et al., 2011)

Nectin-4 is also known as PVRL4 (Poliovirus receptor-like 4) due to its homology with CD155 (Polio virus receptor). The term ‘nectin’ is derived from the Latin word for ‘necto’ meaning ‘to connect’ since they function as cell adhesion molecules along with cadherins. Similar to CD150, this glycosylated protein is a single chain of 66 kDa with immunoglobulin-like domain structures. It is reported to mainly be expressed by epithelial cells of the lung (Proteinatlas.org), in the skin and placenta (and numerous adenocarcinoma cell lines) with moderate expression in other tissues like kidney and urinary bladder, salivary gland, oesophagus, breast, bone marrow and lymphoid tissue. There exists the soluble form of Nectin-4 which is a proteolytic cleavage product by metalloproteinases TACE/ADAM 17. This secreted form, highly released from breast tumors or cancer cells is considered as a prognostic serum marker (Heath et al., 2021).

Structurally, Nectin-4 consists of one terminal V-loop domain followed by two C domains on the extracellular side, a transmembrane region and cytoplasmic tail. Nectin-4 dimerizes via *cis* or *trans* with itself or other nectins so as to form the adherent junctions (Fig. 1.5).

In vitro mutational studies identified a species (as well in ovine and dog) conserved PFAG motif (positions 101,102,103,104) in the V domain probably important for MV H recognition along with similarities of MV H and CDV H in binding to their respective epithelial receptor (Delpeut et al., 2014). Interestingly, Nectin-4 is used late during the infection of an individual, when virus is released to the outside. Infected lymphocytes transport MV to the basolateral side of polarized epithelial layers of the lung thereby leading to infection of these cells and release of virus by coughing. Thus. Nectin-4 has also been designated as an ‘’exit receptor’’ during viral dissemination (although it is an entry receptor), whereas CD150 on immune cells is the principle receptor used by MV during initial phase of infection.

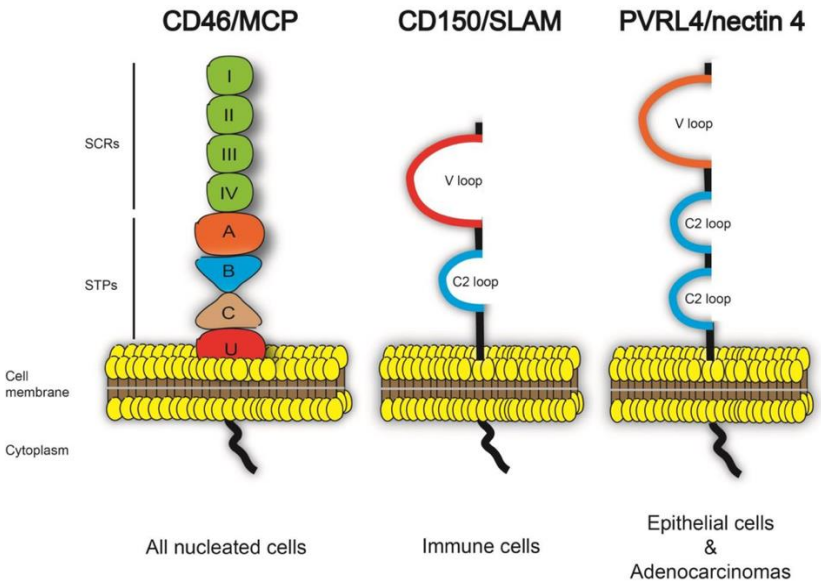

Fig. 1.5:Schematic structure of MV receptors CD46, CD150 and Nectin-4 (figure adapted from Delpeut et al., 2014)

Other Putative or Functional receptors

In the human brain very little or no CD46 and no CD150 is expressed on neural cells (Ogata et al., 1997). Therefore, the exact receptor or mode of entry of MV in neuronal cells is not clear and has still to be elucidated. Studies have identified CD147 to be another function entry receptor used by MV which is based on cellular Cyclophilin B which a

ligand for CD147 and virions incorporated with this ligand may be able to enter the cell via CD147 (Watanbe et al., 2010). Other reported modes of entry reported are use of CAD (cell adhesion molecules) in cis by MV to trigger fusion with neighboring cell (Shirogane et al., 2021) or via movement of the infectious virus as cargo between cells by Nectin-1 mediated endocytic vessels (Generous et al., 2019, Donohue et al., 2019). One may hypothesize here that since its introduction within the human species, transmission and adaptation of MV may have led to evolution of alternative ways to enter the target cell for further propagation.

1.9 Measles as Disease

Transmission and Epidemiology

Transmission of MV particles is by airborne route by inhalation of aerosols or droplet secretions from infected individuals. With the R_0 value of around 17, MV is one of the most efficiently spreading human virus. Individuals susceptible to measles infection are mainly children and unvaccinated populations. Individuals with nutrient deficiencies, inadequate vaccine dose leading to partial acquired immunity or immune deficient or immune-suppressed individuals for e.g. HIV, cancer patients may also be susceptible to wild type infection (Rota et al. 2016).

Economic stability and available health care facilities strongly influence the case fatality ratio which varies between <0.01 % in industrialized countries to >5% in developing countries. Measles is a highly contagious disease as compared to the R_0 of SARS-CoV-2 (the original strain) which lies in the range between 2 to 7 (Burki et al., 2021). Thus, so as to ensure efficient herd immunity and disrupt the transmission chain, at least 95% vaccine coverage in population should be achieved (Rota et al., 2016). Recent Measles outbreaks have been typically observed in unexposed clusters, populations of unvaccinated individuals or island populations – (e.g. 2018 in the Democratic Republic of Congo), or due to vaccine hesitancy due to religious reasons (e.g. 2013-14, Netherlands) or misinformation (2018-2019, USA). High incidences of measles cases are annually reported are often observed in densely populated regions across Asia and Africa for e.g. India, Nigeria etc. supporting the need for complete vaccine coverage. This is important since high cases of acute measles infection may imply higher incidences of MV associated complications and persistent infection in future.

In 2018 a sharp increase of about 58% in measles cases were reported worldwide since 2016. Despite the availability of an effective vaccine, measles remains a

leading cause of morbidity and mortality in young children causing approximately 100,000 deaths each year worldwide (WHO factsheet, 2019).

With the advent of the COVID-19 pandemic, global health agencies issued reports of concern over the effect of pandemic on measles cases. This was due to the fact that with logistical mobility greatly hampered during the pandemic lockdown, more than 117 million children would have been at risk of missing the measles vaccination which would in turn increase the probability of MV neurotropism and immunosuppression related complications. (Roberts, 2020). As per a recent report, 23 million children missed basic childhood vaccine in 2020 with high number of measles cases reported within the first two months of 2022 itself. Nevertheless, such regular reports of caution on incomplete vaccine coverage may serve as awareness at public level so that necessary steps are taken (WHO Press report, 2022).

Clinical Manifestation

The incubation period is between 10-14 days followed by fever. Clinical signs of the prodromal phase are characterized by the 3 ‘C’s – cough, coryza and conjunctivitis. Then follows the phase of specific clinical signs including maculopapular rash over the body and Koplik spots in the buccal cavity along the cheek mucosal lining. Virus shedding and transmission takes place by aerosols from cough and other respiratory secretions. WHO recommended case confirmation based on laboratory confirmed tests of viral RNA (PCR) and/or anti-MV IgM antibodies from patient samples (Rota et al., 2016).

1.10 Viral Pathogenesis

Upon, inhalation, the virus enters the respiratory tract and infects $CD150^{+}$ immune cells namely the local lymphocytes, dendritic cells (DCs) as well as tissue resident alveolar macrophages in the lungs. When these activated immune cells now infected with MV drain into lymph nodes, the viral infection is amplified by spread to other immune cells that interact with these infected cells for and transfer of infection from these antigen presenting cells to T lymphocytes (de Witte et al., 2008). Infected lymphocytes now transport MV via systemic circulation (viremia)- into various organs which leads to multiple immunopathogenic outcomes including the maculopapular rash, lymphopenia and immunosuppression. Mechanisms causing immunosuppression are:

1) Destruction/loss of infected antigen presenting cells (APCs) hampers the cell mediated immune response thereby making the individual susceptible to secondary bacterial or viral infections during measles.
2) Immunosuppression via surface contact with viral envelope proteins leading to T cell paralysis (Avota et al., 2001)
3) Depletion of infected T and B cell populations due to acute viral lytic replication cycle. Particularly the infection of memory and plasma B cells (those which produce antibodies to antigens from previous bacterial or viral exposure) erases the already acquired immunity to previously exposed pathogens (de Vries et al., 2012, Mina et al., 2019).

The MV infected lymphocytes also migrate to the basolateral side of the lung epithelial cell layer and infect epithelial cells via Nectin-4 mediated entry. The infection may also spread via transfer of vRNP complexes between the tight junctions of epithelial cells while progeny virus particles are released by budding from the apical surface. The infected epithelial cells now attract immune cells in vicinity that generate an inflammatory response including release of histamines, nitric oxide, type I IFN independent cytokines and chemokines so as to initiate viral clearance by damaging the infected cells and by other forms of adaptive response. The red skin rash and fever are a result of the chemicals released during the generated inflamed response (Shultz., 2015).

Thus, exit and transmission of the virus is mainly during the prodromal, fever and rash phase by coughing or sneezing from the upper respiratory tract. The virus is shed as released progeny virus or sloughing off of infectious virus associated with epithelial cell debris or active infectious centers (Hippee et al., 2021). After infection, a strong immune response is generated leading to lifelong immunity. Several months post infection, infectious virus particles are cleared but viral RNA may still persist (Lin et al., 2012).

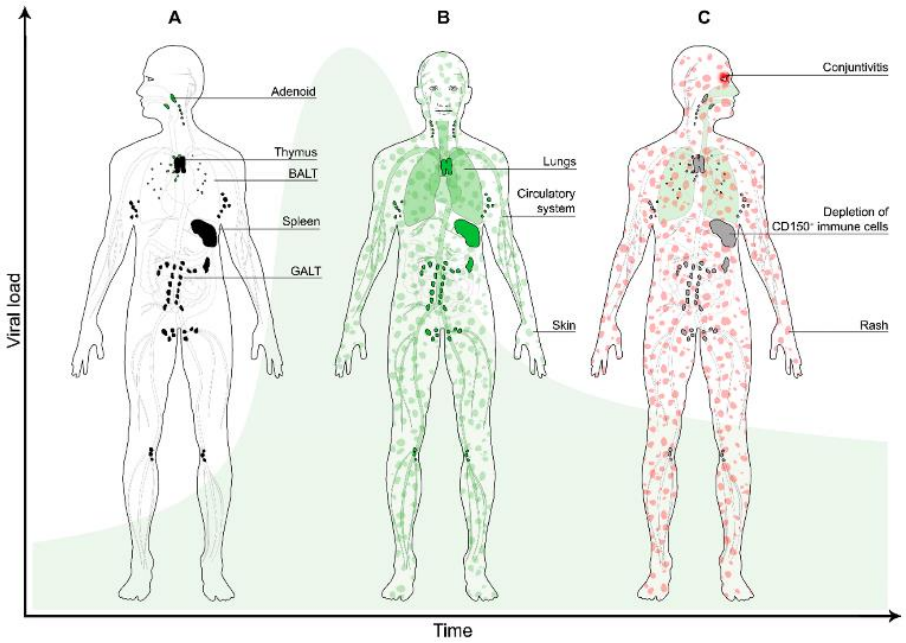

Fig. 1.6: Illustration of MV dissemination leading to systemic spread (figure adapted from Laksono et al., 2016) A) Draining of MV infected immune cells into lymph nodes (black). B) The spread of infection leading to viremia (green) C) Transient immune suppression in lymphoid organs (grey) due to depletion of infected immune cells and the typical maculopapular rash (red). The viral load is represented by the green bell-shaped curve in the background.

1.11.a. Complications during Acute Infections

Complications during and after the acute MV infection may arise due to immunopathogenic mechanisms, as for example the acute post-infectious encephalitis (APME, incidence 0.1%), or due to the immunosuppressive effects as for example secondary bacterial infections or due to persistent viral infection. Common complications include diarrhoea (8%) otitis media (7-9%) leading to hearing loss, pneumonia (1-6%), blindness and subacute sclerosing panencephalitis (SSPE) (see below). Complications in pregnant women who may have not received MMR vaccine may lead to premature birth or low weight baby (ECDC, CDC report, 2020). The **APME** with 20% mortality and severe symptoms like fever, headache and seizures (8) is due to immunopathogenesis and not infection of the brain. CNS lesions observed in APME have been attributed to inflammation and autoimmune reaction to myelin basic protein (mainly expressed on oligodendrocytes) since specific T cells against this protein have been isolated from patients (Schneider-Schaulies J. et al., 1999).

1.11.b. Complications due to Persistent Infections

Immune response mediated by cytotoxic T-cells, antibody mediated B cell response and also cytokines such as IFN- γ usually lead to clearance of circulating infectious virus particles and infected cells. However, when clearance of infectious viral components is not complete, the infection may persist. MV RNA has been reported to persist in lymphoid tissues up to 6 months post infection in rhesus macaques (Griffin et al., 2020).

RNP complex itself is considered to be infectious under certain conditions for e.g. rescue of virus *in vitro* using reverse genetics that lead to assembly of viral RNP complexes or in persistent infections when viral RNP is spread via cell to cell contact. In humans, two neurological complications are based on persistent MV infection: MIBE (measles inclusion body encephalitis) which arises weeks after acute infection in immunocompromised patients in and SSPE (subacute sclerosing panencephalitis) which arises months to years after initial infection (Schneider-Schaulies J. et al., 1999).

MIBE is a rare progressive inflammation of the brain and typically observed in immune-compromised patients. It is characterized by presence of intracytoplasmic or intranuclear inclusion bodies which contain nucleocapsids and observed in neurons, oligodendrocytes and astrocytes. This occurs few weeks or months after acute infection with an onset of febrile focal seizures, behavioral changes leading to coma. Similar to SSPE, MIBE is caused by spread of defective viral nucleocapsid or RNP complexes and characteristic mutations in viral genes that enable cell to cell transmission (Ferren et al., 2019).

SSPE was first documented in 1935 by Dawson and thus also termed as Dawson's disease. Its onset occurs around 6-10 years after acute MV infection and is a result of neuronal loss due to persistent infection and a massive immune response in the brain. SSPE samples and subjected to immunohistochemistry were found to contain MV N and P proteins in lesions surrounded by infiltrating T, B cells and macrophages. A characteristic finding is the high level of MV-specific antibodies in serum and cerebrospinal fluid (CSF). SSPE has a slow onset characterized by cognitive decline, altered behavior, movement disorders like myoclonic jerks (also detected by electroencephalogram to support diagnosis) and seizures. Further deterioration leads to vegetative state or death within a few years (Papetti et al., 2022). The incidence of SSPE is highest in young children (Memon et al.,2021). SSPE developed in 1:1367 cases if measles was contracted before 5 years of age and 1:609 if measles was contracted with less than one year.

1.11.c. Pathogenesis of SSPE

It is not known where MV persists over the years before SSPE is diagnosed as a consequence of massive infection of neurons. Depending on the cellular environment RNP complexes may either remain latent, produce low level viral transcripts / proteins and accumulate mutations in the viral genome. Numerous studies have reported detection of unusual hypermutations in the MV from SSPE brain specimens – defective expression of viral genes (Schneider-Schaulies et al., 1999), hypermutations within the M gene but without or negligible expression of matrix protein, alterations in the cytoplasmic domain of F leading to truncations, elongations, substitutions thereby affecting fusion activity (Schmid et al., 1992) and mutations in H gene (Baczko et al., 1993). Certain mutations in F lead to hyperfusogenic F activity which may enable receptor-independent spread of virus in the brain (Ikegame et al., 2021). This ultimately leads to accumulation of mutated viral products which never the less generates a strong adaptive immune response within the brain including high concentrations of MV-specific antibodies. Furthermore, the persistent infection induces cytokines such as TNF- α, IFN-gamma, Interleukin IL-1ß and IL-2 (Schneider-Schaulies et al., 1999). A recent *in vitro* study reported that mutation in the L polymerase leading to enhanced activity could also promote infection of neuronal cells due to increased F expression (Sakamoto et al., 2022).

As there is no therapy for SSPE available up to date, vaccination is the only possibility to prevent this disease.

1.12 Vaccines: coverage and challenges

All vaccines for MV are in the live-attenuated form most of which are primarily derived from the Edmonston strain isolated in 1954 by Enders and Peebles. Strains derived from this Edmonston strain include the Schwartz, the Edmonston-Zagreb and the Moraten strains. Other independently developed vaccine strains include CAM-70, TD97, Leningrad-16 (used in Russia) and Shanghai 191 (Ji-191 – used in China). The vaccine virus is mass produced using primary chick embryo or Vero cell cultures. Currently, most measles vaccines are administered along with other viral antigens as MCV (Measles containing vaccines) for e.g. MMR (Measles, mumps and rubella) as a part of routine mass immunization in children (WHO measles vaccines, 2022).

Introduction of vaccine since 1963 drastically reduced worldwide incidence of measles cases. Administration of Measles containing vaccine (MCV1) at a public health

routine immunization level within the first year of life significantly reduced reported measles cases. Factors like a single serotype of the virus, absence of a natural animal reservoir and availability of an effective vaccine make measles as an optimal candidate for eradication. These coupled with improved nutritional status and medical facilities in developed and developing countries and a sensitive global network for infectious diseases accelerated the need for elimination at global level. Thus, with the current scenario, an MCV2 (MCV at second year of life) with a target coverage of more than 95% for the both doses is recommended for maintaining measles elimination (Rota et al., 2016).

Till 2009, trends in global reported cases of measles saw a sharp decline until resurgence of measles cases were reported in clustered groups or unvaccinated pockets. In spite of well-coordinated global immunization programs, the two prominent reasons contributing to resurgence were inadequate vaccination coverage (leading to endemic transmission) and vaccine hesitancy. Inadequate vaccine coverage or vaccine shortage was mainly observed in settings like refugee camps, regions of economic and political instability leading to displacement of people groups or even densely population and geographical barriers in economically stable countries – e.g. high cases in Democratic Republic of Congo (DRC), Madagascar, India etc. Vaccine hesitancy occurred in various clusters of people with religious beliefs and misinformation being the predominant reasons e.g. increased cases in USA, Ukraine etc. Vaccine refusal due to beliefs or notions was not restricted to any one particular religion and this refusal was mainly based on components or methods used in the vaccine have been prohibited in the various religious beliefs (Wombwell et al., 2015). Refusal due to misinformation was probably due to vague misinterpretations of scientific data for e.g. link of autism with MMR vaccine or presence of thiomersal a mercury-based preservative used in vaccines (Löffler et al., 2021).

Thus, the best way to prevent spread measles is via vaccination so to maintain herd immunity and prevent transmission to immunocompromised individuals. Since measles is airborne, in case of suspected or measles infected person, all isolation measures should be strictly followed due to its high infectious nature. Routine mass vaccination in children through immunization campaigns have proven effective to reduce global measles death (WHO factsheet, 2019).

1.13.a. Treatment

In probable immunocompromised patients exposed to measles, a possibility of post exposure prophylaxis (PEP) so as to improve the clinical disease is recommended via

administration of MMR vaccine within 72 hours of exposure or immunoglobulin within 6 days of exposure – and not both together (CDC, 2020).

A specific antiviral treatment for measles is not yet in clinical use, but broadly antivirally-active substances like ribavirin have been used in SSPE patients (Reuter et al., 2010). Symptomatic treatment is administered to improve the clinical symptoms for example antibiotics to treat bacterial infections. However, through basic care like adequate nutrition and fluid intake, complications can be reduced. WHO strongly recommends regular administration of Vitamin A supplements to measles infected children since deficiency of this vitamin was found to be risk factor for increased morbidity and mortality (Ferren et al., 2019).

1.13.b Antivirals

An antiviral can be described as a drug or agent that functions against the virus by suppressing its ability to replicate or inhibiting it's multiplication by interfering in the stages of its replication cycle. The mode of action of the drug may be via targeting viral components or host factors that interfere with the viral replication cycle. However, because of side effects of host factor treatment, an inhibitor that specifically targets the viral components is to be favoured. Depending on the mode of action, an antiviral agent can also be specific or broad spectrum against multiple targets. While drugs targeting viral agents are often favored for therapeutic use, inhibitors targeting host cellular factors are used to study the involvement of host factors and their associated pathways in the virus replication within the biological system. Based on available literature, the following table (Table 1.3) summarizes the main list of inhibitors available used for this study:

Inhibitor	Factor	Mode of action	Reference
FIP (fusion inhibitory peptide)	Viral	Z—D-Phe-Phe-Gly-OH is a sequence specific oligopeptide that resembles the N-terminal of MV F protein which is involved in viral fusion and haemolysis. The carbobenzoxy (Z) group increases inhibitory activity and FIP acts by competing with the N-terminal region of viral F polypeptide	Richardson et al., 1980
ERDRP-0519	Viral	Non-nucleoside and highly specific MV RdRp inhibitor which is effective against various	White et al. 2007, Ndungu

		genotypes. This water soluble inhibitor was found to be effective against MV in *in vitro* cell system, ferret and non-human primate model. It interferes in viral RNA synthesis and elongation by blocking the nucleotidyl transferase activity.	et al. 2012, Cox et al. 2021, Krumm et al. 2014, Wittwer et al. 2021
Ribavirin	Viral	It is a synthetic guanosine analog with direct and indirect antiviral effects -like viral RdRp inhibition, introducing mutations in viral genome, depletion of GTP pool, immunomodulatory effects etc. although it's *in vitro* effect depends on cells used. Clinically often used as a broad spectrum antiviral along with Vitamin A so as to reduce disease complications.	Uylangco et al. 1981, Beaucourt et al. 2014, Roy et al. 2013
Favipiravir	Viral	Broad spectrum inhibitor of RdRp of a panel RNA viruses but mainly clinically used against Influenza virus. Upon entering the cells, it gets phosphorylated which get incorporated into viral RNA during synthesis. It's antiviral effect was also observed against Edmonston and SSPE MV strain *in vitro*.	Furuta et al. 2017, Hashimoto et al. 2020
Rapamycin	Host	Inhibits cellular mTOR complex, a nutrient and stress sensor associated with numerous metabolic pathways thus affecting cell survival, proliferation, immunesuppression. Certain analogs have been clinically approved for disease treatment.	Li et al. 2014
SKI-II	Host	Sphingosine kinase inhibitor Refer Section 1.13.c	--
Ceranib-2	Host	Acid ceramidase inhibitor Refer Section 1.13.c	--
17-AAG	Host	A potent binding inhibitor of cellular chaperone Hsp90 protein. It can also induce apoptosis, necrosis, autophagy and mitophagy. Hsp90 chaperoning is required along with viral P to ensure proper and functional folding of viral L polymerase.	Bloyet et al., 2016, NCBI library 6505803, Selleckchem S1141

Table 1.3: Summary of list of inhibitors used for the study

1.13.c. Inhibitors Ceranib-2 and SKI-II

Ceranib-2 is a quinolone based, non-lipid ceramidase inhibitor. It has been reported to inhibit cellular ceramidase activity, and also subsequently decreases levels of downstream biomolecules like sphingosine and sphingosine-1-phosphate and corresponding cell proliferation inhibition (Draper et al. 2011). In vitro, the IC50 was reported to be 28 µM. Ceranib-2 reported to show anti-tumor activity in *in vivo* mouse models. In MCF cancer breast cell line, pro-apoptotic effect of Ceranib-2 via activation of stress and mitogen induced proteins like SAPJ/JNK and p38 (Vethakanraj et al. 2018). Interestingly, prolonged (approx. 48 h) treatment of erythrocytes from healthy blood donors with high concentrations of Ceranib-2 led to hemolysis of erythrocytes (Signoretto et al., 2016) with potential implications on the use of Ceranib-2 in Plasmodium infected erythrocytes.

4-[4-(4-chloro-phenyl)-thiazol-2-ylamino]-phenol **(SKI-II)** inhibitor is non-lipid, non-ATP-competitive sphingosine kinase-2 inhibitor with an IC_{50} value of 0.5 µM, which also leads to the degradation of sphingosine kinase-1 (Sellechem.org S7176). It's antiproliferative effects were observed in various human cancer cells. It has also been studied in mice *in vivo* models via oral and peritoneal administration routes and detected in blood at least 8h post administration. In mouse mammalian adenocarcinoma JC cells, decreased phosho-Akt activation was observed with SKI-II treatment (French et al., 2006). The Akt-mTOR axis is an important factor associated effect of Sphingosine-1-phosphate mediated signaling (Maeurer et al., 2009). Increased SIP production in MV infected DCs thereby contributing to their increase velocity was found to be significantly reduced upon SKI-II treatment (Derakhshani et al., 2019).

From a therapeutic aspect, SKI-II can be used as a potential antiviral. SKI-II (as dual inhibitor of both SphK isoforms) also demonstrated an antiviral effect on early replication of Chikungunya virus and Measles virus via SphK2 and SphK1 inhibition respectively (Reid et al., 2015). Vijayan *et al*., not only reported SKI-II mediated MV replication inhibition in SLAM and Nectin 4 positive cells but also observed decreased expression of viral proteins on the surface of the highly susceptible B95a cells (Vijayan et al., 2014). SKI-II mediated sphingosine kinase inhibition also significantly reduced HSV-1 release not only in infected monocytic THP-1 cells, but also in bone marrow derived macrophages (Lang et al., 2020) implying the significance of S1P driven motility in highly mobile cells like macrophages and DCs.

A few studies have described potential off target effects of SKI-II at cellular level. In primary bronchial epithelial cells, SKI-II was found to enhance Nrf2 (nuclear factor Erythroid 2 related factor) signaling via Keap1 dimer formation and independent of SphK inhibition. Nrf2 is a redox sensitive transcription factor activated in environmental, oxidative and toxic cellular stress so as rescue cell death (Mercado et al., 2014). The activity of Dihydroceramide desaturase (Des1) – another enzyme within the sphingolipid metabolism – was found to be inhibited but without affecting Des1 protein level (Cingolani et al., 2014). An optical based drug array screening study observed with higher SKI-II concentration, cellular protein translation was lowered due to an integrated stress response, along with damage to the endoplasmic reticulum (Corman et al., 2021).

1.14 Sphingolipids

Sphingolipids were first discovered by J. L. W Thudichum in the late1870s from brain extracts and similar to other lipids were hypothesized to function within lipid rafts at the cell membranes. The term ‘sphingolipid’ was inspired from the mythical creature ‘Sphinx’ – whose enigmatic structure used as an analogy to describe its interesting biochemical structure (Bartke et al., 2009).

Structurally sphingolipid consists of a long backbone chain also known as ‘sphingoid base’ i.e. an aliphatic chain with attached hydroxyl group. A fatty acid (of varying chain lengths, predominantly C14-C26) linked to this sphingoid base via an amide bond at the second carbon atom leads to generation of ceramides and form the hydrophobic region. Further, the linkage of the sphingoid backbone head to a phosphate group, single or oligo sugar residues (Sphingolipids chapter UCD ,2021). form the hydrophilic region of this biomolecule (Fig. 1.7). Thus, they are amphipathic in nature since they possess both hydrophilic and hydrophobic properties that enable these bioactive lipids to localize not just at cellular membranes but also transport within the cell and involve / influence a network of signal transduction pathways.

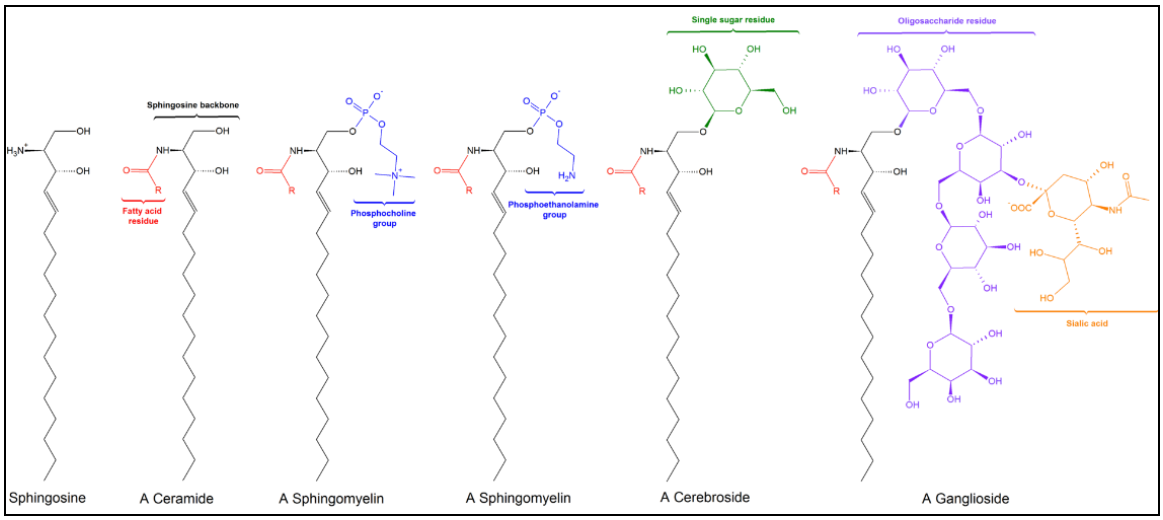

Fig. 1.7: Chemical backbone structure of sphingolipid species. Image adapted from University of California Davis, online Book shelf, Sphingolipids, 2021

1.14. a Sphingolipid Metabolism: Synthesis and Breakdown

Synthesis - *de novo* pathway

The biosynthetic pathway begins in the endoplasmic reticulum (ER) with the generation of ceramides. It is initiated with serine palmitoyltransferase (SPT) acting on preferred substrates serine and palmitoyl-CoA with a series of enzyme catalyzed reactions until Desaturase acts on Dihydroceramide to generate Ceramides (Hannun et al., 2018). Ceramides can also be synthesized from sphingosine pools by ceramide synthases that and fatty acyl groups of various chain length. Variation in length of the sphingoid backbone during *de novo* synthesis can occur when SPT acts on other substrates like myrisate (C14) or stearate (C18).

The fatty acid chain length in ceramides usually consist of 14-16 carbons and can have long C22-26 to ultra-long (more than C26) fatty acyl chains. These saturated molecules tend to form membrane rafts thus restricting the ceramide location cellular membranes – i.e. membranes of cell surface, endoplasmic reticulum or Golgi network. Ceramides are able to interact with proteins on both sides of the lipid bilayer and their modification depends on the enzymes present in the membrane compartment (Sphingolipids UCD,2021).

Ceramides serve as precursors for generation of complex sphingolipids (like sphingomyelin, glycosphingolipids) or can be modified by other enzymes. These modifications (eg. acylation) mainly occur at the Golgi network. In addition, ceramides serve as key mediators of cell signaling process – levels of various ceramide species can determine cell growth or apoptosis. E.g. C16 and C18 species have been reported in cell death, mitophagy while C24 in cell proliferation.

Breakdown of Ceramides

Catabolism mainly involves breakdown of species like sphingomyelin, C1P and glycosphingolipids via hydrolysis into ceramides which constitutively occurs in the lysosome. These ceramides are further broken down by deacylation to generate sphingosine and sphingosine-1-phosphate. The sphingolipid species are finally broken down by S1P lyase to ethanolamine phosphate and fatty aldehyde to form palmitoyl-CoA.

1.14.b Key Enzyme and metabolites: Sphingosine Kinase, Acid ceramidase and S1P

Sphingosine Kinase

Human genome encodes for two Sphingosine kinase genes namely *SPHK1* and *SPHK2* which differ in their overall size to the extra amino acid sequence in SphK2 but are similar in terms of polypeptide sequence. Each gene generates spliced isoforms in total, leading to three SphK1 forms and two SphK2 forms. Based on sequence alignment of reported isoforms sequences (Pitson et al., 2011), in all the known sphingosine kinases there exists five highly conserved regions denoted as C1 to C5. The spliced isoforms within SphK1 only differ at their N termini. As compared to SphK1a, SphK1b has additional 14 amino acids and a Cys residue may be a putative palmitoylation site enabling constitutive localization at the plasma membrane. The two SphK2 arise from and alternative start codon. Functionally both SphKs catalyze the generation of S1P from sphingosine by phosphorylation. Both isoforms harbour kinase and transferase activity along with ATP and nucleotide binding sites. Sphk1 additionally contains a Calmodulin-binding site (Proteinatlas.org).

Sphingosine is the main substrate of **SphK1**. Other reported probable substrates are D-erythro-sphingosine and sphinganine. It is highly expressed in monocytes and DCs. SphK1 mediated S1P generation pushes the cellular rheostat towards pro-survival mechanisms like cell growth / differentiation and trafficking. Activation of SphK1 via phosphorylation enables it translocation to the plasma membrane from cytoplasm. It also activates p38 MAPK signaling and dampens RANTES induction. Activators of SphK1 are growth factors, hormones, pro-inflammatory cytokines, lipopolysaccharide, ligand engagement of IgE, IgG receptors and also G protein coupled receptors. Activation by these factors mainly involve MAPK-ERK mediated phosphorylation activation of SphK1 thereby translocating it from cytoplasm to plasma membrane (Maceyka et al., 2014).

Guanine nucleotides have also been reported to regulate SphK1 activity via the interaction of eIF1a (a factor majorly involved in protein translation) with SphK1.

Contrary to SphK1, **SphK2** has a pro-apoptotic effect on the cell. Only recently, increasing studies have deciphered numerous roles of SphK2 (Maceyka et al., 2005). SphK2 is mainly localized in the nucleoplasm and thus involved in epigenetic regulation of gene expression via interaction with the histones. It is also reported to play a role in the assembly of the mitochondrial respiratory complex and is a major source of mitochondrial S1P. S1P generated via SphK2 is involved in effector events like calcium signaling, NF-κB and cytokine production in mast cells (Proteinatlas.org). Factors that activate Sphk2 are epidermal growth factor (EGF), phorbol ester and protein kinase D.

Acid ceramidase

It is coded by the ASAH1 gene and has an hydrolase activity which under acidic pH breaks down ceramide into sphingosine and fatty acid. Reverse catalytic activity i.e. synthesis of ceramide from sphingosine substrate has also been reported. This enzyme is mainly localized within the lysosomes (Proteinatlas.org). It's constitutive expression within the lysosome is an essential housekeeping function which relates the turnover of bioactive ceramide species since severe diseases like Farber's disease and spinal muscular atrophy have been reported due to dysfunctional Acid ceramidase thereby leading to ceramide accumulation (Gebai et al., 2018). It is reported to be highly expressed within neutrophils and monocytes

Structurally, it is a 50 kDa glycosylated enzyme synthesized as a inactive precursor which upon internal cleavage at a Cys residue forms a heterodimeric enzyme of 13 and 30 kDa subunits. Upon cleavage, a change in conformation of the active form exposes the active site which is a narrow hydrophobic site within the 13 kDa α-helix so as to accommodate the ceramide substrate.

Acid ceramidase enzymes have been found to be upregulated in numerous cancer and tumor cells and thus have been a potential target for anti-cancer therapy.

Sphingosine-1-phosphate

Sphingosine-1-phosphate is generated by the action of both Sphingosine kinases 1 and 2. S1P functions intracellular in numerous signal transduction pathways but can also be secreted extracellularly to function in an autocrine or paracrine signaling. Within the nucleus, S1P can inhibit histone deacetylases thereby preventing deacetylation at lysine

residues of the histone proteins thus contributing to epigenetic regulation. The import and export of S1P across the cell membrane is not only mediated by its specific receptor group S1PRs but also by ATP binding cassette proteins.

At the plasma membrane, S1P generated via SphK1 acts as a co-factor along with TRAF3 which in response to TNF-α stimulation lead to NF-κB and IL-17 secretion (Alvarez et al., 2010). In tumor cells, the autocrine signaling of S1P leads to pro-survival effects like growth, motility and metastasis while in a paracrine signaling, it promotes induction of endothelial cell adhesion (thereby affecting vascular permeability), angiogenesis as well as tumor stromal interactions. Numerous intracellular targets have been also reported, one such example is persistent activation of STAT3 in tumor microenvironment. Due to wide range of cellular targets especially related to metabolism and inflammation, S1P and enzymes involved in S1P generation are often observed to be aberrantly expressed in diseases like cancer or inflammatory conditions in immune system. However, their role in normal essential functions have also been recognized for example. serum S1P levels aid in trafficking of thymocytes and B cells from the lymphoid tissues as well as migration of highly motile DCs (Maceyka et al., 2012, Spiegel et al., 2011)

1.15 Sphingolipid metabolism and MV replication

Literature on the role of sphingolipid metabolism and replication of viruses and other cellular pathogens has been mainly reported in the last decade. With respect to MV replication, Vijayan *et al* (Vijayan et al., 2014) reported that in HEK cells, SphK1 overexpression, but not external supply of S1P, led to enhanced expression of Edmonston MV proteins and infection in the cells and that pharmacological inhibition of SphK1 decreased the viral protein expression in highly susceptible non-human B cell line B95-8. The SKI-II mediated inhibition also resulted in decreased infectious MV titers in Vero cells. The viral replication alone not only induced SphK1 activation within the first replication cycle but also NF-κB. The NF-κB expression was dependent both on viral expression but also linked to Sphk1 activation. Overall, these indicated that more than the bioactive molecule S1P, enzymes related to the sphingolipid metabolism had a role in viral replication.

Recently, a study from our group (Grafen et al., 2019) used a recombinant GFP expressing wild-type MV to study MV mediated pertubations in various aspects of the sphingolipid metabolism using susceptible human BJAB cells and primary blood lymphocytes (PBMCs) along with inhibitors targeting sphingosine kinase and acid

ceramidase. We observed that SKI-II mediated pharmacological inhibition of SphK reduced viral replication in PHA stimulated PBL since low infectious virus titres in dose dependent viable concentrations. Thus, the involvement of SphK was mainly in the later stages of virus replication since viral entry or uptake was not affected by the inhibitor.

Further, using Amitriptyline and GW4868 that reportedly inhibit acid and neutral sphingomyelinase respectively did not have an effect on viral replication in PBL, but a dose and time dependent reduction in viral titers were observed upon inhibition of acid ceramidase using Ceranib-2. The effect of Ceranib-2 and SKI-II treatment on sphingolipid level species in uninfected PBL was detected by mass spectroscopic analysis.

At 24 h after infection SKI-II induced a significant increase of total ceramides and it's key species like C14, C18, C20 and C22 apart from expected decreased S1P levels indicating accumulation of overall ceramides due to shift in the sphingolipid rheostat. In highly susceptible BJAB cells too, treatment with SKI-II and Ceranib-2 resulted in decreased viral titers in a dose and time dependent manner but without affecting the viral uptake. Analysis for sphingolipid composition in MV infected BJAB cells as well as with inhibitor treatment effect demonstrated a transient increase of S1P at 6 hpi in infected cells which was significantly reduced with SKI-II treatment. An increased level of total ceramides was consistently observed at all time points with Ceranib-2 treated infected cells. Overall, the data suggested that the antiviral effect mediated by Ceranib-2 and SKI-II was via accumulation of ceramides and reduction of S1P respectively (Grafen et al., 2019).

1.16 Aim of this study

These findings fall back to the 'Ceramide → Sphingosine → S1P' rheostat that was reported to mediate intracellular signal transduction pathways that drive the cell between pro-apoptotic or cell survival phase (Fig. 1.8). Thus, the aim of my research project was to elucidate the possible downstream pathways affected by this rheostat that would in turn downregulate viral replication in primary human blood lymphocytes (PBL). The regulation between mTOR (mammalian target of rapamycin) and sphingolipid metabolism has been previously reviewed (Tang et al., 2022). The mTORC1 is a cellular nutrient and stress sensor that mediates numerous downstream pathways ranging from protein translation, lipid synthesis to autophagy. Among the numerous pathways, the protein translation is one such cellular function required by the virus for its own replication cycle. Thus, we focused on investigating the ribosomal protein rpS6 and cap dependent EIF4E axis downstream of mTORC1 (Nandagopal et al.,2015).

In addition, as there is not yet a specific antiviral treatment in clinical use against SSPE, it should be investigated if these inhibitors of the sphingolipid pathway and other known inhibitors can be used to reduce or even eliminate MV from persistently infected neuronal cells. So as to explore the efficacy of the inhibitors in neuronal cells and post-mitotic neurons, we decided to use: 1) the neural NT2 cell which can be differentiated into NT2-N neurons – the NT2-N model has been previously used to study Edmonston strain MV, thus we also wanted 2) to generate a persistent infection using a wild type MV in these neuronal NT2 cells and also explore the more recently reported 3) post-mitotic dopaminergic neurons derived from LUHMES cells where MV infection has not yet been reported.

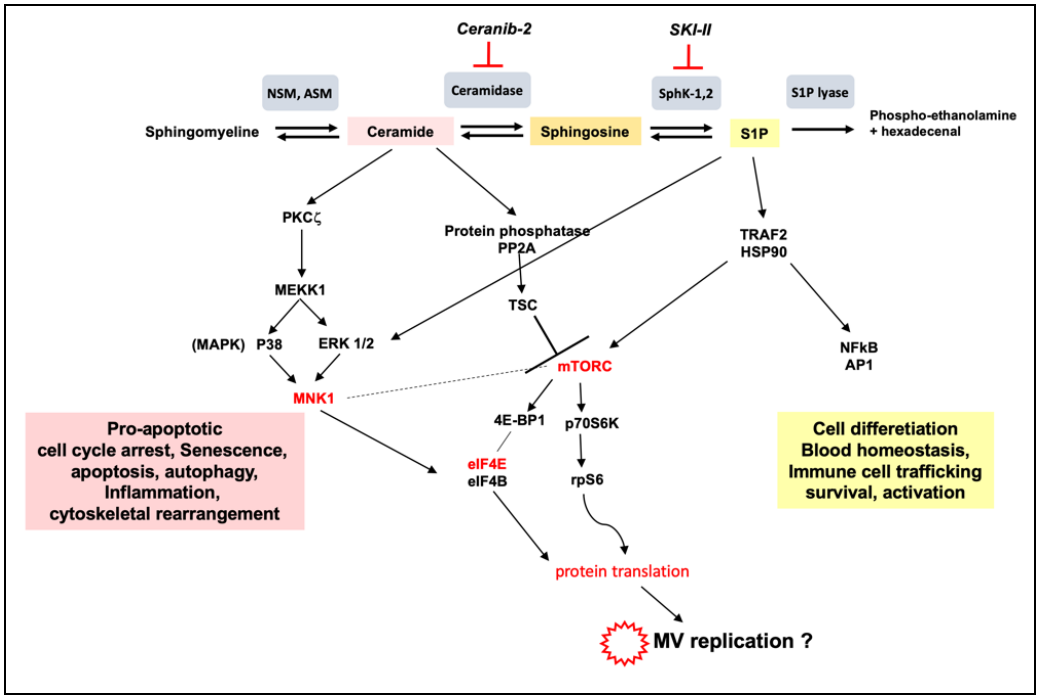

Fig. 1.8: Schematic representation of the sphingolipid rheostat with levels of metabolites like ceramides and S1P affecting the switch between cell apoptosis or survival respectively. The enzymes and metabolites have been reported to influence various downstream signaling pathways – one of which is the the mTOR-EIF4E / rpS6 axis which particularly was the focus of this study

MATERIALS

2.1 Cell Lines And Primary Cells

Name	Type	Origin	Source
BJAB	suspension	Continuous human B lymphobastoid cell line derived from Burkitts lymphoma biopsy of a 5 year old African girl. Negative for Epstein-Barr virus Ref. – *see under* 'BJAB'	DSMZ – German collection of micro-organisms and cell cultures GmbH, Braunschweig
Vero-hSLAM	adherent aneuploid	Vero cell line was established from kidney epithelial cells of a female African Green monkey *Chlorocebus sabaeus*. Vero hSLAM were generated from Vero cells transfected with plasmid encoding human SLAM Ref. – *see under* 'Vero'	A kind gift from Prof. Y. Yanagi (Hashimoto *et al*,. 2002)
NT2	Adherent Hyper-diploid	Human epitheloid clonal cell lineage from TERA-2 cell line which was derived from metastatic (embryonal) teratocarcinoma of a 22 year old Caucasian male. Can differentiate into neurons upon retinoic acid treatment. Ref. – *see under* 'NT2'	DSMZ
pi-NT2	Adherent	Derived from NT2 cells by persistent infection with recombinant wild type MV IC323eGFP. Stably express viral encoded GFP and release low infectious virus titer.	Self-generated and maintained in lab
LUHMES	Adherent	Derived in 1998 from 8-week-old (female karyotype) human brain mecenphalon tissue. Immortal due to tetracycline-controlled, LINX v-myc retroviral vector transfection. Differentiate into post-mitotic neurons	DSMZ, a kind gift from Prof. Dr. med. Lars Doelken (Institute of Virology and Immunobiology, Wuerzburg)
PBMC	Suspension	Primary human peripheral blood cells isolated from healthy blood donors	Institute for Clinical Transfusion Medicine and Hematology, University Hospital Würzburg

Table 2.1: Summary and list of cell lines and primary cells used

2.2 Measles Virus Strain

All experiments were carried out with recombinant MV strain IC323EGFP, a kind gift of Prof. Y. Yanagi. Hashimoto *et al.,* 2002, generated this enhanced green fluorescent protein (EGFP) expressing recombinant MV based on the wild type IC-B (Ichinose-B) strain. This strain has been reported to demonstrate a similar growth kinetics and large syncytium formation as the parent strain. Although this virus predominantly infects SLAMF1 positive cells, it could also infect SLAM negative cell lines to a lower extent and without inducing syncytia – implying that the wild type uses an additional unknown receptor which could be nectin-4, if the cells express it, but is not CD46. Both viral surface glycoprotein H and F were found to be involved with this unknown receptor to aid virus entry.

2.3 Media and Serum

Name	Detail	Source/Catalogue Nr.
MEM	Minimal Essential Medium	Gibco 31095029
DMEM	Dulbecco's Modified Eagle Medium	Gibco 41966029
RPMI 1640	Roswell Park Memorial Institute 1640	Gibco 21875034
DMEM/F12 + L-glutamine	DMEM+F12 Ham (1:1) (for NT2)	Gibco 11330032
DMEM/F12	DMEM+F12 Ham (1:1) (for LUHMES)	Sigma D8437(10565018)
All the above media were supplemented with Penicillin/Streptomycin and FCS or N2 (as required)		
FCS	Fetal calf serum	Biochrom
N2 supplement	Chemically defined, serum free supplement based on Bottenstein's N-1 formulation	ThermoFischer (17502048)
LUHMES Maintenance media	500 ml DMEM/F12 1 % N2 supplement 40 ng/ml Fibroblast growth factor basic (FGF)	+ Pen/Strep
LUHMES Differentiation media	500 ml DMEM/F12 1 % N2 supplement 1 µg/ml Tetracycline hydrochloride 1mM cAMP (2.45ml from 204mM stock) 2 ng/ml rh GDNF (10 µl from 100µg/ml stock)	+ Pen/Strep

Table 2.2: List of media and serum used for cell culture

2.4 Antibodies and Anti-serum

For western blot

Antibody against	Dilution	Type	Source
GAPDH	1:5000	Rabbit polyclonal IgG	Santacruz FL-335 sc-25778
Total p70 S6 kinase	1:2000	Rabbit polyclonal	Cell Signalling(CST) – 9202S
Phospho p70 S6 kinase	1:2000	Rabbit polyclonal	CST (T389) – 9205S
Total ribosomal protein S6 (rpS6)	1:1000	Rabbit polyclonal	Sigma c-terminal antibody SAB4502676
Phospho rpS6	1:2000	Rabbit monoclonal IgG	CST(Ser235/236)(D57.2.2E)XP-4858
Total eIF4E	1:1000	Rabbit polyclonal	CST eIF4E – 9742
Phospho eIF4E	1:1000	Rabbit polyclonal	CST (Ser209) – 9741
Total MNK1	1:1000	Rabbit monoclonal	CST (C4C1) – 2195
Phospho MNK1	1:2000	Rabbit polyclonal IgG	Thermo Fischer - PA5-110137
Total IKK β	1:1000	Rabbit polyclonal	CST – 2684
Phospho IKK α/β	1:2000	Rabbit polyclonal	CST (Ser176/180) – 2694
MV – (Fusion protein)	1:500	Rabbit WTF F serum (wild type F)	SA5353 29.01.1998 – Lab of Dr. Sibylle Schneider-Schaulies
Anti-Rabbit HRP linked secondary antibody	1:10,000	Goat IgG	CST – 7074S

Table 2.3: List of antibodies used for Western Blot

For Flow Cytometry

Antibody	Dilution	Label	Type	Clone	Source
CD69	1:50	FITC	Mouse monoclonal	FN50	BioLegend- 301904
Isotype	1:100	FITC	Mouse IgG2A	PPV-04	Immunotools - 21275523
CD25	1:50	FITC	Mouse IgG	MEM-181	Immunotools – 21270253
Isotype	1:100	FITC	Mouse monoclonal	MOPC-31C	BD Pharmingen – 550616
CD147 (Basigin)	1:50	APC	Mouse monoclonal	MEM-M6/1	Abnova – MAB5047
Isotype	1:50	APC	Mouse IgG1 *κ*,	*MOPC-21*	BioLegend – 400120
CD46	1:100	--	Mouse IgG1	B97-1	SiGi / In-house lab
Isotype	1:100	--	Mouse IgG1 *κ*,	MOPC-	BD Pharmingen –

				31C	550878
Secondary Antibody	1:50	APC	Goat anti-mouse IgG	Poly4053	BioLegend – 405308
MV – N (nucleocapsid protein)	1:50	--	Mouse monoclonal	F227A	SiGi / In-house lab
MV – H (haemagglutinin protein)	1:100	--	Mouse monoclonal	L77	SiGi / In-house lab
Secondary Antibody	1:200	Alexa Fluor™ 647	Goat anti-mouse	polyclonal IgG	Thermo Fischer – A21235
Nectin-4	1:50	--	Mouse IgG_{2B}	337516	R&D Systems – MAB2659
Secondary Antibody	1:200	Alexa 488	Goat anti-mouse	polyclonal IgG	Thermo Fischer – A11001

Table 2.4: List of antibodies used for flow cytometry

2.5 Equipment and Instruments

Equipment	Detail	Manufacturer / Source
Acrylamide gel chamber	N/A	Institute for Virology and Immunobiology
Analytical Balance	EW3000-2M	Kern & Sohn GmbH
Analytical Balance	AC210S MC 1	Sartorius
Biofuge	Fresco Cool centrifuge	Heraeus 75003325
Biosafety Cabinet / Laminar Flow	BSB 4A	Gelaire
Blotting apparatus	N/A	Institute for Virology and Immunobiology
Cell counter	Neubauer improved slide	Assistent
Centrifuge	Rotanta 460R	Hettich
Deep freezer -80°C	MDF-394	Sanyo UltraLow
Dry block Thermostat	BioTDB-100	Biosan
Flow cytometer	FACSCalibur	Becton, Dickinson & Co.
Fluorescence inverted microscope	Leica DMi8	Leica microsystems
Ice flake maker	AF30	Scotsman
Incubator (cell culture – CO_2 incubator)	HERACELL 240i	Thermo Scientific
Inverted Light Microscope	Inverted phase contrast	Leitz Labovert FS
Magnetic stirrer	With aluminium hotplate	Ikamag RCT
Micropipettes	Eppendorf *Reference*	Eppendorf
Microwave	Solo Microwave	OK
Milifuge	Millipore 10k rpm	Hitachi Koki

pH meter	Five Easy	Mettler-Toledo
Photometer	BioPhotometer 6131	Eppendorf
Pipette aid	Accu Jet® Pro	Brand
Power supply (PAGE)	EV243	Peqlab
Refrigerator -20°C	Sikafrost Comfort , *GP1476*	Siemens, Liebherr
Refrigerator 4°C	Sikafrost Comfort, -	Siemens, Liebherr
Rocker	WS5	Edmund Bühler
Thermal printer	DPU-414	Seiko Instruments Inc.
Vortex – for tube	Vortex Genie 2	Bender & Hobein AG.
Vortex Shaker Tray	IKA Vibrax VXR	Hartenstein
Water Bath	1003 Water Bath	GFL mbH

Table 2.5: List of equipments and instruments

2.6.a. Inhibitors Compounds Used

Name	CAS Number	Inhibits	Company / source
17-AAG	75747-14-7	Hsp90	Sigma A8476
Ceranib-2	1402830-75-74	Acid ceramidase	Sigma 219556
ERDRP-0519	1374006-96-8	MV polymerase	AOBIOUS AOB2063
Favipiravir	259793-96-9	RNA polymerase	Sigma SML2427
FIP	4015768.0250	Fusion inhibitory peptide	Bachem H-9430
MNK-1	522629-08-9	Mnk1	Sigma 454861
Rapamycin	53123-88-9	mTOR complex	Sigma R8781
Ribavirin	36791-04-5	Viral polymerase	Sigma R9644
SKI-II	312636-16-1	Sphingosine kinases 1 and 2	Sigma S5696

Table 2.6: List of Inhibitor compounds

2.6.b Inhibitors : Diluent and Stock

Name	Diluent	Stock Concentration
17-AAG	DMSO	10 mM
Ceranib-2	DMSO	1 mM
ERDRP-0519	DMSO	10 mM and 1 mM
Favipiravir	DMSO	100 mM
FIP	DMSO	200 mM
MNK-1	DMSO	1 mM
Rapamycin	DMSO	1 mM
Ribavirin	Sterile dH_2O	50 mM and 100 mM
SKI-II	DMSO	1 mM

Table 2.6: List of Inhibitor compounds with Respective Diluents and Stock Concentration

2.7 Commercial or Prepared Reagents

Reagent	Use	Company/ source
Acrylamide 4K – solution	SDS gel preparation	PanReac Applichem A1672,1000
All trans retinoic acid (RA or ATRA)	NT2 differentiation	Sigma R-2625
Beta-mercaptoethanol	Lammelli buffer	Sigma M-6250
Bicinchoninic acid solution	Protein estimation	Sigma B9643-1L-KC
Bovine serum albumin pH7	Membrane blocking	Applichem A1391, 0100
Chemiluminescent HRP substrate	Blot protein detection	Rockland Femtomax 110A, 110B
Copper (II) sulphate solution	Protein estimation	Sigma C2284-25ML-KC
Cytosine arabinoside	NT2 differentiation	Sigma C6645
cAMP (N^6,2'-O-Dibuyryladenosine 3',3'-cyclic monophosphate sodium salt)	differentiation	Sigma D0627
Dimethyl Sulfoxide (DMSO)	Cryopreservation	PanReac Applichem A3672,0250
Fibroblast growth factor basic	LUHMES media	Sigma GF003A
Fibronectin	Flask coating	Sigma F2006
5-Fluoro-2'deoxyuridine	NT2 differentiation	Sigma F 0503
Gel blotting paper	Whatman® 3MM	Whatman

Lymphocyte separation media	PBMC isolation	Anprotec AC-AF-0018
Matrigel	ECM coat	Sigma E6909
Nitrocellulose membrane 0.2µM	Western blotting	Amersham^{TM} Protran 10600001
Penicillin/Streptomycin 100,000 IU per ml / 100 mg/ml	Cell culture media	In-house (Institute for Virology and Immunobiology)
Phytohemagglutinin-L (PHA-L)	PBMC stimulation	Roche 11249738001
Phosphatase inhibitor tablet	RIPA extraction buffer	Roche PhosSTOP Mini 04906837001
Ponceau S Staining Solution	Gel staining	Cell Signalling Technology 59803S
Poly-L-ornithine hydrobromide	Flask coating	Sigma P3655
2-Propanol	SDS PAGE	Applichem A0900, 0100
Propidium Iodide Solution 0.5 mg/ml	Cell viability staining	BioLegend 421301
Protease inhibitor tablet	RIPA extraction buffer	Roche cOmplete 04693124001
Protein standards 1mg/ml BSA	Protein estimation	Sigma P0914-10AMP
Protein ladder Pre-stained	SDS gel for reference	Thermo Fischer Page Ruler^{TM}
	10 – 180 kDa	26616
	10 – 250 kDa	26619
RIPA Lysis Buffer, 10X	RIPA extraction buffer	EMD Millipore Corp. 20-188
rhGDNF (recombinant human glial derived neurotropic factor)	differentiation	Sigma G1777
Skim milk powder	Membrane blocking	Serva 42590.01 CAS:68514-61-4
TEMED (N, N,N',N'-Tetramethyl-ethylenediamine)	SDS gel	Sigma T9281-100ml
Tetracycline hydrochloride	media	Sigma T7660
Tween-20	Detergent	Sigma P1379-500 ml
Uridine	NT2 differentiation	Sigma U 3750
Versene	PBMC isolation	In-house

Table 2.7 : List of Commercial or Prepared Reagents

2.8 Lab Consumables

Article	Article Number	Manufacturer / Source
6 well tissue culture plate	83.3920	Sarstedt
6 well suspension culture plate	83.3920500	Sarstedt
24 well tissue culture plate	662102	Greiner Bio-one cellstar
48 well tissue culture plate	677180	Greiner Bio-one cellstar
Bacteriological grade Petri plates	633180	Greiner Bio-one GBO
T25 Tissue culture flask with filter	83.3910.002	Sarstedt
T75 Tissue culture flask with filter	83.3911.002	Sarstedt
T125 Tissue culture flask with filter	83.3912.002	Sarstedt
Cell scraper – sterile, non pyrogenic	90020	SPL Life Sciences
Falcon tubes 15 ml	188 271-N	Greiner Bio-one cellstar
Falcon tubes 50 ml	62.547.254	Sarstedt
Cryo-vials	122280	Greiner Bio-one cellstar
Cuvettes Half-micro 1.6ml	Q-vettes Macro	Ratiolab
Eppendorf tubes 1.5 ml	0030120.086	Eppendorf AG
Eppendorf tubes 2 ml	0030120.094	Eppendorf AG
FACS tubes	55.1579	Sarstedt
Glass pipettes	--	In-house (Institute for Virology and Immunobiology)
Mr. Frosty Freezer	5100-0001	Nalgene
Parafilm ‘M’ film	PM966	Parafilm
Pipette tips (0.5-10 µl) long	K138.1	Carl Roth GmbH
Pipette tips (1-200 µl) yellow	8156.1	Carl Roth GmbH
Pipette tips (100-1000 µl) blue	732032	Brand
Plastic serological pipettes 10 ml	607107	Greiner Bio-one cellstar
Plastic serological pipettes 5 ml	86.1253.001	Sarstedt
Sterile filter 0.22 µM Minisart	17597	Sartorius
Sterile filter 0.45 µm Cellulose acetate	514-0063	VWR
Syringe Inject – 5 ml	4606051V	Braun

Table 2.8: List of Lab Consumables

2.9 Solutions, Media and Buffers

2.9.1 For Molecular Biology methods

PBS – T (Phosphate buffered saline with Tween 20)		
PBS	1 L	
Tween 20	0.05 %	500 µl

TBS – T (Tris-HCl buffered saline with Tween 20)		
TBS	1 L	
Tween 20	0.05 %	500 µl

Cathode Buffer		
Tris base	0.025 M	3 g
Methanol	20 % (v/v)	200 ml
6-aminohexanoic acid	0.04 M	5.2 g
Dissolve in 1L dH_2O with pH 9.4		

30 mM Anode Buffer		
Tris base	0.025 M	3.6 g
Methanol	20 % (v/v)	200 ml
Dissolved in 1L dH_2O with pH 10.4		

300 mM Anode Buffer		
Tris base	0.3 M	36 g
Methanol	20 % (v/v)	200 ml
Dissolved in 1L dH_2O with pH 10.4		

10x Protein gel running buffer		
Glycine	1.44% (w/v)	144.4 g
Tris	0.303 % (w/v)	30.3 g
SDS	0.1% (w/v)	10 g
Dissolved in 1L dH_2O with pH 8.7		

Blocking buffer for NC membrane		
Skim milk powder	5 %	5 g
Tween 20	0.05 %	

Dissolved in 100 ml dH_2O

4X Laemmli Buffer (Loading dye)	
1 M Tris-HCl pH 6.8	2.5 ml
100 % glycerine	4 ml
ß – mercaptoethanol	2 ml
SDS	0.4 g
Bromophenol blue (BPB)	2 mg
	10 ml

10x Tris Buffered saline – 500 ml	
Tris base	12.114 g
NaCl (Sodium chloride)	43.83 g
Dissolve in dH_2O	
Adjust pH with HCl to pH 7.4	

Phosphate buffered saline (PBS)	
$CaCl_2$ (Calcium chloride)	1.5 mM
KCl (Potassium chloride)	2.7 mM
KH_2PO_4 (Potassium dihydrogen phosphate)	1.4 mM
$MgCl_2$ (Magnesium chloride)	1 mM
NaCl (Sodium chloride)	137 mM
$NaHPO_4.7H_2O$ (Sodium phosphate dibasic heptahydrate)	4.3 mM
Dissolve in dH_2O pH 7.4	

2.9.2 For Immunological methods

Permeabilization buffer	
Triton X-100	0.1% (v/v)
Dissolve in PBS	

Fixation buffer (4% PFA)	
Paraformaldehye	4% (v/v)
Dissolve in PBS	

FACS buffer	
BSA	0.4 % (w/v)
Sodium azide	0.02% (w/v)
Dissolve in PBS	

2.9.3 For Cell culture methods

ATV (Trypsin versene)	
D – Glucose	5 mM
NaCl	137 mM
Na_2EDTA (disodium salt of EDTA)	200 mg/L
$NaHCO_3$ (sodium bicarbonate)	70 mM
KCl	5.4 mM
Trypsin	500 mg/L
Dissolved in dH_2O	

2.10 Software

Use	Software	Company
Flow cytometry acquisition	CellQuest Pro	Becton, Dickinson & Co.
Flow cytometry analysis	FlowJo™ v10.4.2	Becton, Dickinson & Co.
Western Blot acquisition	Image Studio	LI-COR
Western blot quantification	ImageStudio Lite v5.2.5	LI-COR
Microscope Image acquisition	Las X 1.x	Leica
Data analysis	Excel 2016	Microsoft
Graphical representation	Graph Pad Prism 7.a.	Graphpad Software. Inc.
Text and Data presentation	Powerpoint 2016 and Word 2016	Microsoft
Sequence Analysis	SnapGene Viewer v5.1.1	GSL Biotech LLC

Table 2.9: List of Softwares used

METHODS

Note : All work involving live or infectious cells, fluids, viruses, culture media, carcinogenic reagents were carried out under Biosafety Level 2 hood with laminar flow. Procedures for Biosafety Level 2 were observed for work with Measles virus or blood samples. These were ensured so as to 1) maintain personal safety from infectious or hazardous agents and 2) to maintain aseptic environment so as to prevent contamination of cells, media from external sources.

3.1. Cell and Tissue Culture Methods

All cells were sub-cultured and maintained in sterile plastic tissue culture flasks and placed in humidified incubator at 37°C and 5% CO_2 atmosphere. Each 500 ml media bottle was supplemented with a vial of antibiotic Penicillin/Streptomycin (100,000 IU/ml Penicillin + 100 mg/ml Streptomycin) and required amount of heat inactivated fetal calf serum. Fetal calf serum (FCS) was heated at 56°C for 30 min so as to inactivate heat labile complement proteins. Aliquots of this FCS were prepared and stored at -20°C. Before addition to media, the FCS was also filtered with 0.45 µM pore size filter (Filteration step is optional).

Cells	Use	Media	Percent FCS in Media
BJAB	Maintenance	RPMI	5%
PBL / PBMC	Maintenance	RPMI	10%
BJAB	Maintenance	RPMI	5 %
Vero-hSLAM	Maintenance	MEM or DMEM	5%
	virus stock preparation	DMEM	5 %
	virus titration	MEM	0% and 2%
NT2	Maintenance	DMEM	10%
pi-NT2	Maintenance	DMEM	10%
LUHMES	Maintenance	DMEM/F12+glutamax	1% N2 supplement

Table 3.1: Media and percent FCS used for maintenance of cell lines

3.1.a. Adherent Cell Line – Passage and Maintenance

Flasks with adherent cells showing healthy morphology and 100 to 85% percent confluency were sub-cultured. Briefly, the spent medium was discarded, the monolayer was washed with PBS or ATV to remove residual serum from media. Cells were then detached by trypsinization with ATV for 2-4 min. Next, serum containing medium was added to stop the trypsinization and the cells split at ratio of 1:3 for NT2, 1:5 for Vero hSLAM and maximum of 1:2 for pi-NT2. Cells were passaged every 2-3 days.

3.1.b. Suspension Cell Line - Passage and Maintenance

Flasks with suspension cells showing healthy morphology and dense cell clusters were sub cultured. Briefly, the cell containing medium was collected and centrifuged at 1200 rpm for 5 min. The spent medium was carefully discarded. The cell pellet was gently resuspended in 10 ml fresh medium and split in ratio of 1:3 for BJAB (*It is preferable to split and maintain high density BJAB cultures*). Cells were passaged every 1-2 days.

3.1.c. Thawing of Cell Lines

All cells were revived from frozen stocks in the -140°C deep freezer. Frozen samples in vials were rapidly* (*important since the cryoprotectant DMSO is toxic at +4°C and above*) diluted in 20 ml pre-warmed maintenance medium. This was done by gradually adding approx. 750 µl of warm medium to the vial and collecting the thawed liquid in a falcon tube containing pre-warmed medium until the entire sample was thawed. The tube was then centrifuged at 4°C at 1200 rpm for 5 min in a pre-cooled centrifuge. The supernatant was discarded and the cell pellet carefully resuspended in fresh warm maintenance medium and finally transferred in appropriate tissue culture flask depending on the size of the cell pellet. The medium was changed once within the next 24 h until the cells were ready for scale up or further splitting.

3.1.d. Cryopreservation of Cell Lines

For cryopreservation, cells in the logarithmic growth phase were harvested - thus a 70-75% confluency for adherent cells and for suspension cells - along with microscopic observation for cell density, an orangish colour of RPMI media were considered as indicators. Briefly, the cells were trypsinized and /or pelleted down by centrifugation at 1200 rpm for 5 min at 4°C (*Cell pellets from multiple flasks were pooled so as to ensure*

*even distribution – one confluent middle flask of adherent cells yields minimum 8*10^6 cells which can be aliquoted as 1000µl in one vial or 500µl in two vials. Similarly cells from one large flask can be aliquoted as 1000µl in 3 vials each*). Meanwhile freezing medium (= respective cell line medium + 8% DMSO + 10 to 15% FCS) was prepared and kept on ice. The supernatant was discarded, carefully resuspended in freezing medium and aliquots of 500µl or 1ml were prepared in pre-cooled cryovials (*these steps were performed quickly to minimize DMSO toxicity*). The cryovials were priorly labelled. The step wise slow freezing was done as the cryovials were placed in Mr. Frosty^{TM} freezing container at -20°C for 2 h , then -80°C overnight and finally in -140°C until further use.

3.1.e. Propidium Iodide Staining for Cell Viability

Propidium iodide (PI) staining was used to measure live and dead cells to check the toxicity of various inhibitor concentrations. This is based on the dye exclusion principle. Live or viable cells have a selectively permeable cell membrane and thus do not take up the PI stain. In dead cells, due to the dysfunctional or disrupted cell membrane, the dye diffuses into the cell and binds to the DNA by intercalating between the base pairs. The bound dye now emits an enhanced fluorescence (at 617 nm) which can be measured in the red channel of the flow cytometer (Biolegend v2).

Safety measures were followed since PI is a suspected carcinogen. The viability staining procedure was as follows: 10,000-20,000 suspension cells were aliquoted in FACS tubes – for adherent cells, (in 48 well plates) the spent medium was discarded, monolayer washed with 40 µl ATV, further incubated with 75 µl trypsin for 3-4 min, the detached monolayer was then collected with 125 µl media(containing FCS) and collected in the FACS tubes. 300 µl FACS buffer was added to the tubes and centrifuged at 4°C / 1600 rpm for 5 min Meanwhile a 1:40 dilution of PI from 0.5mg/ml stock was prepared in FACS buffer. Following steps were performed on ice. The supernatant from the tubes were swiftly discarded using vacuum pipette without disturbing the cell pellet. 50 µl of the PI solution was added to each tubes. The tubes were then vortexed well and incubated on ice in dark for 10 min. Finally 100 µl of FACS buffer was added and the samples were FACSed. Heat killed cells were used as positive controls for forward (FSC) versus side scatter (SSC) and PI uptake positive gating.

3.1.f. Isolation of Peripheral Blood Cells / Lymphocytes

Isolation of peripheral blood mononuclear cells (PBMC) was done from blood deposited by healthy blood donors at the Transfusion medicine center at Universitätsklinikum, Würzburg – with approval from ethical committees. The blood (approx. 10 ml) is obtained in conical shapes leucocyte reduction chamber (LRC) which are granulocyte reduced and concentrated with mononuclear cells (i.e. lymphocytes and monocytes (Bio-sharing.org). The blood from the chamber was collected in a sterile Falcon tube. Next 40 ml of Versene was added to this tube and the tube was mixed by inverting it twice. Next 9 ml Histopaqe solution was added in two new 50 ml tubes each. 25 ml of the blood-versene suspension was carefully added to each of the Histopaqe containing tubes so as to allow the blood-versene suspension to form a layer and avoid mixing the two phases. The tubes were centrifuged at 20°C, 1200 rpm for 30 min with slow 2 and 2 break speed so as to not disturb the gradient. The white buffy coat layer containing PBMC was carefully collected into another tube. For washing, the supernatant was discarded and the pellet resuspended with PBS (without Ca^{2+} and Mg^{2+}) up to 50 ml and centrifuged at 20°C, 1600 rpm for 5 min. with 9 and 9 regular break speed – this washing step was repeated up to 4 times. Post washing, the PBMC pellet was resuspended in 10 ml of 5% FCS-RPMI medium and added to a 175 cm^2 cell culture flask. Additionally 40 ml more medium was added to the flask. The flask in horizontal position, was incubated at 37°C for 2 h for monocyte adherence. As most of the monocytes adhered to the flask, the cell suspension (lymphocyte enriched) was carefully collected and cells were counted using Neubauer chamber. For stimulation and further experiments, high density cell cultures in 10% FCS-RPMI media were prepared : $1*10^8$ PBLs in 50 ml medium for 75 cm^2 (middle) flask or $2*10^7$ PBLs in 10 ml medium for 25 cm^2 (small) flask and incubated at 37°C CO_2 incubator. For PHA stimulation, 2.5 µg/ml PHA was added and incubated overnight along with unstimulated control flasks. Flasks were checked next day for cell clumping under microscope and surface expression of CD25 and CD69 by flow cytometry – as indication of stimulated cells.

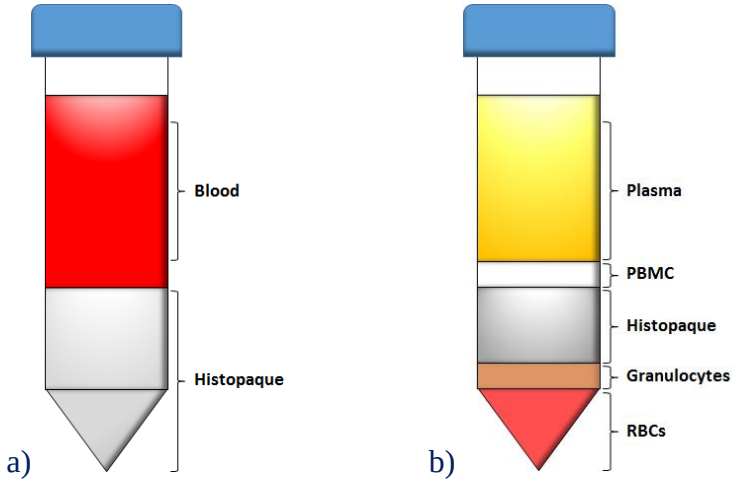

Fig. 3.1. Schematic of PBMC isolation by Histopaque gradient a) layering of suspension before centrifugation b) post centrifugation separated layers

3.1.g. Stimulation of PBL

PBMCs were stimulated with phytohaemagglutinin (PHA). This was done by incubating overnight the freshly isolated PBMCs with PHA concentration 2.5 µg/ml. Briefly, $1*10^8$ cells were resuspended in 50 ml of 10% RPMI medium. 125 µl PHA (from 1mg/ml stock) was added to this cell suspension and the suspension mixed well. The cells in tissue culture flasks were incubated upright at 37°C CO_2 incubator. For PHA stimulation, PHA was added and incubated overnight along with unstimulated control flasks. Flasks were checked next day for cell clumping under microscope and surface expression of CD25 and CD69 by flow cytometry.

3.1.h. Experimental Setup for Inhibitor Treatment of BJAB and PBMC

The cell density for the inhibitor treated cells for western blot and FACS analysis were as follows: $3*10^6$ BJAB cells in 3 ml medium per well and $1*10^7$ stimulated PBMC in 3 ml medium per well.

Setup for uninfected cells:

Cells were counted using Neubauer chamber → Required cell suspensions were prepared for each sample → Inhibitors were added → 3 ml cell suspension was aliquoted as per time point collection in 6 well plates → RIPA protein extracts for western blot were prepared along with an aliquot of sample analyzed by flow cytometry for cell viability.

Setup for inhibitor treatment for Infected cells:

Cells were counted using Neubauer chamber → For the infection phase, high density cell suspension i.e. $3*10^6$ per 500 µl or $1*10^7$ per 500 µl were prepared in serum free RPMI medium → The cells were pooled so as to ensure even infection and were infected with MV with an MOI of 0.5 for BJAB cells and MOI of 1 for PBMC → During this infection phase, the Falcon tube was incubated at 37°C in water bath for 2h with intermittent vortexing every 15 min. → After incubation, the unbound virus was washed by with serum free medium by pelleting the cells at 2000 rpm for 5 min → The pellet was then resuspended in PHA containing medium as per original cell density and aliquots as per samples were prepared → The inhibitors were added to respective samples and the tubes briefly vortexed once → 3 ml of the cell sample suspensions was aliquoted as per time point collection in 6 well plates. → RIPA protein extracts for western blot were prepared along with an aliquot of sample analyzed by flow cytometry for cell viability.

3.1.i. Differentiation of NT2 Cells to Neuronal NT2-N and Infection Experiment Setup

Numerous protocols have been reported for generation of neurons from NT2 cells. Here, differentiation of neuronal precursor NT2 cells into NT2-N neurons was performed as described by Paquet-Durand et al., 2003. For differentiation, $5*10^6$ NT-2 precursor cells were seeded in bacteriological grade Petri dishes so as to avoid cell adherence and promote free floating cell spheres. DMEM/F12 medium supplemented with 10% FBS, 1% Penicillin/streptomycin and 1% glutamine was used for cell seeding and further steps. On the next day and further on until two weeks retinoic acid (RA) yielding a final concentration of 10 µM was added to the media. During this period, the differentiation medium was replaced every 2-3 days by centrifuging the cell suspension at 200 g for 5 min, resuspending and reseeding the cell pellet with fresh medium on a new plate. After the first week, the cell sphere culture were transferred from petri dish into T75 cell culture flasks and maintained up to the end of the second week. At approximately day 14-16, the flasks were covered with aggregates or monolayer of cells. At this stage, the cells were trypsinized with ATV and replated into new T75 flasks with fresh medium now supplemented with following final concentrations of mitotic inhibitors - 1 µM Ara C (cytosine arabinoside), 10 µM FudR (5-Fluoro-2'-deoxyuridine) and 10 µm Urd (Uridine) and maintained for another 7-10 days (approx. 2 weeks). The post mitotic NT2-N cells were the trypsinized and $5*10^4$ cells per well (in medium now containing 10ng/ml Nerve growth factor) were seeded into 24 well plate precoated with extra cellular matrix Matrigel. The next day post seeding, neuron like

morphology can be observed on the NT2-N differentiated cells as compared to the undifferentiated cells. NT2-N cells were infected by incubation for 2 h with wild type IC323eGFP MV of MOI of 1. The wells were then washed to remove unbound virus and further incubated with 1 and 3 µm ERDRP-0519. Infection and effect of the inhibitor was noted by observing GFP positive cells under the microscope at day 1, 2 and 3 post infection.

3.1.j. Coating of Flasks and Plates for LUHMES Culture

For adherence of LUHMES cells, the tissue culture flasks and 24 well plates were pre-coated with poly-L-ornithine and fibronectin before seeding (Edwards et al., 2019). For the first coat, 50 µg /ml poly-L-ornithine, was added to each flask as per the following calculation:

1 T75 cm^2 flask: 6 ml dH_2O + 30 µl poly-L-ornithine (stock = 10mg/ml)

6 ml per flask or 500 µl per well was added and the flasks/plates incubated overnight at 37°C in CO_2 incubator. The solution was discarded the next day and the flasks nicely washed thrice with 5 ml sterile dH_2O. For the second coat, 1µg/ml fibronectin was added to each flask as per the following calculation:

1 T75 cm^2 flask: 5 ml PBS + 25 µl fibronectin (stock = 1 µg/ml)

The flasks were then incubated for 3 h at 37°C in CO_2 incubator. The solution was then discarded and the flasks thoroughly washed thrice with sterile distilled water. After washing the flasks were let to completely dry under the hood without allowing any traces of moisture to remain. The flasks/plates were then wrapped in plastic and stored at 4°C up to 2 weeks.

3.1.k. Maintenance of LUHMES Cells

Adherence ability of the LUHMES cells to the flasks is dependent on the cell density. Flasks showing 75-80 % confluency (approximately $9*10^6$ cells) were used for splitting and passaging the cells. Meanwhile new pre-coated flasks stored at 4°C were placed in the incubator to warm them up. The spent medium was discarded and the cell layer washed once with 3 ml PBS (without Calcium /Magnesium). Cells were trypsinized by incubating them with 1 to 1.5 ml of 0.25% trypsin-EDTA for 2-3- min until all cells detached. Trypsinization was stopped with 9 ml of LUHMES proliferation medium (+ 40ng/ml FGF final concentration). 2.5 ml of these cells were transferred into a new flask for a 1:4 split. Remaining fresh proliferation medium was added to the flask. The flask was then swirled well to mix the cell suspension and incubated at 37°C in the incubator.

3.1.l Generation of Neurons from LUHMES Cells

Differentiation of LUHMES cells was performed in pre-coated 24 well plates. Cells from flasks trypsinized as described in 3.1.f and centrifuged and counted using the Neubauer chamber. For a seeding density of $2.5*10^4$ cells per well, a suspension of $6*10^5$ cells is 12 ml medium (+5.4 µl FGF) was prepared and 500 µl aliquoted on each well.

Approximately 2 days post seeding, when the cell confluency in the wells was 70-80 %, the medium from the wells was carefully discarded and 500 µl of Differentiation medium was added per well and the plate further incubated. After 24 h incubation, the spent differentiation medium was replaced with fresh one. During the course of infection, the differentiation medium (Table 3.1.a) was replaced every 48 h.

Components	For 50 ml total volume	
DMEM F12/glutamax	50 ml	Prepare for 500 ml and store
N2 supplement (1% final concentration)	0.5 ml	
FGF basic (40 ng/ml)	20 µl from 100 µg/ml stock	Add fresh each time
Tetracycline hydrochloride (1µg/ml final)	50 µl from 10 mg/ml stock	
cAMP (1 mM)	245 µl from 204 mM stock	
rh GDNF (2ng/ml)	1 µl from 100 µg/ml stock	

Table 3.1.b.: Composition of Differentiation Media for LUHMES cells

3.2. Molecular Biology Methods

3.2.a. Protein Extraction from Cells

For experiments with suspension cells BJAB and PBMCs, total protein lysates were prepared with RIPA extraction buffer. 100 µl RIPA extracts were prepared from $3*10^6$ BJAB cells or $1*10^7$ PBLs. All the following steps were done on ice. Sample cell suspension were collected in sterile 1.5 ml Eppendorf tubes and centrifuged at 4°C / 1600 rpm for 5 min. The spent medium was discarded. Two washing steps followed involving each time resuspending the cell pellet in 750 µl ice cold PBS and centrifuging at 4°C, 1600 rpm for 5 min and discarding the supernatant. The pellet was resuspended in 100 µl freshly prepared cold RIPA extraction buffer (see table.3.2) and incubated on shaker at 4°C for 1 h. The lysate was clarified by centrifugation for 5 min at 10,000 rpm at 4°C to get rid of debris. The clear supernatant was carefully transferred in pre-cooled Eppendorf tubes and stored at -20°C until further use. The samples were further quantified for protein content by BCA

method. Avoid frequent freeze thaw of samples to prevent sample protein degradation (*especially for phosphorylated proteins detection by western blot*).

RIPA extraction buffer (fresh)	For 1000 µl (1 ml)
1x RIPA buffer	756.2 µl
7x protease inhibitor stock	142.8 µl
10x phosphatase inhibitor stock	100 µl
1 M DTT	1 µl

Table 3.2.: Constituents for fresh RIPA buffer for protein extraction

3.2.b. Protein Quantification by BCA Method

Protein concentrations were estimated by the colorimetric bicinchoninic acid (BCA) method. The BCA solution is highly alkaline and also contains copper sulfate. The peptide bonds in the protein reduce the Cu^{2+} ions to Cu^{1+}. This temperature dependent reduction reaction is thus proportional to the amount of protein present in the solution (Olsen et al., 2007). Further, two molecules of bicinchoninic acid chelate with one Cu^{1+} ion to form a purple complex that absorbs light at 562nm. Protein concentration can thus be measured using this absorbance property and comparing it with known protein standards. A higher temperature range of 37°C or 60°C is recommended to increase assay sensitivity (ThermoFischer Cat No.23225).

The protein samples were thawed and placed on ice. Meanwhile, BCA reaction mixture was prepared as follows: 20 µl $CuSO_4$ + 980 µl BCA solution for 1 sample, thus BCA reaction mixture was prepared for samples including blank and standard, vortexed well and 1ml was aliquoted in 2 ml labelled Eppendorf tubes. 5 µl of sample was added to each tube and the tubes vortexed well. The tubes were incubated at 37°C for 30 min and further cooled on ice for 1 min. to stop the reaction. Samples were then transferred to cuvettes for absorbance measurement. The colorimetric readings were taken in Eppendorf Photometer as per manufacturer's protocol.

3.2.c. Western Blotting for Protein Detection

The western blot or protein immunoblot is a widely used analytical technique in molecular biology to detect protein expression in biological samples. For above experiments, the western blot procedure steps followed were:

Sample preparation → 2) SDS – PAGE for separation of proteins on gel → 3) Semi-dry transfer of proteins from gel to nitrocellulose membrane → 4) Detection of proteins on membrane with antibody.

1) Sample preparation: Sample preparation (protein lysate) and storage was a key step especially important for detection of phosphorylated proteins or non-constitutive proteins. Handling at low temperatures during sample preparation inhibits the action of proteases and prevents protein degradation. Cell quantity for sample preparation not only depends on cell size but also size of SDS gel being used. Samples here were prepared as previously described in and should contain 1 to 3 µg/µl protein (3.2.a)

2) SDS-PAGE (Sodium Dodecyl Suphate – Polyacrylamide Gel Electrophoresis):

Here the proteins are separated by electrophoresis using polyacrylamide gel containing SDS as a denaturant. SDS is a surfactant that binds to the protein and confers a uniform negative charge. One molecule of SDS binds to approximately 2 amino acid. Thus as the proteins migrate towards the anode, they separate based on molecular size (typically between 5kDa to 250 kDa). In discontinuous PAGE, two gels are used to separate the proteins. Proteins first migrate within the stacking gel at pH 6.8. The neutral pH enables to concentrate the sample before actual separation within the resolving gel at pH 8.7. This pH difference gives a stacking effect resulting in sharp bands.

The gel chamber apparatus was assembled as follows: two clean dry glass plates were aligned separated by spacers and securely fixed with clamps on the side and sealed with rubber tubing below. The assembly was checked for leakage. The resolving gel was prepared (see table) and poured carefully up to three fourth filling capacity. The gel was layered with 2 ml iso-propanol to even the surface and avoid bubbles and the gel was allowed to polymerized (usually 25-30 min). Next, the iso-propanol was discarded and the prepared stacking gel was poured on top. The comb was carefully inserted and the gel allowed to polymerize for 25-30 min. The electrophoresis unit was then filled with 1x protein gel running buffer and the comb carefully removed from the stacking gel. The wells were gently flushed with protein gel running buffer to remove air bubbles or gel residue.

a. Resolving Gel preparation

% of gel	10 %	12 %
d/W	12.9 ml	10.8 ml
1.5 M Tris pH 8.7	8 ml	8 ml
30 % Bis acrylamide	10.6 ml	12.8 ml
20 % SDS	160 µl	160 µl
TEMED	18 µl	18 µl
10 % APS	280 µl	280 µl

b. Stacking Gel preparation

Stacking Gel	1 Gel
d/Water for 30 % Bis	6 ml
1.5 M Tris pH 6.8	1.25 ml
30 % Bis acrylamide	1.3 ml
20 % SDS	50 µl
TEMED	10 µl
10 % APS	100 µl

Table 3.3: Volumes of components for preparation of a) Resolving (lower) gel and b) Stacking gel. The sequence of components to be added is from first to last row. The solution was mixed well before pouring.

For protein expression/detection equal amount of proteins were loaded in each well. The prepared protein lysates were thawed and kept on ice. All following steps were performed on ice. Loading samples per well was prepared with 35 or 70 µg sample protein + 10 µl of 4x Laemelli buffer + RIPA buffer to a total volume of 40 µl for 15 well comb (The loaded volume per well depended on number of wells in the comb). The tubes were then vortexed well, briefly spun down and heated at 95°C for 5 min. and then placed on ice. The samples and pre-stained protein marker (5-6 µl) were then loaded in the wells. The gel was run at 50 mA for 2-3 h till the bromophenol blue covered ran at least three fourth of the gel.

3) Semi-dry transfer of proteins from gel to nitrocellulose membrane

The proteins separated on the gel were now transferred onto a solid nitrocellulose membrane so as to immobilize them. Once the gel run was complete, the gel was cut and placed in Cathode buffer so as to remove the running buffer salts and detergents (8). Whatman filter papers were cut and soaked in each of the buffers – 300 mM Anode buffer, 30 mM anode buffer and Cathode buffer. The gel / pre-wetted membrane sandwich (in sequence as in the image) was carefully set up to prevent excess moisture or air bubbles. This gel / membrane sandwich was set up between the two electrodes. Transfer was carried out at 125 mA for 65 min. Transfer was checked by successful transfer of all bands of the protein marker.

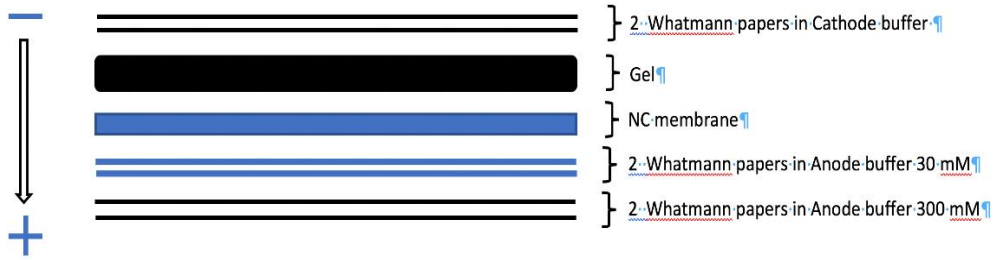

Fig. 3.2: Schematic layout of sequence of electrode , membranes and gel sandwich for semi-dry transfer

4) Detection of proteins on membrane with antibody

After protein transfer to the membrane, to avoid background signal due to antibody binding at unoccupied sites, the membrane was blocked by incubating it at room temperature on a shaker for 30 min. in 5% non-fat dry milk in PBS-T or BSA in TBS-T (for phosphorylated proteins). The membrane was then washed with PBS-T or TBS-T for 5 min. The blocked membranes were then incubated with respective primary antibodies (1:1000 – 1:2000) diluted in 5% milk-PBST or 5% BSA-TBST overnight at 4°C with gentle shaking. Membranes were then washed thrice for 5 min each with PBST/TBST and further incubated with HRP- labelled secondary antibody (1:10,000 dilution in milk or 5% BSA) and incubated for 1h at room temperature with gentle shaking. The membranes were again washed thrice with PBST/TBST. For visualization of protein bands, 1:1 ratio of Chemiluminescent FemtoMax^{TM} Super Sensitive HRP substrate (Rockland) was added over the membrane before acquiring images in the Chemi channel if theh Li-cor Odyssey Fc Imaging system.

3.3. Immunological Methods

3.3.a. Flow Cytometry

Flow cytometry is widely used to detect expression of biomolecules on the cell surface and also intracellular. Additionally, numerous other parameters like cell size, shape, heterogeneity within the cell suspension can also be analyzed using appropriate channels, antibodies and fluorescent/ chemical labelled probes. The basic principle involves light scatter and/ or fluorescence detected as the single-cell suspension pass through a nozzle. The sheath fluid channels the cell suspension such that one cell at a time that passes the laser light beam thus affecting the path of light. The forward (FSC) or side scatter (SSC) of light by the cell correlates with cell size and cell granularity respectively, while target proteins can be detected by fluorescence emission of the probes used for staining the cells. For detection of multiple fluorescent probes from the same sample it is important to select

probes with different / distant emission spectra to avoid interference. For example GFP and propidium iodide used together.

All flow cytometric measurements were performed in BD FACS Calibur and the acquired experimental data then analyzed by FloJo version 10.4.2 software. Cells were treated/ prepared as per the experimental requirement. All washing steps were done with 1ml cold FACS buffer with cold centrifuge for 5 min at 1600 rpm. For every experimental analysis, required controls were set up along with tests – isotype control, unstained control, only fluorescent antibody control and dead cell control.

3.3.a.1. Viral GFP Detection

Detection and measurement of viral encoded GFP by FACS was done to check and quantify infected cells. GFP measurement was done simultaneously along while measuring cell viability by propidium iodide staining (Protocol: 3.1.d. Propidium Iodide Staining for Cell Viability).

3.3.a.2. Cell Surface Staining of Proteins

Between $1*10^4$ to $4*10^4$ cells were aliquoted in FACS tubes – <u>for adherent cells</u> (from 48 well plates) the spent medium was discarded, monolayer washed with 40 µl ATV, further incubated with 75 µl ATV for 3-4 min, the detached monolayer was then collected with 125 µl FCS-medium and collected in the FACS tubes. For suspended cells, the cells were counted and aliquoted in the FACS tubes. 300 µl cold FACS buffer was added to each tube and the cells washed by centrifugation at 4°C / 1600 rpm for 5 min. Meanwhile respective primary antibody dilution was prepared in FACS buffer or PBS and kept on ice. (Antibody dilution was calculated as per 200µl volume per tube). After centrifugation, the supernatant from the tubes were swiftly discarded using vacuum pipette without disturbing the cell pellet. 200 µl of respective primary antibody / isotype was added per tube, the tubes vortexed well and incubated for 45 min. on ice in dark. Next, the cells were again washed twice each time with 1 ml of cold FACS buffer. 200 µl of fluorescently labelled secondary antibody was added per tube, the tubes vortexed well and incubated for 45 min on ice in dark. Cells were washed twice with cold FACS buffer and finally the pellet resuspended in 100 µl FACS buffer and proceeded for FACS. *(For direct staining, i.e. where the primary antibody itself was fluorescently labelled the 2° antibody step omitted).*

3.3.a.3. Intracellular / Total Staining of Proteins

Suspension or adherent cells were added in FACS tubes as described previously in the above protocol (3.3.a.2) up to wash step with cold FACS buffer. Fixation was carried out by adding 200 µl 4% PFA to the tube and resuspending the cell pellet by vortexing. The tubes were incubated on ice for 15-20 min and further at R.T. for 10 min. Cells were washed thrice 1 ml cold FACS buffer to get rid of PFA.

For permeabilization of large cell line cells, 200 µl of 0.1% Triton X-100 was added per sample and incubated for 10 min at R.T. Cells were washed once with cold FACS buffer. For permeabilization of PBMC, the mild detergent Saponin buffer was used.

All antibody dilutions for PBMC total staining were prepared in Saponin buffer while p.i.NT2 or NT2 cells, FACS buffer or PBS was used as diluent. 50µl of primary antibody was added per sample, tubes vortexed and incubated at R.T., dark for 45 min. Cells were then washed twice with cold FACS buffer. Next cells were incubated with 50 µl secondary antibody at R.T., dark for 45 min followed by subsequent washing steps twice. The washed pellet was resuspended in 100 µl FACS buffer and measured by FACS.

3.4. Virological Methods

3.4.a. Measles Virus Stock Preparation

For all infection experiments in BJAB, PBMC, Vero-hSLAM, NT2 and LUHMES cells, recombinant wild type IC323eGFP MV was used. The virus was cultivated in Vero-hSLAM cells and crude purified stocks were used. Briefly, Vero-hSLAM cells were cultured in 175 cm^2 flasks with 5% FCS-DMEM medium until the cell confluency was 60-70 %. Then, the spent medium was discarded and the flask rinsed once with warm serum free medium or sterile PBS (*to remove serum traces*). A virus inoculum of 0.01 MOI in 4 ml serum free medium per flask was added and cell flasks were incubated at 37°C for 2 h with regular intervals of shaking. Next, 20 ml of 2% FCS-DMEM medium was added to each flask and the flasks incubated for further one hour at 37°C. All flasks were then shifted to 33°C incubator for 2-3 days until typical cytopathic effect of 75% or more syncytium was observed (*begin the harvest before the monolayer detaches*). Media from each infected flask was carefully reduced to 5 ml, the cells were then scraped using a cell scraper within the flask media, the flasks then sealed with parafilm and frozen at -80°C for 48 h. The flasks were then thawed at 37°C and all the subsequent steps carried on ice. The scraped cell-virus suspension was pooled and cooled in a homogenizer. Using a douncer, cells were

homogenized for 6-8 times (*to disrupt cells and release cell associated virus*). This lysate was then centrifuged at 4°C , 1600 rpm, 15 min to get rid of the pellet cell debris. The supernatant was further centrifuged twice for 5 min each so as to obtain a clear supernatant. The virus supernatant was finally aliquoted in labelled and pre-cooled cryovials and stored at -80°C. (*Repeated freeze-thawing of virus aliquots to reduces infectious virus titers*).

3.4.b. Titration of Measles Virus

Samples from virus stock preparations, BJAB, PBMC and p.i.NT2 experiments were titrated on Vero-hSLAM cells. Vero-hSLAM cells ($1*10^4$ cells/well) were seeded in 48 well plates and incubated overnight at 37°C. On the next day, ten fold serial dilutions from 10^{-1} to 10^{-6} of the test virus sample were prepared in cold 2% FCS -MEM medium in a total volume of 800 µl (720 µl medium + 80 µl virus). Using sterile glass Pasteur pipette connected to vacuum source, the spent medium from the wells of the seeded plate was discarded. The medium was now replaced with serially diluted virus beginning from the highest dilution to the lowest (200 µl per well). Each dilution along with uninfected control was performed in triplicates. The plates were incubated at 37°C for 72 h. Infection induced syncytia were observed microscopically and the GFP positive syncytia were counted. The PFU / ml was determined by the formula: (mean number of plaques * respective dilution factor) / volume of inoculum (µl)

RESULTS

4.1. PHA Stimulation Upregulates Surface Expression of Lymphocyte Activation Markers Coinciding with MV Infection

In the first part of my thesis, I performed experiments with primary human PBL, which were obtained from healthy blood donors from the Transfusion medicine center of the Universitätsklinikum, Würzburg, with approval from the ethical committee of the medical faculty.

PBL were prepared by Histopaque gradient centrifugation and stimulated with PHA as described in 3.1.f and 3.1.g. After the plastic adherence step, the isolated PBMC consisting of (T cells, B cells, NK cells and monocytes and macrophages) are now devoid of most of the adherent monocytes and enriched as PBL (peripheral blood lymphocytes). Activation of the PBL by overnight PHA stimulation prior to inhibitor and infection experiments was checked by flow cytometric analysis for surface expression of known activation markers like CD25 and CD69. While both are expressed on PBMC population, CD69 is also expressed on platelets and granulocytes and is an early activation marker involved in proliferation and signaling. As expected, PHA treatment led to upregulation of surface CD25 and CD69 expression (Figure 4.1.A) and CD69 positive cells coincided with higher MV infection (Fig 4.1.B). As the example in Fig. 4.1.B shows, infection of 24 h PHA-activated PBL with recombinant wild-type MV IC323eGFP at an MOI of 0.1 led to approximately 8% of infected, GFP positive cells in culture, a twofold increase in comparison to unstimulated PBL. Due to the limited expression of CD150, at most 15 to 20% of PBL can be infected with higher MOIs of wild-type MV (Fig.4.1.C)

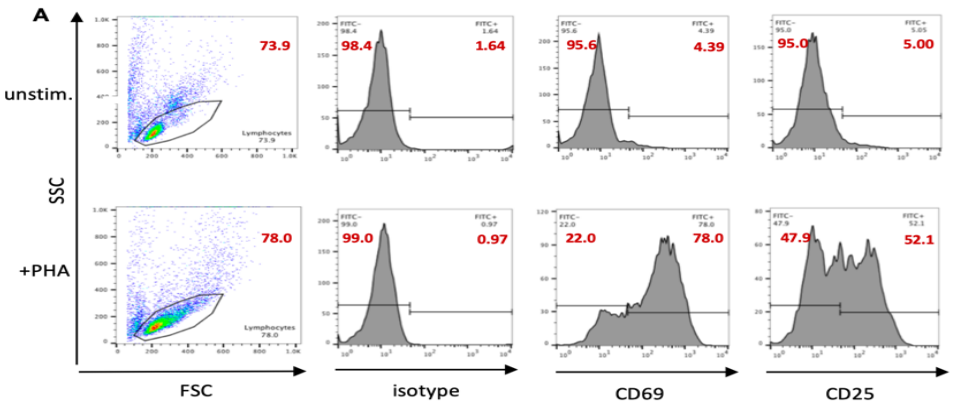

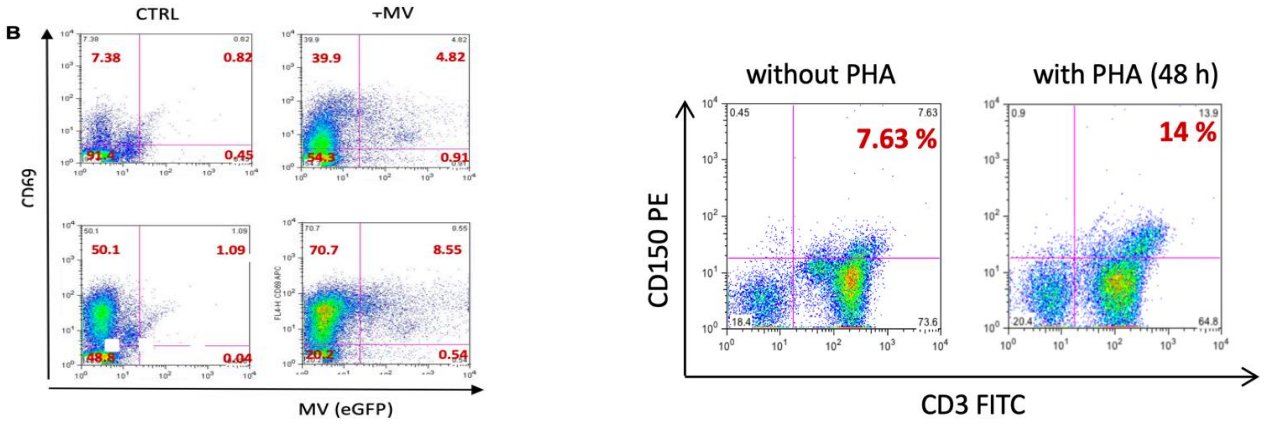

Fig. 4.1: Activation of PBL increases the percentage of MV susceptible cells

PBL from healthy donors were stimulated with PHA for 24 h prior to inhibitor treatment and/or infection experiments. (A)The cells were then stained with FITC conjugated CD25 and CD69 antibodies along with respective isotype controls. The histogram shows increased CD69 and CD25 intensities with PHA treatment (B) An example of dot plot graph showing difference between percent infected cells determined by viral eGFP positive cells observed in stimulated versus unstimulated PBL plotted by CD69 on Y axis. PBL were infected with MV-IC323eGFP at a MOI of 0.1 for 48 h (Grafen et al., 2019). (C) Increased surface expression of CD150 in PHA stimulated PBL as compared to unstimulated PBL (lab generated, data unpublished).

Pre-stimulation of PBL overnight with PHA resulted in almost double percent of infected cells by MV at 24 hpi as compared to unstimulated PBL. This can be attributed to the increased CD150 surface expression observed in stimulated PBL (Fig. 4.1.C). Increased infectious virus titers from PHA stimulated PBL were also observed at 48 hpi as compared to titers from unstimulated PBL (data not shown).

4.2. Ceranib-2 and SKI-II Reduce mTOR Activity in Uninfected BJAB and Primary PBL

The group of Prof. Jürgen Schneider-Schaulies found that the two inhibitors of the sphingolipid metabolism Ceranib-2 and SKI-II (1.13.c) reduced MV replication in primary human PBL and BJAB cells and thus based on tested viability assays as reported in Grafen et al, 2019, we treated both BJAB cells and stim PBL each separately with 3µM Cer-2 and 5µM SKI-II. It was not known that and how these compounds may lead to this effect, and therefore I investigated the underlying mechanisms. Studies from our group by Tiwarekar et al., 2018 and Grafen et al., 2019 also reported the involvement of cellular nutrient sensor

mammalian target of rapamycin complex (mTORC) in MV replication in PBLs (See Section 4.6 and Fig. 4.6).

As it is known that alterations of cellular ceramide concentrations and S1P, and Sphk 1/2 activities can affect intracellular signaling and the mTORC1 activity, we hypothesized that corresponding pathways might be involved in the reduction of MV infection by Ceranib-2 and/or SKI-II. Thus, we further explored the effect of Ceranib-2 and SKI-II on mTORC activation in BJAB cell line as well as PHA stimulated PBL in the absence and presence of viral infection. Their effects on mTORC1 activity were checked by assessing for a known marker substrate downstream i.e. phosphorylation of p70 S6 kinase (activation) at various timepoints using western blots. In PBL (Fig.4.2.A), Cer-2 significantly reduced phosphorylation of p70 as compared to DMSO treated cells, while in BJAB cells (Fig.4.2.B) – p70 activation was reduced by both Cer-2 and SKI-II.

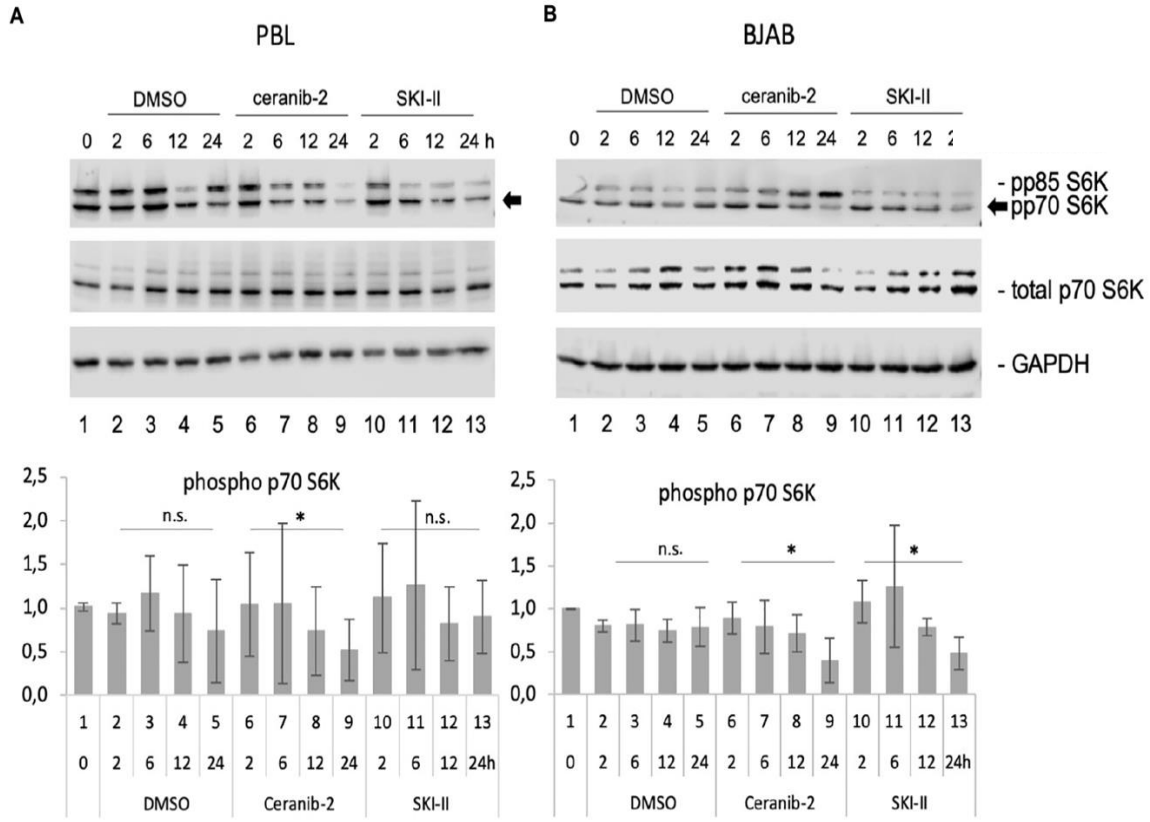

Fig. 4.2: Cer-2 and SKI-II reduce p70 phosphorylation in stimulated PBL and BJAB cells Representative image of western blots from total cell lysates of PHA stimulated primary human PBL (A) and (B) which were treated with 0.2 % DMSO as control and 3 µM Cer-2 and 5 µM SKI-II for 2. 6. 12 and 24 h as indicated and were probed using antibodies against phosphorylated and total p70 S6K (also bind to it's 85 kDa isoform) and GAPDH as loading control. Graphical representation of quantified phosphorylated p70 (normalized to GAPDH) of the PBL (from three independent blood donors) and BJAB from three independent experiments (n=3) are shown.

4.3. Ceranib-2 and SKI-II Treatment affect rpS6, EIF4E and MNK Expression in Uninfected Primary PBL

The mTORC1 sensor orchestrates numerous downstream pathways associated with metabolism, survival and growth of the cell. From a virus point of view, for its own successful replication cycle, it requires host cell machinery for production of its viral proteins. Thus, I further assessed the effect of the two inhibitors on protein translation associated proteins downstream of mTORC1 i.e. ribosomal protein S6 (predominantly associated with translation of proteins containing TOP motifs) and EIF4E (involved in capped mRNA dependent protein translation). Effect of the inhibitors on MNK expression (a protein activated by MAPK and reported to be associated with mTOR complex) was also assessed (Batool et al., 2020).

Phosphorylation of rpS6 (indicating activation) showed a tendency of reduction by both Ceranib-2 and SKI-II especially between 6 and 15 h post treatment as comparted to DMSO control (Fig. 4.3 A.). However, this reduction difference was significant with Ceranib-2 treatment especially at 6 and 15 h (Fig. 4.3.B.). We observed, significant reduction in expression levels of phosphorylated EIF4E at 15 h and 24 h post treatment with both the inhibitors (Fig 4.3 C, D). When probing for MNK1 expression levels, we observed that both phosphorylated and total MNK1 expression was not significantly affected by both inhibitor treatment especially Ceranib-2 (Fig 4.3 E, F). However as compared to control cells which showed increased total MNK1 expression over time (indicating turnover as the cells divide) we observed a low level MNK1 expression in the presence of SKI-II (Fig 4.3 G. last graph).

These data indicated that treatment of the primary PBL with Ceranib-2 and SKI-II mainly affected the phosphorylation of EIF4E and also moderately affected rpS6 activation in the absence of MV infection. Thus, we pursued further to check the effect in the same experimental set-up but now also in the presence of MV infection.

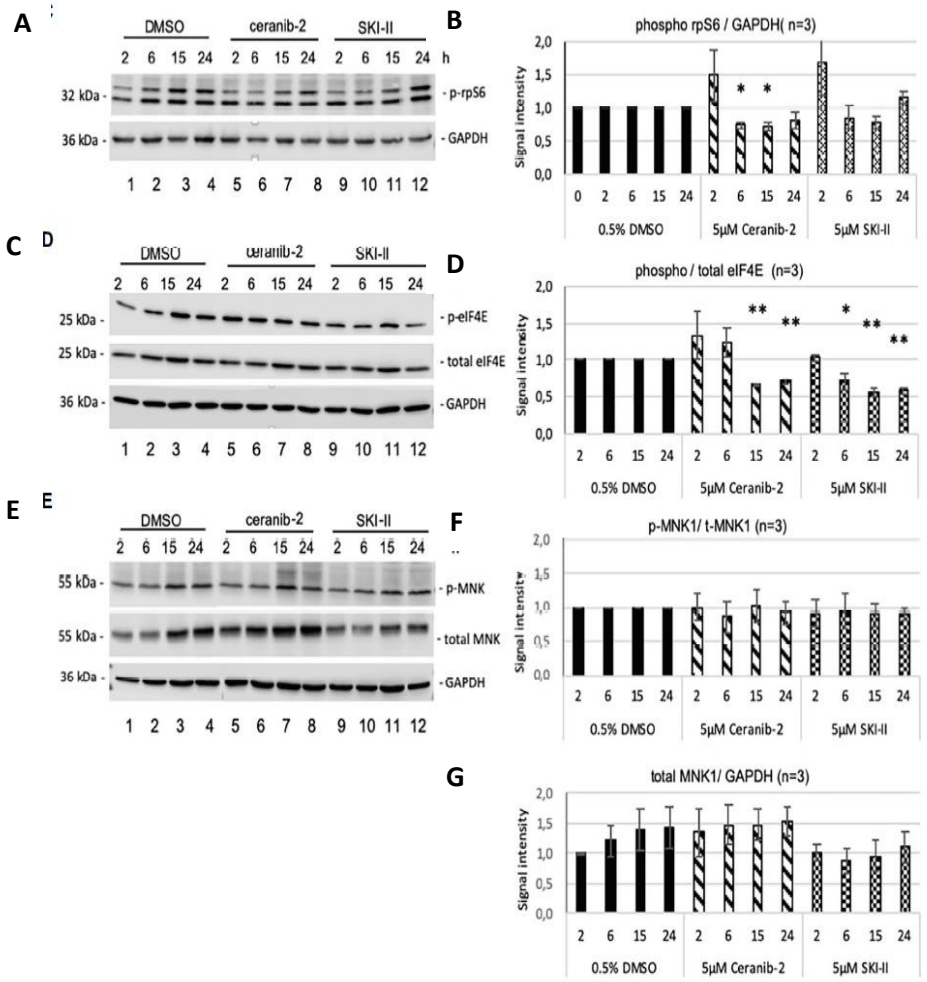

Fig. 4.3: Cer-2 and SKI-II affect rpS6, EIF4E and MNK1 expression in uninfected primary PBL Representative image of western blots from total cell lysates of PHA stimulated primary human PBL and (B) which were treated with 0.2 % DMSO as control and 5 µM Cer-2 and 5 µM SKI-II for 2. 6. 15 and 24 h as indicated and were probed using antibodies against (A) phosphorylated rpS6 (32 kDa) and GAPDH as loading control (B) phosphorylated and total forms of EIF4E and (E) phosphorylated and total forms of MNK1. Graphical representation of quantified phosphorylated proteins (normalized to total protein or GAPDH) of the PBL (from three independent blood donors) (n=3; with *p≤ 0.05 and **$p \leq 0.01$ calculated by student's t-test) are shown.

4.4. Ceranib-2 and SKI-II Treatment affects rpS6, EIF4E and MNK Expression in MV Infected Primary PBL

Next, I further assessed the effect of treatment of inhibitors in stimulated primary PBL infected with wild-type MV. The PHA stimulated PBL were infected with recombinant wild-type MV IC323 eGFP at MOI of 1.5 and further in the absence or presence of 5 µM Ceranib-2 and SKI-II along DMSO uninfected and uninfected controls. Cell lysates using RIPA buffer extraction were prepared at 3, 6, 16 and 24 h and processed and equal amounts

were loaded for Western blot. We observed that MV infection stimulated expression of total rpS6 as compared to uninfected control (Fig. 4.4 A lanes 8,9 compared to lanes 4,5) and treatment of the infected cells with Ceranib-2 and SKI-II reduced the rpS6 expression (Fig 4.4 A). For rpS6 phosphorylation, we found a significant reduction at 16 and 24 h post SKI-II treatment in infected cells indicating reduced translational capacity of the cells. The observed increased intensity of the phosphorylated rpS6 bands at 16 and 24h (Fig 4.4 A lanes 8 and 9) indicate upregulation of rps6 activity during viral replication cycle.

We observed that the cap dependent translation associated protein EIF4E phosphorylation was increased at 16 h post infection which was significantly decreased by Ceranib-2 and SKI-II at 16 h and 24 h respectively (Fig. 4.4 D,E)

Although phosphorylated MNK1 expression was not significantly affected by both infection and inhibitor treatment (Fig 4.4.F evaluation not shown). However, Ceranib-2 slightly reduced total MNK1 expression in infected cells (Fig. 4.4 G).

Since previously IKK and NF-κB were shown to be affected by SKI-II in H3358 cell line – a bronchioalveolar epithelial carcinoma cell line (Vijayan et al. 2014), we also probed for IKK expression levels. We observed a significantly decreased expression of IKK levels in SKI-II treated MV infected cells indirectly indicating decreased NF-κB activity (Fig. 4.4. H,I).

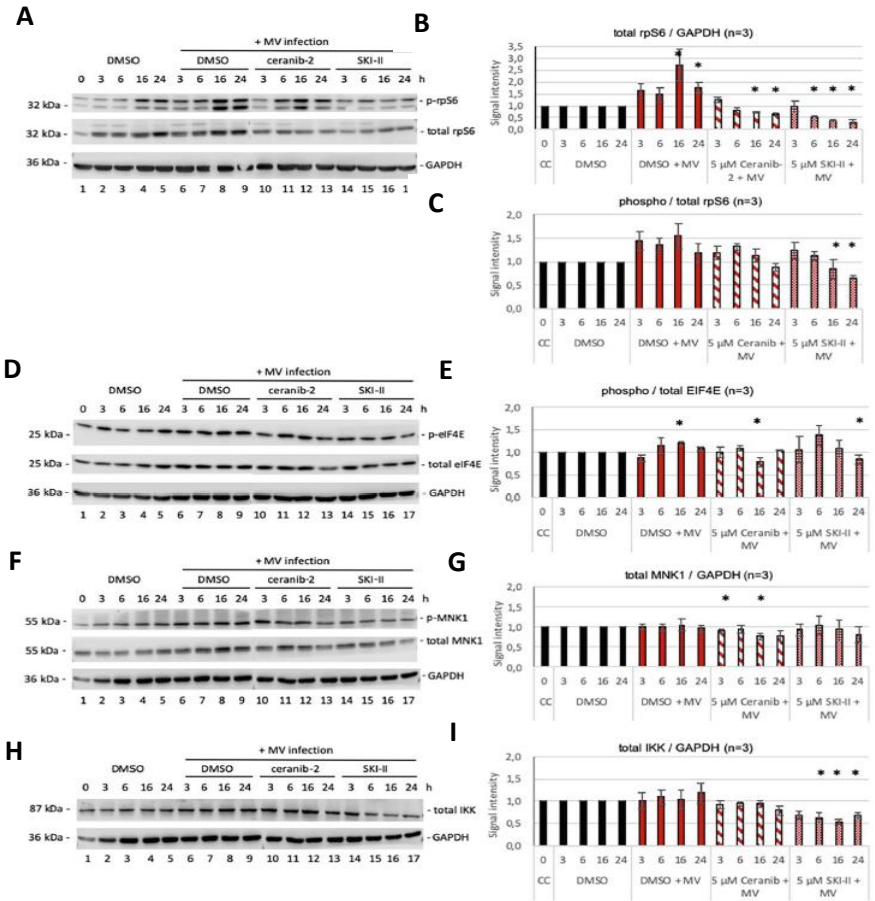

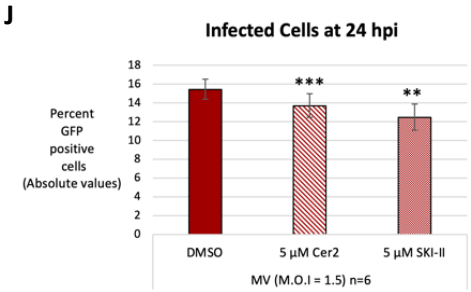

Fig. 4.4: Cer-2 and SKI-II affect rpS6, EIF4E and MNK1 expression in infected primary PBL Representative image of western blots from total cell lysates of PHA stimulated primary human PBL which were first infected with 1.5 MOI MV IC323eGFP and then treated with 0.2 % DMSO as control and 5 µM Cer-2 and 5 µM SKI-II with lysates prepared for 3. 6. 16 and 24h as indicated and were probed using antibodies against (A, B,C) phosphorylated and total rpS6 (32 kDa) and GAPDH as loading control (A,B,C) phosphorylated and total forms of EIF4E and (D, E) total forms of MNK1 (F, G) and IKK-β (H, I). Graphical representation of quantified phosphorylated proteins (normalized to total protein or GAPDH) of the PBL (from three independent blood donors) (n=3; with *p≤ 0.05 and **$p \leq 0.01$ calculated by student's t-test) are shown. (J) Graph of percent infected (GFP positive cells) PBL with control DMSO and 5 µM Cer-2 and SKI-II treated which was estimated by flow cytometry (Methods 3.1.d and 3.3.a.1) at 24 hpi along with lysate preparation for Western blot. Results from six independent blood donors) (n=6; with *p≤ 0.05, **$p \leq 0.01$ and ***$p \leq 0.001$ calculated by student's paired t-test) are shown.

4.5. Ceranib-2 and SKI-II Treatment affect Viral Protein Expression in MV Infected Primary PBL

Based on the immunoblots where we observed an overall dampened expression profile of mTOR activity, rpS6 and EIF4E in Ceranib-2 and SKI-II inhibitor treated infected and uninfected cells indicating decreased translational capacity in the cell, we sought to check the effect of these inhibitors (along with known mTOR inhibitor Rapamycin) on viral protein expression in the PBL at 24 h (where there would be sufficient accumulation of viral proteins for detection by flow cytometry).

Although, we observed significantly reduced viral encoded GFP MFI expression in SKI-II and Rapamycin treated cultures at 24 h as expected, the GFP fluorescence in the Ceranib-2 treated sample rather had an increased tendency. (Fig 4.6 A). We also quantified for two other viral proteins MV-N (nucleocapsid) and MV-H (hemagglutinin) using monoclonal antibodies. We observed that expression of nucleocapsid was not significantly affected by any of the inhibitor treatment (Fig.4.5.B). However, MV-H expression was reduced by Ceranib-2, SKI-II and Rapamycin at 24h (Fig.4.5.C). These results not only

indicate a dampened protein translation effect by the inhibitors but also that Ceranib-2 and SKI-II have differential effects on the mode of downregulation.

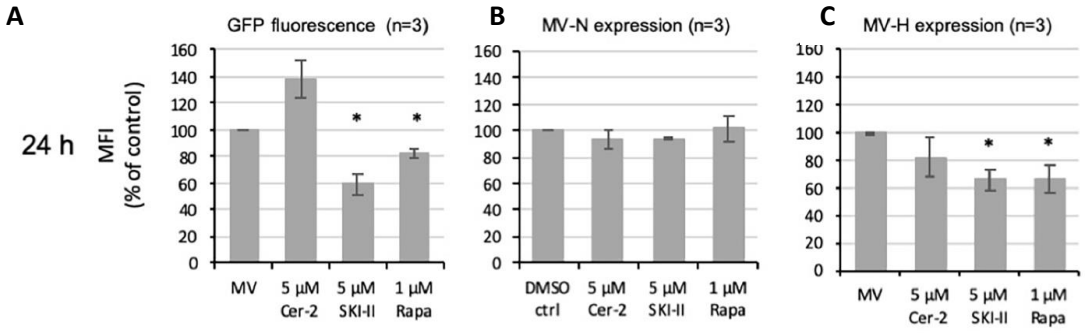

Fig. 4.5: Cer-2 and SKI-II affect viral protein expression in MV infected PBL

The PHA stimulated PBL were infected for 2h with wild type MV IC323eGFP and further incubated with the respective inhibitors and analyzed at 24 h by flow cytometry (MFI) for GFP, MV-N and MV-H (A, B, C). Quantification is presented in relation to percent of the control. Significant differences in comparison with the control were indicated with $*p \leq 0.05$ calculated by student's *t*-test (n=3).

4.6. Antiviral Effect of Various Inhibitors on Acute MV Infection in PBL

We also tested the panel of inhibitors (mentioned in Introduction Section) on their ability to prevent MV replication in primary PBL during acute infection. First, inhibitors targeting cellular host factors were investigated. MTOR inhibition by 1µM Rapamycin significantly reduced MV replication especially at 48 hpi (Fig 4.6 A). With pharmacological inhibition of mTORC1 activity by Rapamycin, a dose dependent inhibition in infectious viral titers and reduction in infection induced cell fusion was observed indicating that mTORC1 activity enhanced MV replication in PBL (Fig 4.6 A). Rapamycin treatment reduced the infectious titers (from stimulated PBL) to a level similar to the unstimulated untreated control.

Further, inhibitors SKI-II and Ceranib-2 that predominantly target the sphingolipid metabolism enzymes sphingosine kinases and acid ceramidase, respectively, effectively inhibited MV replication at concentrations 5 µM and 1 µM respectively at 72 hpi (Fig. 4.6 Panels B, C). Maximal reduction of MV titers were approximately 1 log step. Such an antiviral effect of both inhibitors was observed for MV replication in PBL as well as BJAB (Grafen et al., 2019).

MV replication in PBLs was found to be sensitive to low concentrations of Hsp90 chaperone inhibitor 17-AAG, since 0.5 and 1 µM 17-AAG strongly reduced viral titers at 48 and 72 hpi but not yet at day 1 (Fig 4.6 D) emphasizing the role of functional Hsp90 for proper folding of newly synthesized viral L polymerases.

Furthermore, inhibitors targeting viral proteins and their activities were investigated. (Fig. 4.6 E, F, G). Inhibition of viral F protein activity by 200 µM FIP was significant at 48 and 72 hpi indicating FIP activity mainly on the newly synthesized viral particles (Fig 4.6 E). Among the panel of inhibitors, ERDRP-0519 had the most specific antiviral mode of action and this was also observed by the dose dependent significant log fold reduction in viral titers (Fig 4.6 G) at 48 and 72 hpi. As a known control, we also tested effect of Ribavirin (a broad spectrum clinically used antiviral and also used in treatment during SSPE) and observed that a high concentration of Ribavirin (100 µM) significantly reduced production of infectious MV titers at 48 and 72 hpi (Fig 4.6 F).

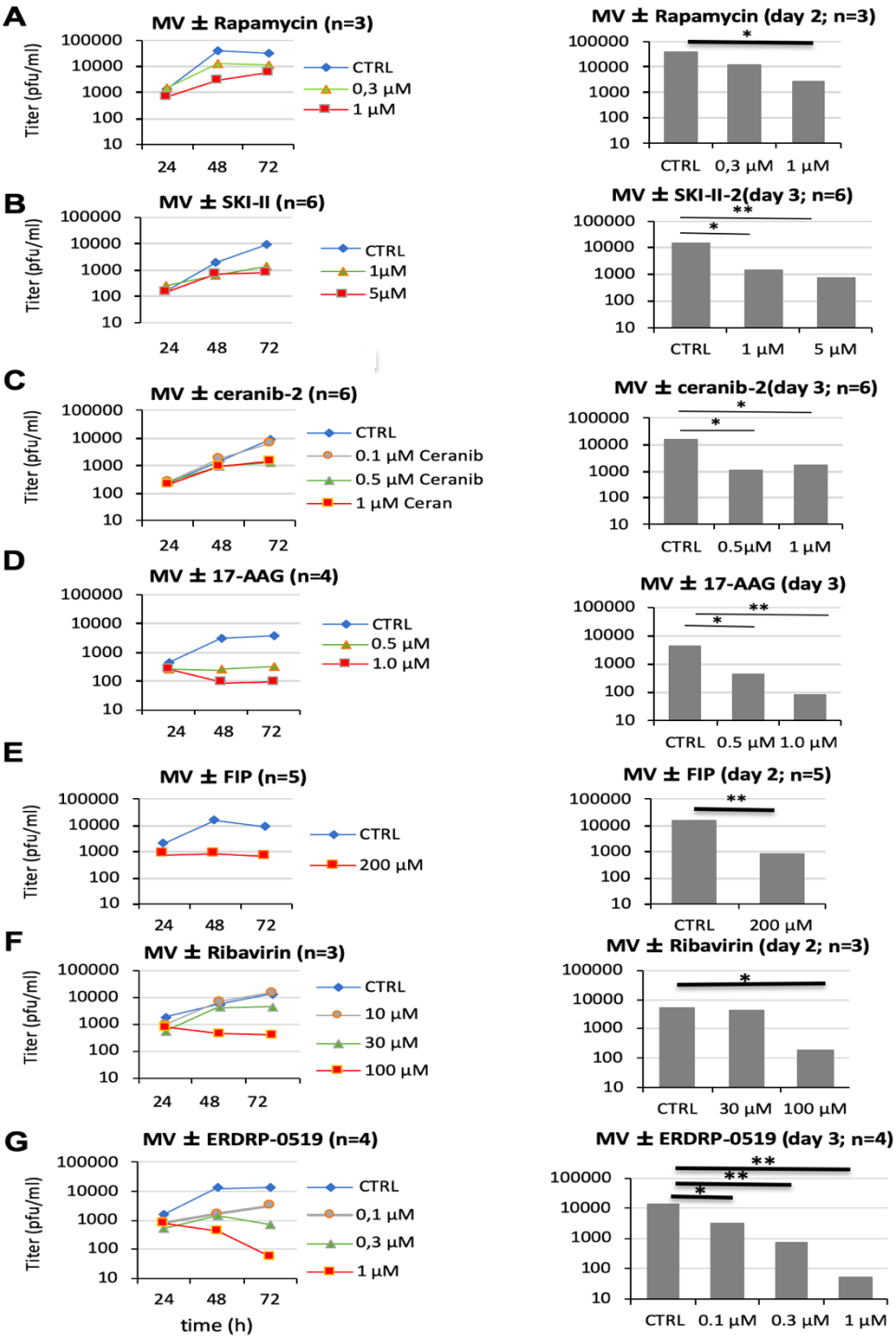

Fig. 4.6: Antiviral effect of various inhibitors on acute MV infection in PBL

Primary human PBL were stimulated with PHA (2.5µg/ml) for 24h and pretreated with DMSO (control) or increasing concentrations of inhibitors as indicated (A to G) 1h prior to infection with MV (MOI=0.1) for 2h. cells were then washed to remove the unbound virus and resuspended in PHA-media along with the inhibitor concentrations and the plate incubated with cell and media collections from 1,2 and 3 dpi stored at -80°C. Newly synthesized infectious virus (cell bound plus supernatant) from the freeze-thawed samples was titrated on Vero-hSLAM cells. Significant differences in comparison with the control were indicated with *$p \leq 0.05$ with statistical evaluation

calculated by student's *t*-test (n=3). Viability of the inhibitor concentrations was previously checked using Propidium iodide uptake assay. Data A-G collectively contributed by Hannah Franke and Nora Laender.

4.7 Ceranib-2 and SKI-II Reduce Viral Infection in 'Residual Monocytic' Population

Isolation of PBL from blood samples obtained in LRC chambers was performed by density gradient centrifugation followed by plastic adherence step to get rid of other monocytes like macrophages and trace amounts of dendritic cells (DC). However, this method may retain a residual portion of the adherent monocytes. For all the PBL based western blot experiments for infection and inhibitor treatment, gating of the PBL population was performed based on flow cytometry based FSC (forward) and SSC (side scatter) using linear scale for both (Fig 4.15 B) . This linear scale gating is commonly used to identify the various cell populations within the blood sample based on their physical parameters (Fig 4.7 A) (Barnette, n.d. Biorad).

During the initial experimental set up, due to an unaccounted procedural difference in set up, the data for gating got recorded using FSC (linear scale) versus SSC (LOG scale). During analysis of these plots, two distinct cell populations were observed (Fig 4.7.B) which we tentatively defined as 'residual adherent monocytes' based on the dot plot pattern in Fig 4.7 A and found that this constituted about 10% of the gates cell group (Fig 4.7 C). Upon further analysis of infected (GFP positive) cells in this group, we found a high percentage of infected cells (71.8%) which showed significant reduction especially with Ceranib-2 treatment. These results indicated that the inhibitors were also effective in MV infection inhibition in these cell population.

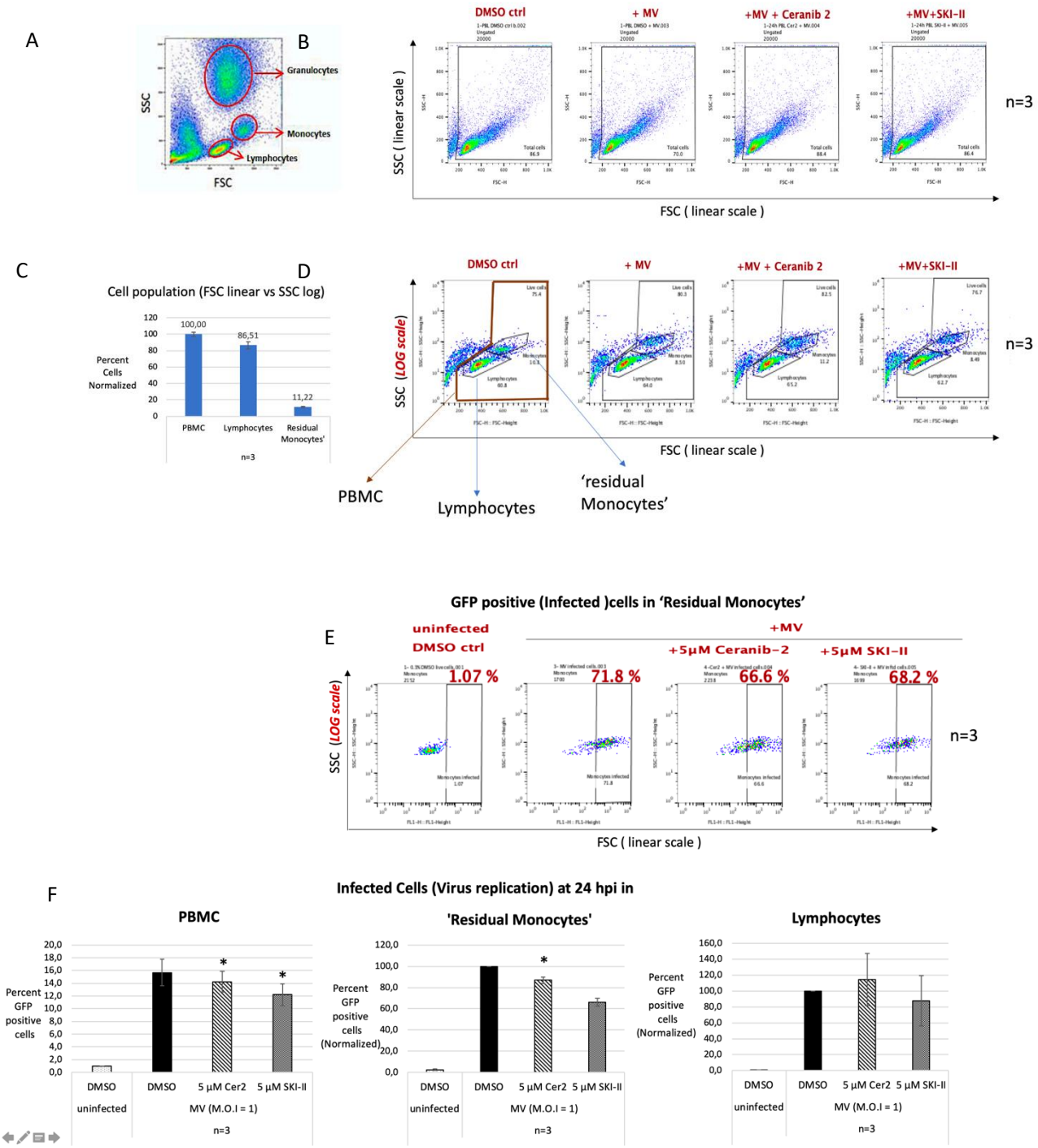

Fig. 4.7: Ceranib-2 and SKI-II reduce viral infection in 'residual monocytic' population

(A) Dot plot representation of different cell populations from PBMC when assessed by flow cytometry using linear scale for both forward (FSC) and sideward scatter (SSC). (B) Representative FSC versus SSC dot plot and gating strategy used PBL uninfected and infected along with inhibitor treatment for western blot analysis. (C) Percentage of the two gated populations with the total events gated – the 'residual monocytes' account for around 10%.(D) Representative of FSC (linear scale) versus SSC (LOG scale) dot plot and gating strategy used earlier in PBL uninfected and infected along with inhibitor treatment during initial set up of experiments. (E) Percentage of GFP positive (infected cells) from the gated 'residual monocyte' population indicating a high percentage of

infected cells which is reduced with the inhibitor treatments. F) Graphical representation of GFP positive infected cells in different gated populations – PBMC, 'residual monocytes' and 'Lymphocytes'. Significant differences in comparison with the control were indicated with $*p \leq 0.05$ calculated by student's *t*-test (n=3).

4.8 Identification of Putative TOP Sequences Upstream of Viral Genes

Based on experiments in stimulated PBL infected with wild type MV we observed an increased upregulation of phosphorylated and total forms of ribosomal protein (rpS6) and also to an extent EIF4E expression in comparison to uninfected control at the respective time points. The EIF4E is a part of the large protein complex EIF4F (eukaryotic translation initiation factor 4F). However, it is the main component that binds to the 5' mRNA cap structure thus mediating and initiating cap dependent protein translation (Gingras et al., 1999). The MV associated RNA transcripts have a methylated cap as well as a poly (A) tail which has been previously reported (Yoshikawa et al., 1986). Simultaneously, Rapamycin mediated mTOR inhibition has been reported to dampen translation of mRNAs containing a TOP sequences via mTOR downstream p70 S6K -rpS6 axis (Jefferies et al., 1997).

Thus, my aim was to check for putative TOP sequences mainly upstream of each viral gene from available published genome sequences from the NCBI databank. 5'TOP RNA are vertebrate mRNA transcripts which contain a 5' terminal oligopyrimidine tract (TOP) sequence. This sequence begins with Cytidine followed by a stretch of further 5 to 15 pyrimidine nucleotides – this sequence acts as a translation regulator and is often found in mRNAs coding for peptide elongation factors and ribosomal proteins.

Hence, a basic search analysis to search for putative TOP sequences upstream of each viral gene using SnapGene software. Seven random whole genome sequences were selected so as to represent vaccine, wild type and recombinant strains. The sample size also represents multiple genotypes from samples across global locations and along various time points and upgraded methods of sequencing (Phan et al., 2018)

It was observed that the upstream of surface viral protein F had the most number (around 24) of putative TOP like sequences followed by upstream of gene for viral surface H which was 4 for all the strains. The mostly abundantly produced protein N had no TOP like sequences in all the natural strains except for the recombinant IC323eGFP which could be attributed to probable addition of intergenic sequence of following gene (gene P) during cloning and rescue of the virus. Similarly, the least abundantly produced viral L protein also

did not have any TOP like sequences upstream it's gene. One to two TOP like sequences were also observed upstream of the P ORF and the M ORF respectively.

The distance between the pairs of TOP like sequences particularly upstream of P, F and H genes were found to follow the 'Rule of Six' – i.e. the nucleotide distance being a multiple of 6.

		Genotype	A	B3	D3	D4	D8	D8	D8			
		Strain	vaccine strain	wild type	wild type	wild type	wild type	wild type	wild type			
		Location	Croatia	Sudan	Japan	USA	Netherland	India	Israel			
		Name / Accession No.	Edmonston Zagreb AY486083	MG912590.1	IC323eGFP LC420351.1	KY656518.1	MG912592.1	MH356240.1	MZ712065.1			
function	**type**	**Number of 5'TOP sequences upstream of gene**								Mean	StDEV	SEM
enhanced green Fluroscent protein	recombinant (inserted)	eGFP upstream	not valid	not valid	0	not valid	not valid	not valid	not valid	0.00	0.00	0.00
Nucleoprotein	viral	N upstream	0	0	2	0	0	0	0	0.40	0.89	0.37
Phosphoprotein	viral	P/V/C upstream	2	2	2	1	2	2	2	1.75	0.45	0.18
viral accessory proteins	viral											0.00
	viral											0.00
Matrix	viral	M upstream	1	1	1	1	1	1	1	1.00	0.00	0.00
Fusion	viral	F upstream	24	25	22	25	24	25	24	24.00	1.22	0.50
Hemagglutinin	viral	H upstream	4	4	4	4	4	4	4	4.00	0.00	0.00
Large	viral	L upstream	0	0	0	0	0	0	0	0.00	0.00	0.00
			master seed lot	endemic circulating in Sudan in 1997	recombinant virus with EGFP insert	CDC generated	from large measles outbreak in in 2013	throat swab from 4 month old male child	during outbreak collected from urine sample, sequence directly from sample			

Fig. 4.8 / Table 4.1: . Identification of putative TOP sequences upstream of viral genes

4.9. Neural NT2 cells are susceptible to wild -type MV infection

In the second part of my thesis I investigated if the above mentioned inhibitors have the same capacity to inhibit the MV infection in persistently infected neural or differentiated neuronal cells. We used the two cell lines NT2 and LUHMES, which can be differentiated in culture to post-mitotic (non-proliferating) neuronal cells

In order to evaluate the susceptibility and permissiveness of NT2 cells to MV infection by observing expression of GFP and syncytia formation, cells were incubated with three different MV strains at various MOI and observed upto day 3 post infection. Highly susceptible Vero-hSLAM cells were used as positive control. The three strains used were:

a) IC323eGFP → wild type MV strain

b) Edmonston-GFP → lab adapted MV strain (de Vries et al., 2010)

c) Edmonston-GFP-CAM/RB → Rat brain adapted (neurovirulent) MV strain (Duprex et al., 1999)

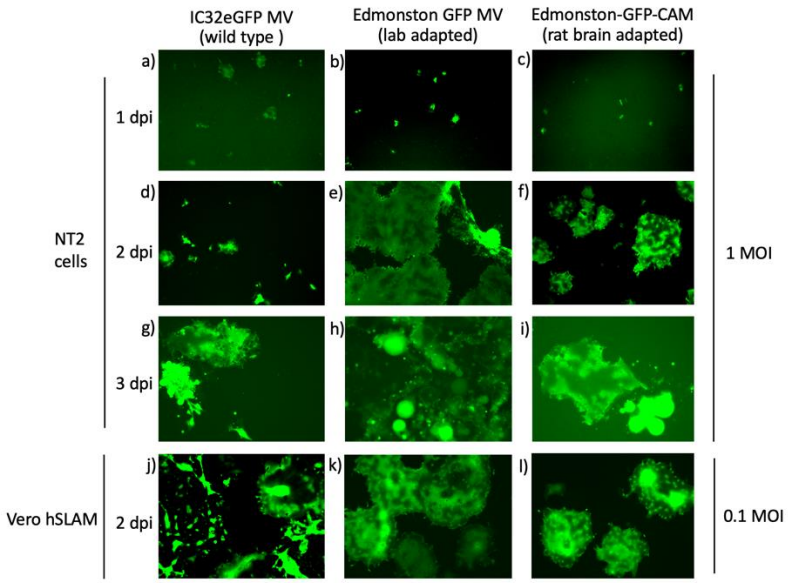

Fig. 4.9.a. : Susceptibility of NT2 cells to various MV strains

$4*10^4$ NT2 cells and $1*10^4$ Vero hSLAM cells were seeded per well so as to obtain confluent cell layer at 24 h. On the next day, spent media was discarded and cells infected with virus strains IC323eGFP, Edmonston-eGFP and Edmonston-eGFP-CAMH as indicated (magnification 100x).

The neuronal NT2 cells were found to be susceptible to all the three virus strains as GFP positive infected cells were observed at 1 dpi including with the wild type strain which predominantly uses CD150 as its entry receptor. However, the spread of wild type infection (as observed by syncytia formation) in the neuronal NT2 cells (d) was highly restricted in comparison to its spread in highly susceptible and permissive Vero-hSLAM (j). This indicates that the NT2 cells are susceptible (have a receptor) for wild-type MV, but are not as permissive as the Vero-hSLAM cells. The pattern of few single GFP-positive cells observed at 1 dpi with all three strains suggested that a probable common receptor is used for entry into the neural cells. Since the aim of this experiment was to check for susceptibility of the NT2 cells to wild-type MV strain, the results clearly indicated that further experiments can be carried out using wild-type MV-IC323eGFP.

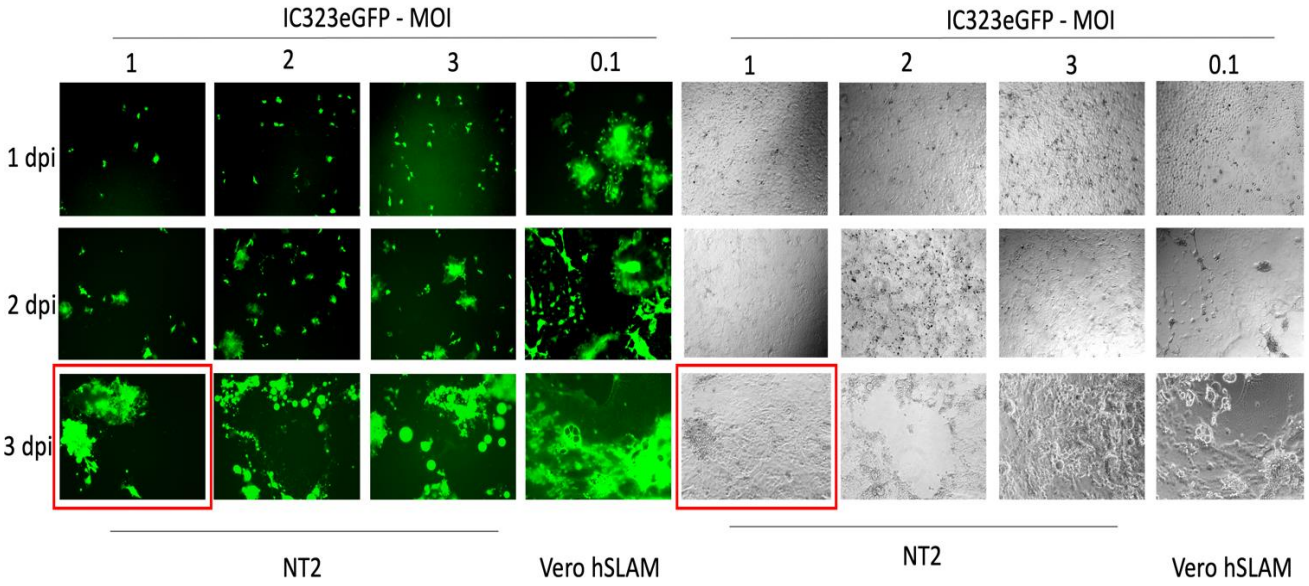

Fig.4.9.b: Increased viral load contributes to cytopathic effect in NT2 cells

The seeded NT2 cells and Vero-hSLAM cells were infected with wildtype MV-IC323eGFP with MOI of 1, 2 and 3 while the Vero-hSLAM cells were infected with 0.1 MOI of wild-type MV. Images of the GFP positive infected cells were taken at 1, 2- and 3-days post infection (magnification 100x)

First, I checked if increasing of the MOI of the wild type MV leads to more infected NT2 cells. The increased MOI did have corresponding effect on viral uptake especially at 1 dpi since observed number of individual GFP positive infected cells increased with higher MOI. However, at 3dpi higher viral load did have a cytopathic effect on NT2 cells since cell fusion and rounded clumps were observed with MOI of 2 and 3 which was comparable to the respective day infection in Vero-hSLAM cells. With lower viral load (MOI=1 image highlighted in red boxes), very less syncytia were observed with the cell layer being still confluent as compared to rounding and cell detachment with 0.1 MOI at 3 dpi in the Vero-hSLAM cells.

4.10 NT2 Cells Lack the Predominant Wild-type MV Receptor CD150

Based on the above experiments, we observed that the wild type, lab adapted and the rat brain adapted neurovirulent CAMH-MV strains were capable of infecting and replicating in the NT2 cells indicating presence of functional MV receptor/s on NT2 cells. Thus, we checked for surface expression of known MV receptors used by wild-type and lab-adapted strains. According to available literature, the presence of these receptors is cell-type specific and summarized in the Introduction (Table 1.8):

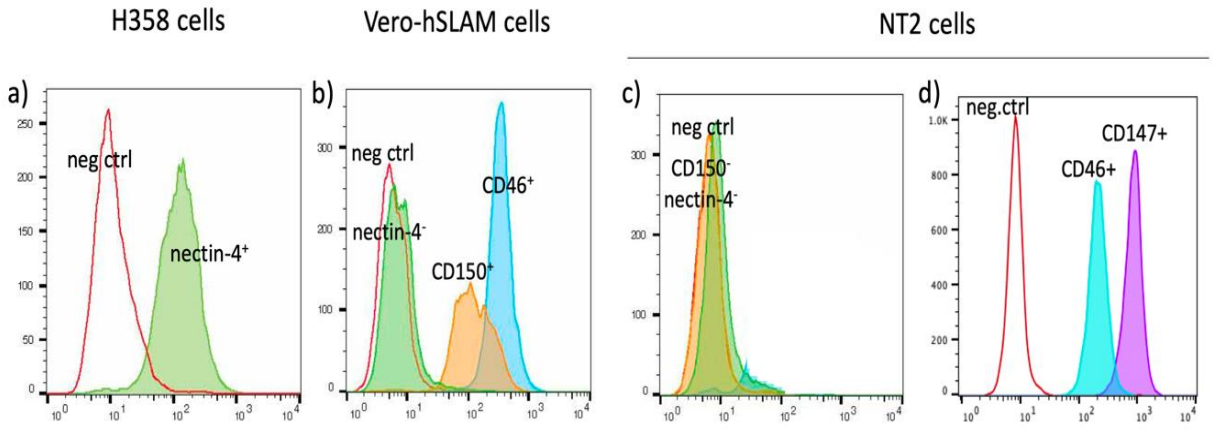

Fig. 4.10: NT2 does not express the predominant wild type MV receptors CD150 and Nectin-4 Representative histograms from surface staining for MV receptors (On X-axis is the cell count and Y-axis is the channel used for fluorochrome excitation of the labelled antibodies as indicated) Data a,b contributed by Hannah Franke

The surface of NT2 cells did not express CD150, the wild-type MV receptor (Fig. 4.10 C). This was expected since CD150 expression is restricted to lymphoid and hematopoietic cells. It also did not express Nectin-4 a cell adhesion surface molecule which is also considered as a tumor associated marker and present on adenocarcinomas of lung, breast and colon. Surface staining procedure for Nectin-4 was validated using control H358 cells (a non-small cell lung cancer line) which were positive for surface Nectin-4 expression. The NT2 cells, however, expressed CD46 (mainly used by lab-adapted and vaccine MV strains) and CD147. The usage of CD147 by the wild-type MV is questionable since CD147 was found to be highly expressed. Such a highly expressed receptor should thus enable increased viral cell entry which was not observed in the infection experiments. These data indicate that the mode of entry of wild-type virus in NT2 cells is via an unknown receptor or unknown mechanism.

4.11. Generation of NT2 Cells Persistently Infected with Wild-type MV

Our group had previously established a NT2 cell line model persistently infected with recombinant MV-CAMH-HcRed, a MV strain which expresses neurovirulent rodent brain adapted H and a HcRed reporter protein, to study viral clearance by short hairpin RNA (Zinke et al., 2009). For further analysis with inhibitors, we wanted to establish a NT2 cell line persistently infected with MV-IC323eGFP so as to obtain a model of neural cells persistently infected with wild-type MV. This will allow a highly sensitive quantification

and microscopic visualization of the viral infection by measurement of GFP. In addition, it is non-overlapping with filter channels of other fluorochrome labelled antibodies used in microscopy and for flow cytometry channels.

After initial few unsuccessful attempts and optimization with respect to cell confluency and virus MOI, a NT2 cell line persistently infected with MV-IC323eGFP was established and maintained. (Figure 4.11 A) shows images taken at day 1, 7 and 11 post infection. During this period, the media was changed every 2-3 days to renew nutrient supply and to also discard detached and infected cells. Unlike typical syncytia mediated spread of infection in Vero-hSLAM cells, spread of infection via long processes was mainly observed in NT2 cells (Fig. 4.11 b). During passaging, cell to cell contact was important so as to maintain more than 80% GFP positive infected cells.

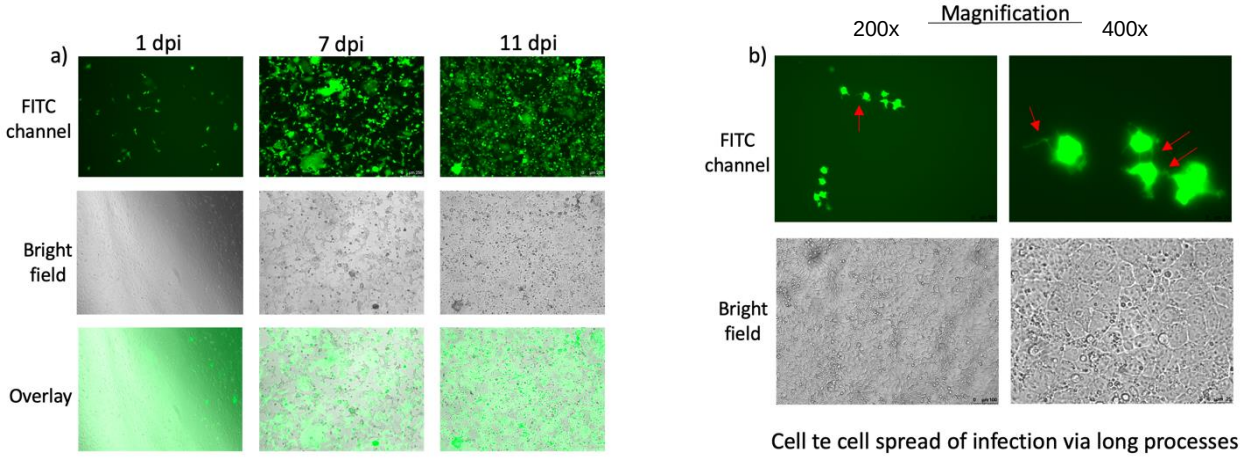

Fig. 4.11: Establishment of persistent infection in NT2 cells

(a) NT2 cells were trypsinized, counted and $2*10^5$ cells were incubated with 0.8 MOI of MV-IC323eGFP in an Eppendorf tube at 37°C for 1h. The cells were then seed into wells of 6 well plate and media in each well reconstituted upto 3 ml. The plate was then incubated at 37°C in CO_2 incubator and checked for infection under microscope each day. Overlay images show that the viral GFP infection was across the complete cell layer. (magnification 100x) Panel (b) Spread of infection via long processes in infected cells (red arrows). (magnifications 200x and 400x scale bars= 100 µM)

4.12. Characterization of Persistently Infected NT2 Cells (pi-NT2)

4.12.A Persistently Infected NT2 Cells Express Viral Encoded Proteins

MV-IC32eGFP is a recombinant virus with eGFP encoded upstream of all other viral genes. As MV follows a transcription gradient during viral replication and thus with GFP

transcripts being transcribed the most, the protein expression is very high (Schematic figure 4a). Furthermore, GFP is a soluble protein evenly gets distributed in cell cytoplasm and thus can also be used to track fine neuron-like cell processes and extensions e.g. spines in *ex vivo* neurotropic infections (Malinow et al., 2010). To characterize the persistent infection of the NT2 cells I checked for presence of other viral proteins and also determined infectious virus titers from these cells.

We observed that the pi-NT2 cells also expressed other viral proteins. More than 75% of piNT2 cells were found to be GFP positive as per the flow cytometric quantification. A previous study (Duprex et al., 1999 b) using astrocytoma cells (tumorous glial cells) as a CNS model for MV-GFP infection reported that GFP expression was a sensitive method to detect viral infection. GFP was detected in early stages of virus infection and was also useful to trace spread of infection.

A)

B)

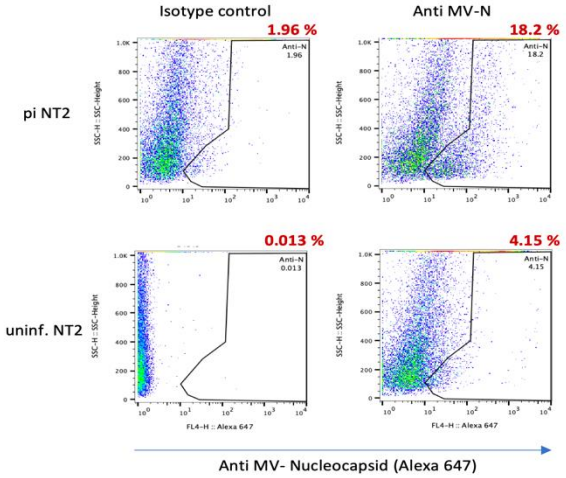

C)

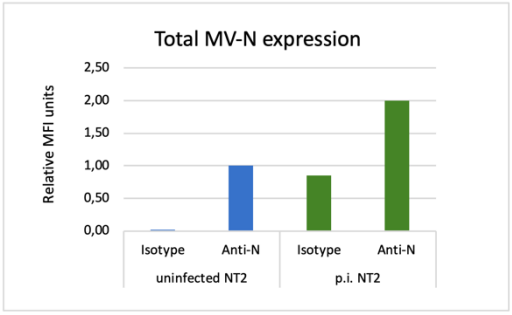

D)

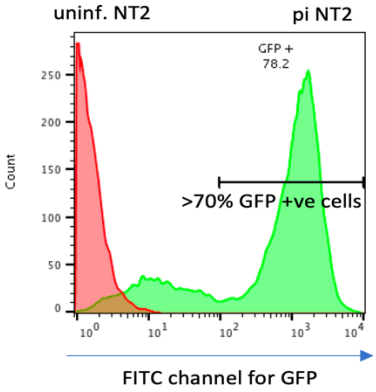

E)

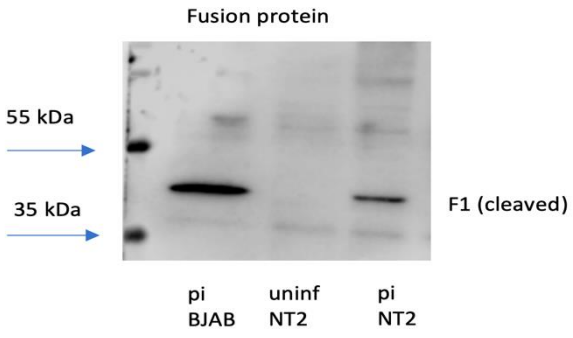

F)

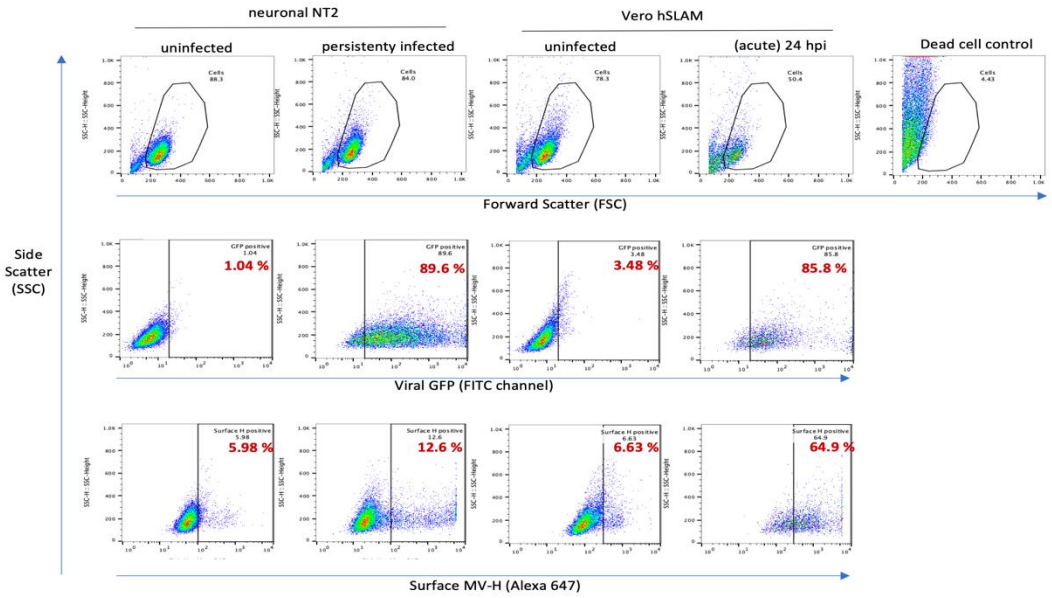

Figure 4.12.A: Persistently infected NT2 cells express viral proteins

(A) Schematic picture of genome organization of recombinant wild-type MV- IC323eGFP wild type MV – in sequence of genes transcribed and translated. (B) Dot plot representative of total staining for MV nucleocapsid (N) protein analyzed by flow cytometry – $6*10^4$ pi NT2 cells and $5*10^4$ NT2 cells were seeded in 48 well plates for confluent cell layer. The next day cells were trypsinized, washed and fixed for antibodies (primary Ab: F227 anti -N mouse mAb, Isotype anti-mouse IgG and secondary Ab: Alexa 647 goat anti mouse IgG). (C) Graphical representation of MFI expression of total MV nucleocapsid in pi-NT2 cells. (D) Histogram plot of percent infected cells by reporter GFP positive cells. (E) Expression of viral Fusion protein (cleaved F1 form) as detected by Western blot using WTF F rabbit serum SA5343 and HRP labelled secondary antibody, Uninfected NT2 and pi-BJAB cell lysates were used as negative and positive controls, respectively. (F) Dot plot graphs for comparison between pi NT2 and acutely infected Vero-hSLAM cells for cell morphology (first row – FSC versus SSC), infection via viral GFP positive cells (middle row – FITC-GFP versus SSC) and cell surface expression for viral H protein (last row – FL4-Alexa 647 versus SSC).

With FACS analysis by total staining for downstream viral N protein we observed that 18.2% of pi-NT2 cells expressed the viral nucleocapsid (Fig. 4.12.A c) and had higher MFI values as compared to uninfected and isotype controls. Besides, detection of 40 kDa band by western blot showed that the pi-NT2 expressed the cleaved F1 form of fusion protein indicating the functional use of this protein probably for spread of infection (Fig 4.12.A e). Surface expression of the other surface viral glycoprotein H in the pi-NT2 cells was also determined by flow cytometry and was also compared with Vero-hSLAM acutely infected with 0.3 MOI of virus. Integrity of cell morphology between the pi-NT2 and acutely infected Vero-hSLAM cells versus uninfected or dead cells was observed with the FSC

versus SSC plots (Fig 4.12.A f top row) – the pi-NT2 cells had a morphology similar to healthy uninfected NT2 and Vero-hSLAM cells. Due virus lytic cycle induced cytopathic effects like fusion and syncytia in the highly permissible Vero-hSLAM cells, the fusion of cells could be viewed as an undefined cell cluster on the dot plot. However, in terms of viral infection, similar percentages of GFP positive cells (89.6% and 85.8 % respectively) were observed in both pi NT2 and acutely infected cells indicating active viral infection (Fig 4.12.A middle row). Interestingly, inspite of similar percentages GFP positive cells, a low percentage i.e. 12.6% of pi-NT2 cells expressed surface H as compared to 64.9% of infected Vero-hSLAM cells.

4.12.B Persistently Infected NT2 Cells Release Low Infectious Virus Titers

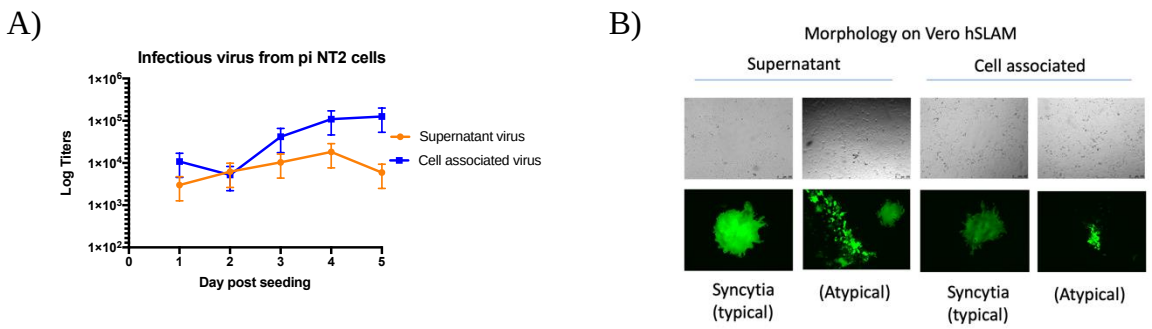

Fig. 4.12.B.: Persistently infected NT2 cells release low infectious virus titers

(A) Estimation of infectious virus from piNT2 released in supernatant or cell-associated by serial diluted titration on Vero-hSLAM cells. $4*10^4$ piNT2 and NT2 cells per 500 µl media were seeded per well in 48 well plate and incubated at 37°C / CO_2 incubator. Supernatant media containing virus were collected in vials and stored at -80°C. The cells were then detached by trysinization, resuspended in FCS + media and subjected to one freeze thaw cycle to (at -80°C for 15 mins followed by 37°C for 2 mins) releases the cell associated virus and samples stored at -80°C until titration n=3. (B) Micrographs showing the morphology of Vero-hSLAM cells infected with piNT2-derived virus. (magnification 100x scale bar= 100 µM)

Accumulation of viral F and H at the cell surface is important for budding of progeny infectious virus particles. The pi NT2 were also checked for release of infectious progeny virus into the supernatant. Assuming slow replication of virus in these cells, we collected supernatant and cell associated virus up to 5 days after seeding. We observed low titers of infectious virus released in supernatant as compared to increasing cell associated virus titers in the day 3, 4 and 5 samples. It should be noted that normalization of virus titers with the cell count for the respective day was not included in the above data. Thus, the increased cell

associated virus titers could also be attributed to the increased cell number along the days due to normal cell division. However, with this trend of increasing cell associated virus , we observed rather the contrary with released virus in the supernatant with almost a log difference between the supernatant and cell associated titers at day 5 indicating that the pi NT2 release only low infectious virus (Fig 4.12.B). Apart from few syncytia CPE on Vero-hSLAM cells, infectious virus from both samples shows an atypical cell-to-cell spread type infection pattern on Vero-hSLAM cells.

4.13. Effect of Antiviral Compounds on Viral Inhibition in Persistently Infected NT2

The panel of inhibitors were now tested 1 to 7 days (D1 to D7) for their antiviral effect in pi-NT2 cells. In addition to the panel of inhibitors mentioned in Table : . We also tested antiviral effect of Favipiravir, a clinically available broad spectrum antiviral, as well as IFN-α , IFN-γ and inosine pranobex. Of these inhibitors, Ribavirin, IFN-α and inosine pranobex are used with limited effectivity in clinical treatment of SSPE.

We observed that both 1 µM and 3 µM ERDRP-0519 led to a complete disappearance of viral GFP. 100 µM Ribavirin reduced the percentage of GFP positive cells by approximately 15 %. With doses of 30 µM and 100 µM of Favipiravir, we also observed a significant reduction between 50 and 60% respectively in viral GFP expression, whereas a high dose of 200 µM Favipiravir affected cell proliferation as observed by microscopy on day 7 (data not shown) indicating that high doses of Favipiravir has an off target effect on cellular polymerases. We also observed reduction in GFP infected cells and expression with 200 µM FIP treatment indicating that the viral fusion protein was actively involved in spread of infection even in the persistently infected cells (Table 4.13).

Among the panel of inhibitors that targeted cellular proteins, we observed a reduced GFP expression with 1 µM Rapamycin treatment but observation of these cells under the microscope revealed that this reduction was due to reduced cell number, which suggests reduced cell proliferation due to mTOR inhibition. Interestingly we observed a reduction in GFP MFI expression also with 5 µM SKI-II treatment which suggests an active involvement of sphingosine kinase in viral GFP production. However, we did not observe effects of IFN-α, IFN-γ and inosine pranobex on reduction of viral GFP. For inosine pranobex, this was not expected, because it has an immunomodulatory or immunostimulatory effect in clinical treatment of SSPE indicating that its predominant mode of action against the virus is

indirectly by mediating cell mediated immune response for e.g. T cells which are absent in this persistently infected NT2 cell model (Table 4.2).

Since we observed an effective reduction of viral GFP by both ERDRP-0519 concentrations, we treated further with these doses so as to reveal the time frame required for complete viral clearance in these persistently infected cells. Similar to previous experiment, the cells were treated up to a week, with presence and removal of inhibitor at D7 and incubated up to D10. We observed that with 1 µM, but also with 3 µM dose, although there was negligible GFP positive cells at D10, upon removal of the inhibitor the number of GFP positive cells increased again due to spread of infection (figure 4 panel A – red highlighted box) indicating incomplete viral clearance. We further treated the cells with the inhibitor doses up to two weeks with intermittent removal of inhibitors at D17 (observed on D22) and D22 (observed on D25). In the case of 1 µM ERDRP-0519 we still observed spread of viral GFP to neighboring cell at D22 even if a single cell was positive. Given the fact that viral GFP indicates active viral protein translation and not simply uptake of soluble GFP by neighboring uninfected cells, this can probably be explained by two factors : 1) dilution of GFP would occur due to soluble uptake by a cell or cell division of the infected cells would decrease the fluorescence intensity as observed or by FACS while comparing with untreated control samples and 2) By observing D22 (-) image, the cluster pattern indicates cell to cell spread of infection and GFP intensity indicates active GFP production. To summarize the above, we conclude that so as to obtain a complete virus clearance in pi-NT2 cells, a treatment with 3 µM dose is required for a minimum of 2 week duration.

		At Day 7 post treatment	
		Viral GFP reduction	
		% GFP positive cells (FACS)	GFP expression (MFI) FACS
ERDRP-0519	1 µM	***	***
	3 µM	***	***
Favipiravir	30 µM	-	*
	100 µM	-	*
	200 µM	-	#
Ribavirin	100 µM	*	-
	200 µM	-	-
FIP	200 µM	*	*
Rapamycin	1 µM	-	* #
IFN-γ	100 U	-	-
ERDRP-0519 + IFN-γ	1µM + 100 U	***	***
Interferon α	100 U	-	-
Inosine Pranobex	0.5, 5, 50 µg/ml	-	-
SKI-II	3 µM	*	*

* = significant reduction ; # = reduced cell proliferation ; - = no significance

Table 4.13: Overview of effect of antiviral compounds on viral GFP expression in p.i.NT2 cells $6*10^4$ p.i.NT2 cells/ 500 µl media per well were seeded into 48 well plates with the day of seeding considered as D0. The next day D1, spent media from the confluent wells was discarded and replaced with medium containing respective inhibitor concentrations. Viral GFP quantification was done by FACS analysis along with propidium iodide staining on D0, D3 and D7. On D3 (or every 3 days for longer duration), Cells in wells were split 1:3 or 1:4 and seeded with fresh medium and inhibitor to maintain confluency upto D7 and further. GFP quantification was normalized with DMSO or sterile used as untreated controls and uninfected NT2 was used as GFP negative control for gating. The results are n=1 with technical replicates for all inhibitors except for ERDRP-0519 samples n=3. (Data also contributed by Nora Länder)

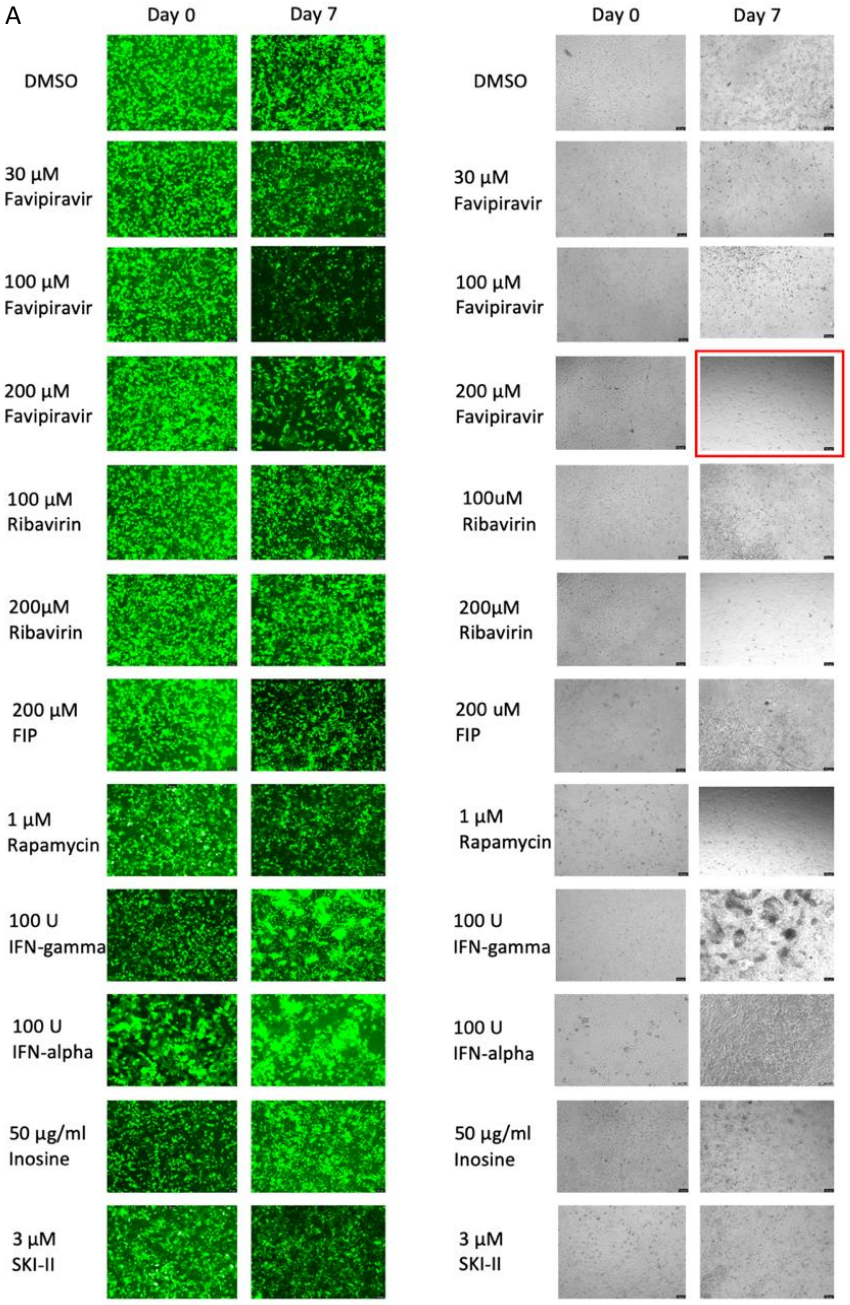
A
Day 0
Day 7
DMSO
30 µM Favipiravir
100 µM Favipiravir
200 µM Favipiravir
100 µM Ribavirin
200µM Ribavirin
200 µM FIP
1 µM Rapamycin
100 U IFN-gamma
100 U IFN-alpha
50 µg/ml Inosine
3 µM SKI-II
Day 0
Day 7
DMSO
30 µM Favipiravir
100 µM Favipiravir
200 µM Favipiravir
100uM Ribavirin
200µM Ribavirin
200 uM FIP
1 µM Rapamycin
100 U IFN-gamma
100 U IFN-alpha
50 µg/ml Inosine
3 µM SKI-II

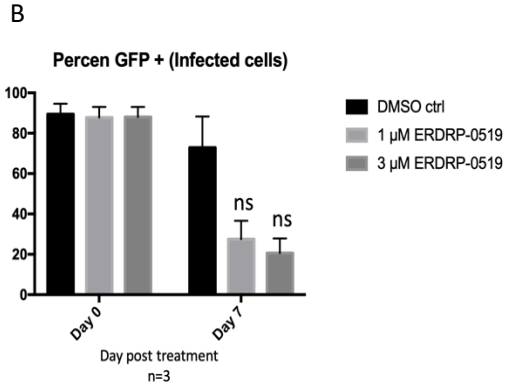
B
Percen GFP + (Infected cells)
100
80
60
40
20
0
ns
ns
Day 0
Day 7
Day post treatment
n=3
DMSO ctrl
1 µM ERDRP-0519
3 µM ERDRP-0519

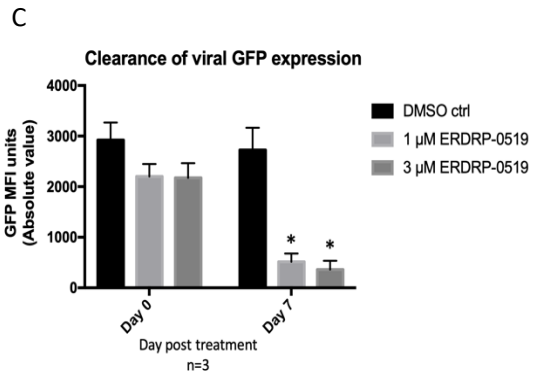
C
Clearance of viral GFP expression
GFP MFI units (Absolute value)
4000
3000
2000
1000
0
*
*
Day 0
Day 7
Day post treatment
n=3
DMSO ctrl
1 µM ERDRP-0519
3 µM ERDRP-0519

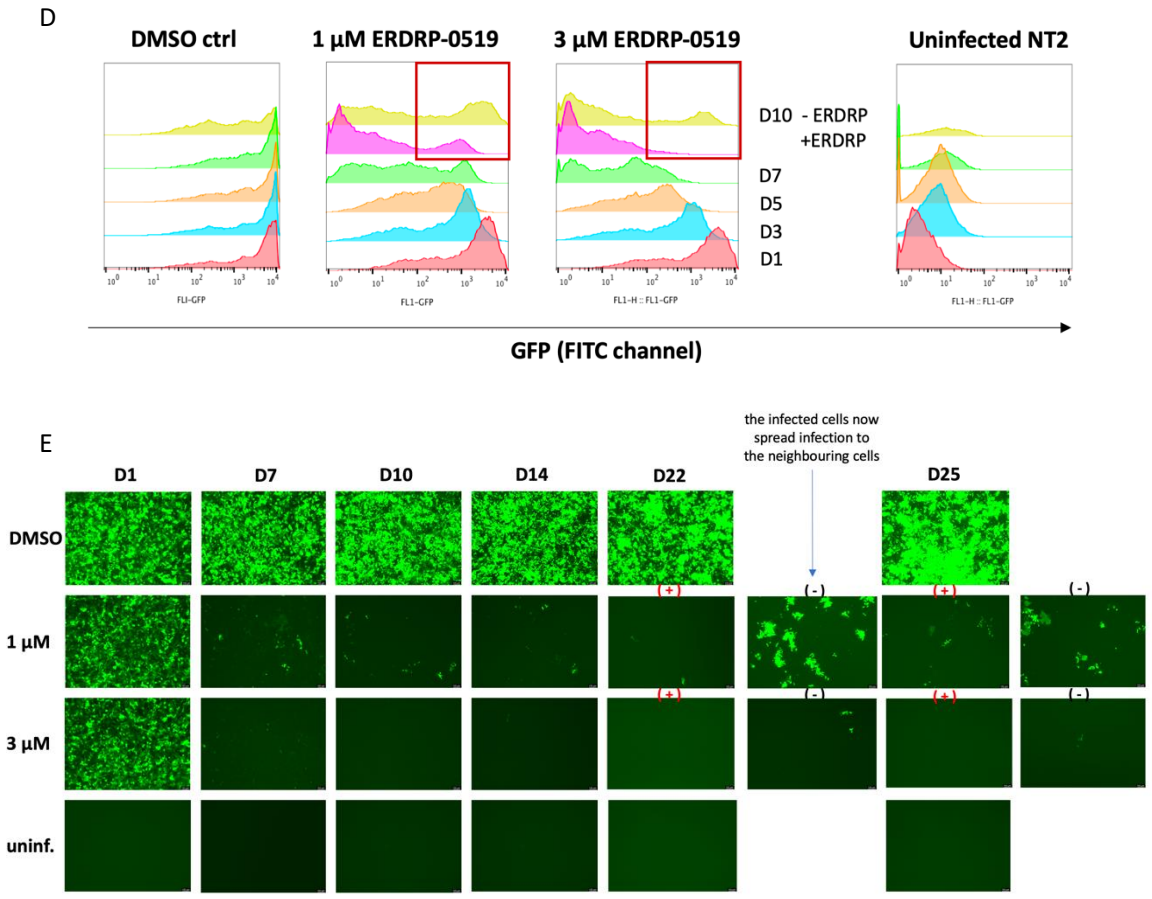

Fig. 4.13: Time dependent viral clearance by ERDRP-0519 in pi-NT2 cells

Experimental setup was previously described as mentioned under Table 4.12 with microscopy imaging and flow cytometric analysis on mentioned days. (A) shows micrographs taken of seeded pi-NT2 cells on day 0 (D0) and day 7 (D7) of various inhibitor treatment. The images were taken for blank field (right column) as well as FITC exposed to observe GFP positive cells. (magnifications 100x). (B) shows graphs of effect of 1 µM and 3µM ERDRP-0519 treatment for 7 days on reduction of GFP positive (infected cells) and in (C), the GFP MFI (viral protein expression) in the pi-NT2 cells (n=3). Significant differences in comparison with the control were indicated with $*p \leq 0.05$ calculated by student's *t*-test (n=3). (D) shows the histogram overlay of the samples from D1 to D10 plotted with FITC channel. Highlighted in red box is the difference increase in GFP positive cells observed on D10 after with and without ERDRP-0519 inhibitor removal at D7. (E) shows micrographs of the cells further treated with ERDRP-0519 up to D25. The (+) and (-) sign denotes presence or removal of inhibitor. The results are n=1 with technical replicates. (magnifications 100x, size bar = 100 µM)

Neuronal Infection

4.14 Infection Inhibition in Differentiated NT2-N Cells

The stem cell-like NT2 teratocarcinoma cells can be differentiated into post-mitotic neurons upon treatment with retinoic acid and other mitotic inhibitors. Since, the gene expression pattern of differentiated NT-2 cells (NT2-N) was reported to be similar to that of neuronal precursors during neurogenesis, we decided to use differentiated NT2-N as an *in vitro* model for SSPE to test the antiviral effects.

For a preliminary study, we analyzed for antiviral effect of MV L polymerase specific ERDRP-0519 on acute infection in the differentiated NT2-N cells. The differentiation procedure takes 3 to 4 weeks. After the differentiation procedure, the seeded NT2-N cells were infected by incubating for 2h with wild-type MV-IC323eGFP MV followed by washing to remove the unbound virus and further treated with 1 µM and 3 µM ERDRP-0519 up to 3 days post infection. Microscopic images for infected GFP positive cells indicated that 1) differentiation protocol treated NT2-N cells were susceptible to MV infection and 2) Both concentrations of the inhibitor were able efficiently inhibit MV infection in these cells up to 3 dpi (Fig. 4.14).

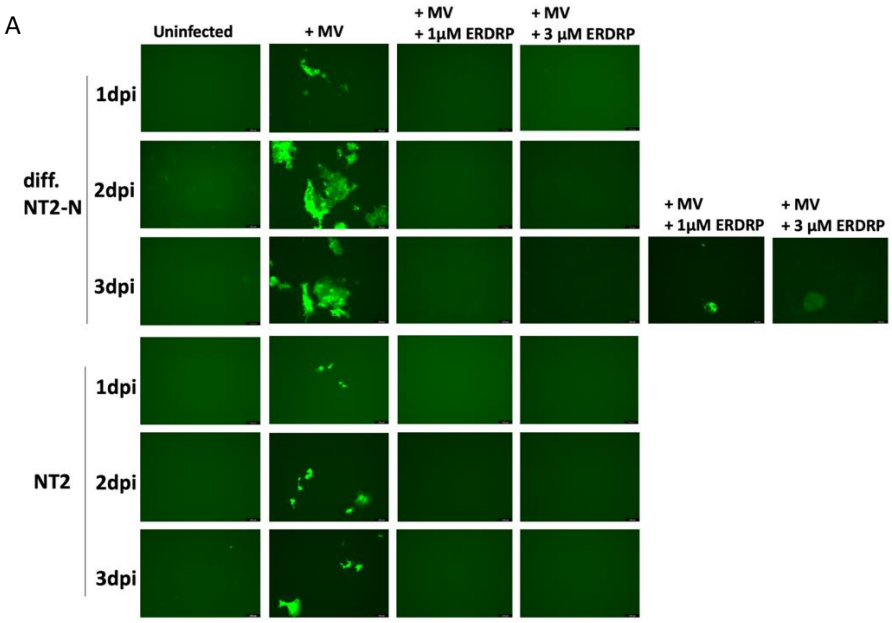

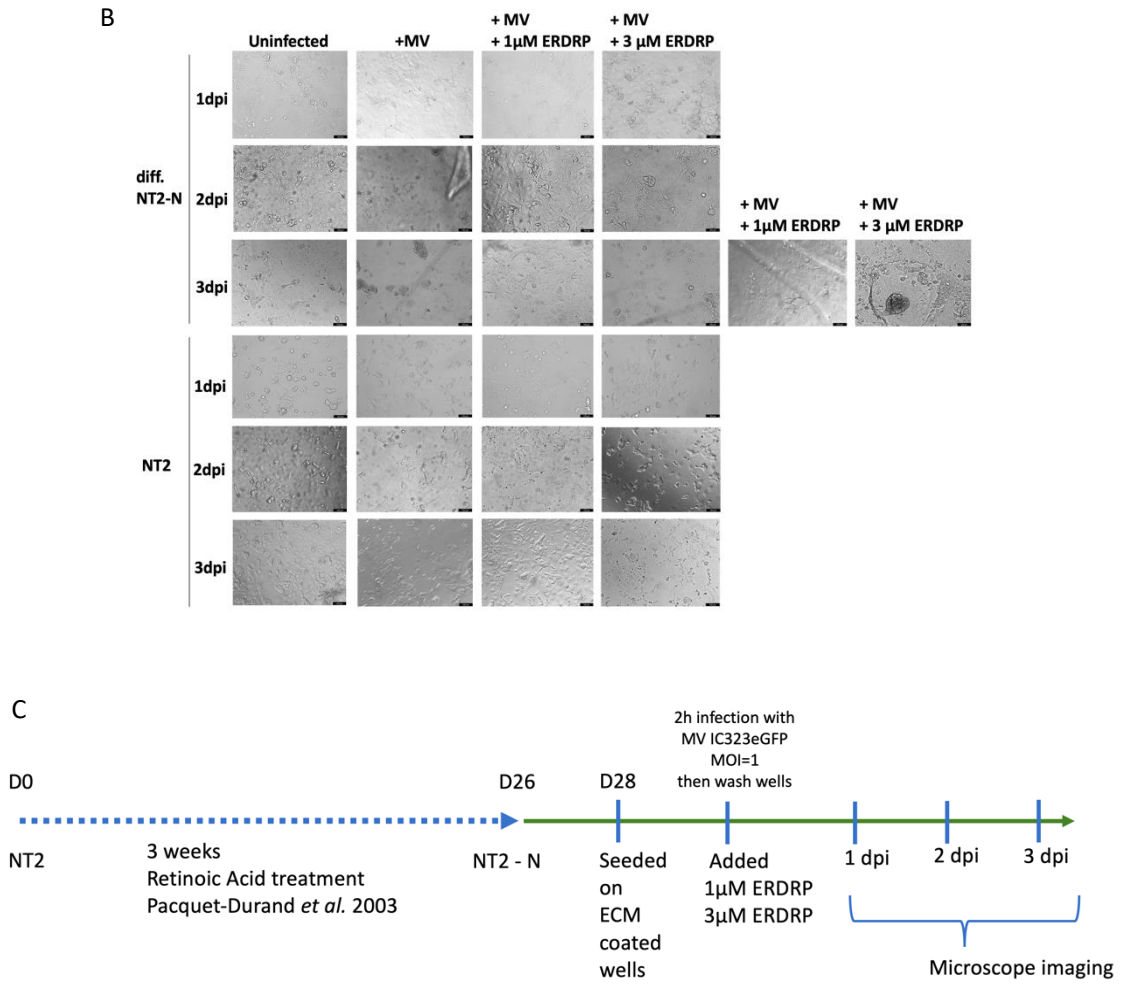

Figure 4.14: ERDRP-0519 mediated infection inhibition in differentiated NT2-N and NT2 cells (A) and (B) Microscope images show that the viral GFP infection (magnifications 100x, size bar = 100 µM). (C) Schematic representation of procedure NT2 cells were differentiated to NT2-N cells as per protocol described in 3.1.i (Section methods). The seeded cells were then infected with MV-IC323eGFP and further incubated with the inhibitor. The plate was then incubated at 37°C in CO_2 incubator and checked for infection under microscope each day.

These results demonstrate that the NT2 model can be used to study antivirals and their effect on wild type MV infection. However, owing to the long duration of differentiation procedure (approx. 3 weeks) and low neuron yield as compared to the initially seeded cells, we further decided to explore another and more recently described *in vitro* neuron model for the antiviral studies.

4.15 Differentiation and Infection of Post Mitotic Neurons Derived from LUHMES Cells

The LUHMES (Lund human mesencephalic) neuronal cells are a subclone derived from human mesencephalon cell line MESC2.10. These subcloned cells contain a tetracycline controlled v-*myc* overexpressing gene that immortalizes these otherwise post -mitotic neuronal cells. By supplying the maintenance media with additional factors like tetracycline, cAMP and glial derived neurotrophic factor (rhGDNF) (Materials section 2.3 and Methods section) , tetracycline induced v-myc shut off shifts the cells from proliferation to differentiation phase which can be observed by changes in the cell morphology under microscope- from flat epithelial like morphology on day 1 to stretched neuron like morphology with long neurites and synapses on day 5 (Fig. 4.15.A,B). Cells at the day 5 stage of differentiation were found to be positive for neuronal specific markers like neurofilament H and synaptophysin (Edwards et al., 2019) and are dopaminergic type neurons (Schoelz et al., 2011). Further, we were able to infect these differentiated neurons with low MOI (=0.1) of the wild type MV-IC323eGFP and not only observed GFP positive infected cells but also infection spread via the long neurite network (Fig 4.15.B) indicating that these dopaminergic neurons are susceptible and support the replication of wild type MV (image data not shown).

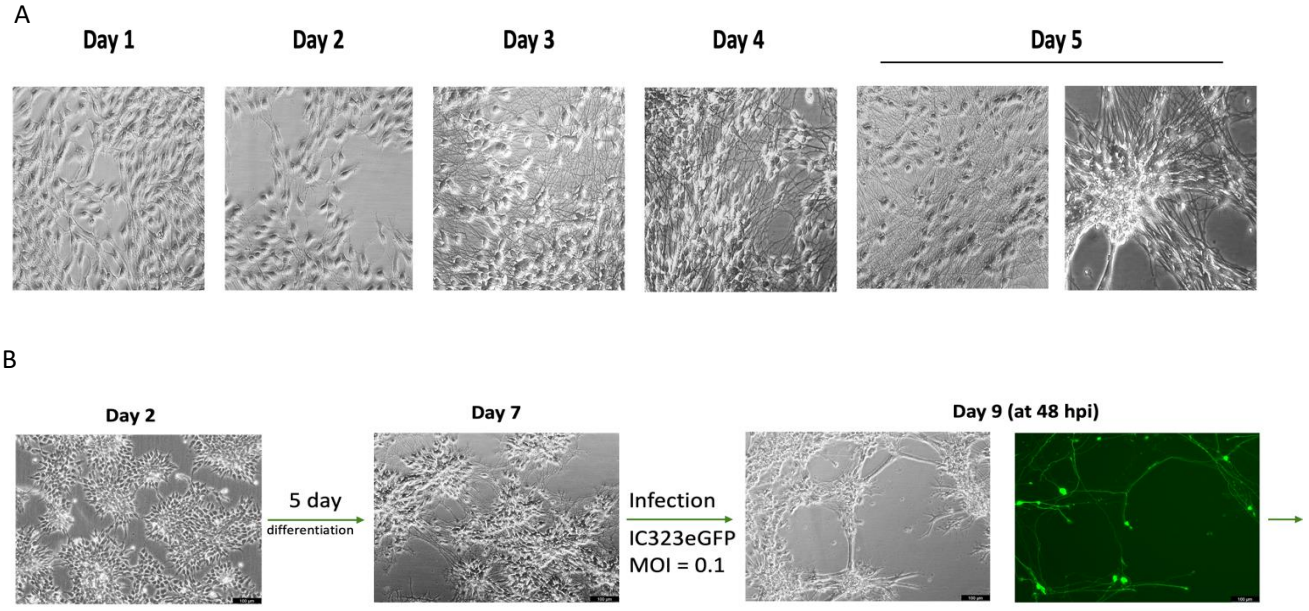

Fig. 4.15: Differentiation and infection of post mitotic neurons derived from LUHMES cells (A) Changes in morphology of the LUHMES cells across the upon treatment with differentiation media over the 5 days (magnification 200x scale bar=100 µM). (B) Micrograph of post-mitotic

neuron at 48 hour post infection with MV IC323eGFP. Microscope images show that the viral GFP infection (magnification 100x scale bar=100 µM). Data A contributed by Julia Thoma

4.16 Effect of Antiviral Compounds on Viral Inhibition in Post Mitotic Neurons

Using the above described model, we tested two antivirals that interfere with an important viral protein involved in its replication cycle – the viral Large polymerase complex. The inhibitor ERDRP-0519 specifically targets and blocks the viral polymerase activity thereby preventing synthesis of new viral RNA, and 17-AAG which binds to cellular protein Hsp90 thereby preventing its essential chaperoning activity important for proper folding of newly synthesized viral L protein. The schematic representation of the treatment of the cells is shown in Fig. 4.16 A

We observed that treatment with both 1 µm and 3 µM ERDRP-0519 were effective in reducing viral infection (GFP positive cells Fig.4.16 B) as well as spread of infection as observed by reduced GFP positive neurite network when compared to infected controls. 0.01 µM and 0.1 µm 17-AAG also reduced viral infection (Fig 4.16 B) to some extent and spread of infection as compared to infected control. However, the overall infection inhibition by 17 AAG was to a lesser extent when compared to ERDRP-0519.

A

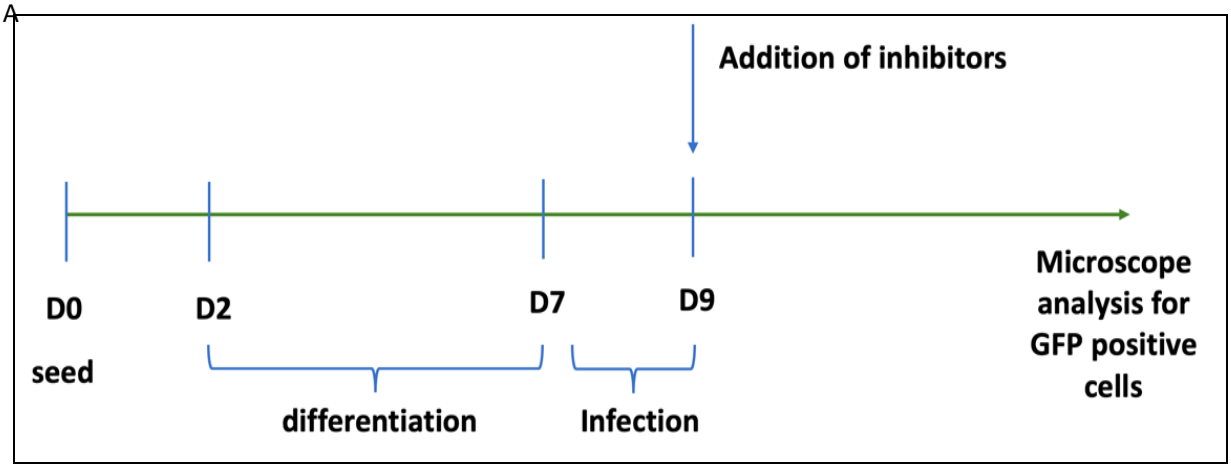

B

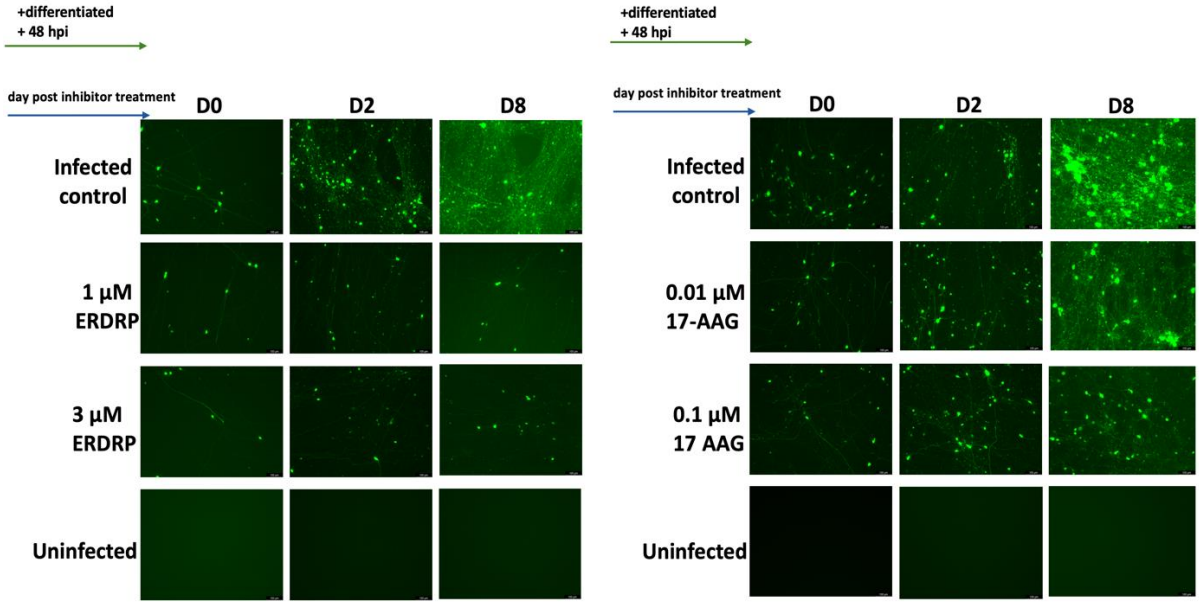

Fig. 4.16: Effect of antiviral compounds on MV replication in post-mitotic LUMES neurons

(A) Schematic representation of experimental setup for differentiation and subsequent infection inhibition experiments. B) Micrographs of infected post mitotic neurons treated with ERDRP-0519 and 17-AAG over a period of 7 days. After the five days differentiation, the neurons were infected with 0.1 MOI of MV-IC323eGFP for 2 h. The virus suspension was then discarded and the cell monolayer was then gently washed to remove unbound virus and finally replaced with fresh differentiation media. At 48 hpi the medium in the wells was replaced with fresh differentiation medium now containing the inhibitors and incubated further up to a week. Microscope images for GFP positive cells were recorded to observe infection inhibition (magnification 100x scale bar=100 µM).

DISCUSSION

In this study, our broad aim was to target viral and host factors so as to optimize anti-measles virus therapy. With respect to host factors, the main focus was to study the involvement of two key enzymes of the sphingolipid metabolism – the acid ceramidase and sphingosine kinase in acute measles virus infection of primary lymphocytes. The effect of their pharmacological inhibition using inhibitors Ceranib-2 and SKI-II respectively on MV replication in primary lymphocytes as well as on cellular protein expression in key metabolic pathways was the focus of this part of the study. Secondly using a persistently infected neural cell culture model as well as *in vitro* post-mitotic neuronal model we investigated the antiviral effect of a panel of inhibitors.

5.1. Involvement of Sphingolipid Metabolism in MV Infection

The involvement of sphingolipids or components of the sphingolipid pathway in various steps of replication cycle of numerous viruses and also other pathogens has been previously studied. The following table 5.1 summarizes some of the examples from available literature including a review (Avota et al., 2021) from our research groups:

Stage	Examples	Ref.
Receptor binding and attachment	Cell surface gylcosphingolipid 3 (Gb3) binding to V3 loop of HIV surface gp120 protein thereby modulating the virus fusion and uptake within the cell. Usage of globotetraosylceramide by parvovirus B19 for cellular entry Murine polyoma virus and SV40 reportedly also use gangliosides GM1 as entry receptors	Schneider-Schaulies, J et al., 2015
Uptake and cell entry	Attachment by certain rhinoviruses lead to acid sphingomyelinase (ASMase) translocation to cell surface along with ceramide enriched lipid clusters for viral endocytosis Attachment of Ebola virus to its receptor NPC1 was found to be dependent on expression of sphingomyelin and ASMase at the surface	

Viral Replication	Sphingosine kinase was found to regulate MV replication post its cellular entry via involvement of NF-kB SphK2 was found to co-locate with Chikungunya viral RNA and replication complex indicating a proviral involvement Distribution of ceramides and their interaction with non-structural protein NS4B of Zika virus. Influenza A virus activates Sphk1-NF- κB axis which acts proviral by promoting viral RNA synthesis	Reid et al., 2015, Vijayan et al 2014, Avota et al. 2021
Maturation and budding	Ceramide transfer protein (CERT) via regulation by PKD was found to influence HCV maturation and release along the Golgi network	Avota et al., 2021

Table 5.1: Reported involvement of sphingolipid metabolism in replication cycle of viruses

Acid ceramidase (aCDase) is considered as a potential target for anti-cancer therapy. Acid ceramidase was found to be overexpressed in a number of cancer of various tissues like prostrate, glioblastoma, head and neck cancer, melanoma, breast as well as gastrointestinal tissue (Vijayan et al., 2019). Complete aCDase knock down in melanoma cells prevented cell cycle progression and formation of invasive cancer cells (Lai et al., 2017). Between the two sphingosine kinase isoforms (Sphk), SphK1 has been extensively studied. Similar to aCDase, overexpression of SphK1 has also been linked to tumor progression in various cancers for e.g. breast, lung etc (Zhang et al., 2014). The SphK2 isoform was also found to be moderately overexpressed in a variety of cancers (Neubauer et al., 2016), however depending on its cellular location and extent of overexpression it could have both cell survival or pro-proliferative effect (Maceyka et al., 2005). Thus, well characterized inhibitors like Ceranib-2 and SKI-II have been described with potential for anti-cancer therapy since as compared to cancer cells (expressing high aCDase and Sphk), normal primary cells would be less sensitive to the apoptotic effects with the inhibitor treatment.

We checked for viability of various concentrations of Ceranib-2 and SKI-II treatment in proliferative lymphoma BJAB cell line and in normal PBL from healthy blood donors. A significant reduction in percent viable BJAB cells were observed with concentration above 1 µM for both inhibitors (Grafen et al., 2019). In PBL from healthy donors, the cells remained viable even upto 10 µM Ceranib-2 treatment but were viable upto 5 µm SKI-II treatment (Grafen et al., 2019). The viability threshold was set when ≥ 80 % cells did not uptake

Propidium iodide. These data reflect the sensitivity of (cancer) BJAB cells to Ceranib-2 and SKI-II as compared to less sensitive (normal) PBL. Nevertheless, we observed that viable concentrations of Ceranib-2 and SKI-II reduced mTORC1 activity (as determined by expression of p70 S6K downstream substrate) in both BJAB and PHA stimulated PBL over 24 h treatment (Fig.4.3) indicating that pharmacological inhibition of acid ceramidase and sphingosine kinase affected nutrient sensor mTORC1 downstream activity. Next, focusing mainly the on normal PBL (in absence of MV infection), we observed that Ceranib-2 and SKI-II affected phosphorylation of EIF4E and rpS6 (Fig. 4.4) which indicates perturbations in the protein translation pathways downstream of mTORC1. In the presence of MV infection, upregulation of rpS6 and EIF4E at 16 hpi especially indicated the probable usage of these factors during viral replication (Fig 4.5).

SKI-II mediated downregulation of rpS6 and EIF4E in the infected cells was also reflected by reduced viral protein expression of GFP and Hemagglutinin. In case of Ceranib-2 treatment, we observed significantly reduced infectious viral titers at 72 hpi (Fig 4.7.C), reduced percentages of infected (GFP positive cells Fig. 4.5.J.) at 24 hpi, but surprisingly increased GFP expression (per remaining GFP-positive cells in terms of MFI Fig.4.6.A.) at 24 hpi. This observation can be explained that the antiviral activity of Ceranib-2 is mainly via acid ceramidase inhibition thereby leading to reduction of MV replication in a fraction of the cells (low percentage of infected cells at 72 hpi) and accumulation of viral proteins within the cell or even lysosomes due to reduced virus exit (explaining the high GFP expression in remaining GFP-positive cells) in the other fraction of cells. Clinically, acid ceramidase deficiency is known to result in a rare lysosomal storage disorder or 'Farber's disease' due to ceramide accumulation in lysosomes (Yu FPS et al., 2018). In a recent report, acid ceramidase inhibition using another inhibitor led to retention of SARS CoV-2 within the lysosomal compartments along with ceramides (Geiger et al., 2022).

Apart from their pharmacological inhibition of respective enzymes, both the inhibitors may have off target cellular effects. SKI-II not only inhibits both the isoforms of SphK but also later was found to inhibit dihydroceramide desaturase-1 (Des1) – another sphingolipid metabolism related enzyme (Cingolani et al., 2014). The SKI-II mediated downregulation of global protein translation was found to be via activation of integrated stress response (ISR) in U2OS (human osteosarcoma) cells which also occurred upon knockdown of both Sphk (Vethakanraj et al., 2018). However, the ISR was observed with 10 µM of SKI-II, a high concentration as per our viability data with BJAB cells (Grafen et al., 2019). Interestingly, SKI-II mediated damage of the endoplasmic reticulum (ER) was observed (Corman et al.,

2021) by electron microscope. This could explain its effect of disrupted protein translation due to dislocation of ribosomes from the ER. In certain breast cancer cell lines, anti-cancer or apoptotic effects of ceranib-2 were found to be via nuclear changes, loss of mitochondrial membrane potential and also activation of mitogen and stress related pathways (Vethakanraj et al., 2018)

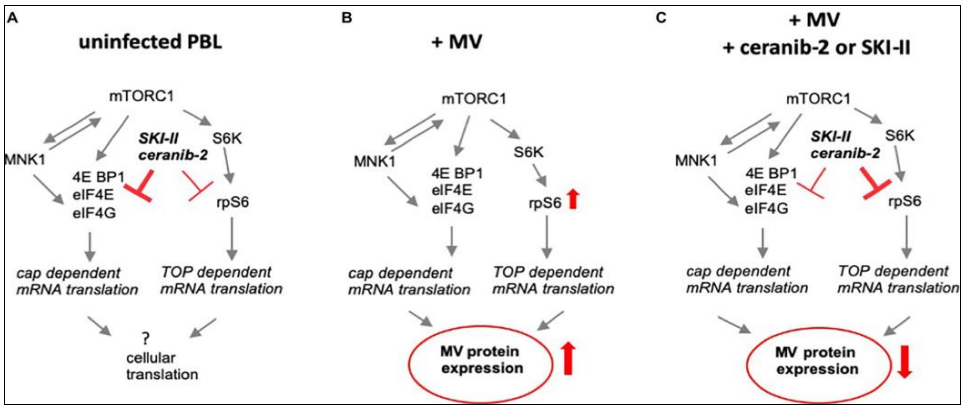

Fig. 5.1. Schematic summary of key observations

(A) The observed effects of Ceranib-2 and SKI-II in uninfected PBL, (B) effect of MV replication on signaling pathways downstream of mTORC1 and (C) the effect of the two inhibitors on infected PBL – as compared to reduced phosphorylation of EIF4E by the inhibitors in uninfected PBL, the inhibitors predominantly reduced the effect of infection by reducing rpS6 expression

Rapamycin has been used as an immunosuppressant and one of the suggested mechanisms of this effect has been via its effect in lymphocytes. The mTOR – EIF4E/rpS6 translation axis in lymphocytes was not only found to highly sensitive to rapamycin but also that this axis coordinated the lymphocyte between phases of growth and/or proliferation via ribosomal protein S6 and EIF4E respectively (So et al. 2021). In B lymphocytes, interestingly, antibody class switching was found to reduce by genetic and pharmacological inhibition of EIF4E leading to disruption of the cap translation complex (Chiu et al., 2019)

In summary, the inhibitors Ceranib-2 and SKI-II did inhibit MV replication in PBL, however, this antiviral effect was not very strong. Inspite of these limited antiviral activities, these inhibitors could be used along with other specific antiviral compounds to obtain a synergistic effect – especially as they are used already in the clinic against certain tumourous diseases.

5.2 Role of Monocytes and Macrophages in MV Infection

A study by Esolen et al. 1993 of clinical samples from acute measles patients observed that within the PBMC population, viral F gene was detected more abundantly in the

monocyte (adherent) enriched cells as compared to the non-adherent (lymphocyte enriched) cells implying that adherent monocytes were the predominantly infected cells as compared to lymphocytes. In PHA stimulated monocytes, CD150 was found to be the main receptor for MV (Minagawa et al. 2010). During natural MV infection, dissemination of the virus from the respiratory tract is carried out by infected immune cells that drain into the lymph nodes. Among the types of immune cells, monocytes are cells that can differentiate into highly motile and phagocytic macrophages and dendritic cells (Ginhoux et al. 2014) that are a part of innate immune system to capture pathogens and thus may function as predominant carriers of the measles virus during its systemic spread in blood circulation. The bioactive sphingolipid metabolite S1P is known to egress and trafficking of immune cells via a receptor sensitive gradient maintained intra and extra cellularly (Lewis et al. 2013).

From our FACS dot plot analysis (Fig 4.15), two distinct cell populations were observed and based on larger size (as determined by the forward scatter) the upper population was designated as 'residual monocytes' that may have retained even after the adherence step. Thus, we also analyzed this 'Residual monocyte' population for MV infection with inhibitor treatment. Based on the high percentage of infection in these cells (Fig 4.15), it is certain that this is a monocyte population and the both inhibitors (especially Cer-2) significantly reduced the infection. In 3D culture models, significantly impaired MV transmission from DCs to epithelial cells as well as reduced DC velocity was observed with SKI-II treatment (Derakhshani et al. 2019). These findings reflect or highlight the interplay of sphingolipid metabolites and MV infection in an organism. Nevertheless, further study of this 'Residual monocyte' population may have to be verified further by staining expression of surface CD14 – a marker mainly used for monocyte and macrophage identification.

5.3 Putative TOP like sequences in viral infections

Genetic material like RNA and DNA apart from storing genetic information of the organism also contain numerous non-coding sequences, motifs, nucleotide modifications or even associated protein modifications that may serve as signals for initiation, termination, gene expression and more importantly regulation in important processes like replication, transcription, translation etc. One such regulatory motif is the 5' TOP (terminal oligopyrimidine tract) observed in RNA of vertebrate mRNA transcripts particularly those coding for cellular ribosomal proteins and elongation factors. Since these proteins are essential machinery of cellular protein synthesis, the 5'TOP containing transcripts are thus under translational control especially during stress conditions. LARP (La related protein 1)

and key cellular sensor mTOR are majorly associated with repression and promotion of TOP RNA translation respectively (Cockman et al., 2020, Philippe 2018 and Jian-Jun et al. , 2021). Recently, an interactome study identified TOP like motifs within the 5' leader region in viral RNA of SARS CoV-2 and that cellular LARP1 was found to bind TOP motifs within the viral (positive sense) RNA and restricted viral replication (Schmidt et al., 2021). Also based on our observation (Fig. 4.5 A,B) that ribosomal protein (rps6) was upregulated in MV infected PBL, a basic search analysis for putative TOP motifs within the coding sequence genome of MV was done.

As described in 4.16, we observed that the upstream of the genes for viral surface proteins F and H there were 24 and 4 putative TOP like sequences respectively – more than with the other viral genes. Based on the mTOR → LARP1 → 5'TOP regulation axis, I hypothesize that the rpS6 overexpression (especially at 16 and 24h) occurs as a side effect of the virus translation especially of F and H genes that are expressed in late stage of the replication cycle during assembly and exit. Thus, the virus replication, may indirectly promote rpS6 expression thus contributing to increased cell growth (enlarged cells observed in MV infected cells) – these enlarged cells now also expressing viral surface proteins may bind to neighboring cells to spread infection further. In a knock out mice model, *rps6* deficiency was associated with mTOR regulated diminished cell size (Ruvinsky et al., 2005). In a plant model, rpS6 not only acted as a pro-viral factor for the virus infection but also gene silencing of various forms of the *rpS6* led to phenotypically distinct stunted plant growth (Helderman et al., 2022).

Nevertheless, practical validation involves confirmation of the putative TOP sequences as regulatory. For a TOP sequence to have regulatory effect it has to be immediately adjacent to the 5' cap structure. Since capping is a post-transcription event indicating that the validation of TOP sequences has to be checked in the capped viral transcripts. Additionally, growth assays of MV can be done using in LARP deficient/overexpressing cells to confirm the involvement of LARP1.

5.4.a. Persistent MV infections of neurons

With the aim to study MV infection and subsequent antiviral inhibition using an *in vitro* model for neural cells and post-mitotic neurons, we first used the NT2 cell line – that neuronal precursor cells and is committed to differentiate into neurons only (Pleasure et al., 1993). Previous reports using this cell were studied with respect to acute MV infection using the recombinant Edmonston B strain expressing GFP. Infection and spread of MV in NT2

and NT2-N was found to be CD46 independent, lack of syncytia formation along with low released extracellular virus titers and observation of incomplete budding structures at cell membrane by electron microscopy and spread of infection mainly via synapses formed by connecting neuronal processes (Lawrence et al., 2000). In astrocytoma cells, a similar pattern of MV infection was observed with diffusion of eGFP to adjacent fused cells considered as a sensitive marker for early viral infection. Both acute and persistent MV infection of NT2 and NT2-N cells was found to be independent of CD46 (McQuaid et al., 1998, Ludlow et al., 2005) and interestingly, the NT2 cells persistently infected with Edm-eGFP MV when superinfected with related Morbillivirus like MV or CDV did not demonstrate a cytopathic effect. A recent report observed that the cell to cell spread of the wild-type IC323eGFP MV between NT2-N still mainly depended on the attachment and fusion by viral H and F but not via syncytia formation (Sato et al 2018). In addition, the persistently infected (with rat brain adapted CAM-H -HcRed MV) NT2 cell line was also used successfully as an *in vitro* model to study viral clearance using short hairpin RNA (targeting multiple MV sequences) delivered via lentiviral system (Zinke et al., 2009).

5.4.b. Antiviral Activity of Inhibitors in Acute and Persistent MV Infections of NT2 Cells

In this study, we established a NT2 cell line persistently infected with wild-type MV-IC323eGFP – a wild type strain (Fig 4.9) and checked for expression of typical characteristics like expression of viral proteins and low release viral titers (Fig 4.10.A and Fig. 4.10.B). The spread of infection was mediated by a functional activity of viral F since we observed significant reduction in GFP positive cells with FIP treatment (Table 4.12). In order of significance, the compounds showing best antiviral effect in terms of viral GFP expression were ERDRP-0519, Favipiravir and SKI-II. While clinically used broad spectrum Favipiravir may function by inhibiting viral polymerase activity, with higher doses of 200 µM, cell division was also affected. In pi-NT2 cells, SKI-II mediated viral GFP downregulation could be possibly via:

1) Downregulation of cellular protein translational capacity similar to that observed in PBL
2) Inhibition of SphK activity in neuronal cells – S1P and SphK have been reported to be crucial in rodent brains and enriched at synapses in *C.elegans* nervous system models (Blondeau et al 2007, Chan et al., 2012). A possible direct interaction of Sphk can be hypothesized since both isoforms contain nucleotide binding sites that can bind possibly

bind also bind to viral RNA and Sphk2 isoform was found to co-localize with viral RNA od Chikungunya virus.

Characterization, development and specific antiviral activity of small non-nucleoside inhibitor ERDRP-0517 had been extensively reported and proved (refer Table 1.3) using *in vitro* replication systems, bioinformatic analysis as well as in biological systems like ferret and non-human primate models. The unique aspect of our study was that the significant antiviral effect of this compound was also observed in *in vitro* acute infection of lymphocytes from healthy human donors (Fig. 4.7 Panel G, unpublished). Additionally, we observed almost viral (GFP) clearance in the wild type persistently infected neuronal NT2 model (Fig 4.11)

5.4.c. Differentiation of NT2 and LUHMES Cells and Infection Inhibition

We observed that NT2-N cells obtained by differentiation of NT2 cells were susceptible to wild-type MV infection which was efficiently inhibited with both doses of ERDRP-0519 upto day 3 post infection (Fig. 4.12). However, owing to time constraints due to the long differentiation procedure (approximately 3 weeks) and low neuron yield, we decided to use another system i.e. post-mitotic dopaminergic neurons derived by differentiating LUHMES cells. This system not only had a short differentiation time (approx.5 days) but has also not been previously studied for MV neurotropic infections. We not only observed that these post-mitotic neurons could be infected with wild-type MV (Fig. 4.13) but also explored the antiviral effect of two inhibitors and observed that (Fig 4.14) the compounds ERDRP-0519 and 17-AAG had an antiviral effect as in proliferating cells like stimulated PBL or p.i.NT2

5.5 Final Note: Persistence of viral infections

Persistence of MV infections has been previously documented in numerous cell culture models. Fisher *et al* reported that wild type Edmonston, vaccine strain Schwarz, Halle SSPE strain and even a temperature sensitive Edmonston strain were able to establish persistent infection in Vero cells. Typical features include absence of cytopathic effect, persistence of viral RNA, reduced cell free virus production. Not just in *in vitro* models, presence of viral RNA was detected upto 3 months post-acute infection in samples from infected patients (Riddell et al., 2007) as well as prolonged shedding of viral RNA from HIV positive immunocompromised patients (Sallie et al., 2001). Such a prolonged persistence

was also detected for vaccine viral RNA from vaccinated children (McMahon et al., 2019). Viral RNA persistence in multiple sites was also observed in rhesus macaque models suggesting that such a viral RNA persistence is possibly a part of the acute phase dynamics with the viral RNA being remnants after infectious viral clearance (Lin et al., 2012). The detection MV RNA has been reported to persist in lymphoid tissues up to 6 months post infection in rhesus macaques even when no replicating virus was detected (Griffin et al., 2020). There also exists singular summary of evidence of integration of viral RNA into host genome in chronically infected cells for a number of RNA viruses including measles (Zhdanov et al., 1975).

Not just MV, viral persistent infections have been observed and reported (Randall et al., 2017) among animal RNA viruses belonging to almost all virus families ranging from simple *Picornaviridae* (single positive RNA genome) to complex tripartite negative sense *Bunyaviridae* or even ambisense *Arenaviridae* indicating that persistence of viral RNA is a common feature and may imply that cellular factors may predominantly contribute to extent of viral persistence. One probable mechanism could be RNA modification for e.g. m6A (N6-methyl adenosine) which is reported to be abundantly detected in mammalian RNA but also in viral RNA. Such a modification did not stimulate a cellular innate immune response like TLR as compared to strong stimulation by bacteria or *in vitro* transcribed RNA (Kariko et al., 2005). During acute phase infection, viral proteins generated may initiate an antigenic immune response within the host so as to clear the infection. But since viruses utilize cellular biomolecules for building up its own structure during replication, although, a certain amount of newly progeny viral RNA may still persist over time as they escape intracellular detection due to the fact that since they were produced within the host cell itself, their RNA obtained the modification features imparted by the cell thus rendering them as non-foreign RNA.

MV persistence in SSPE is one such example persistent viral infection that has negative consequences in terms of morbidity and mortality thus requiring specific and effective therapy. From our study, we found that polymerase inhibitor ERDRP-0519 and similar such inhibitors are very good candidates in inhibiting wild type MV infection in primary human lymphocytes, neuronal NT2 cells as well as post-mitotic neurons derived from LUHMES cells.

REFERENCES

Alvarez SE, Harikumar KB, Hait NC, Allegood J, Strub GM, Kim EY, Maceyka M, Jiang H, Luo C, Kordula T, Milstien S, Spiegel S. Sphingosine-1-phosphate is a missing cofactor for the E3 ubiquitin ligase TRAF2. Nature. **2010** Jun 24;465(7301):1084-8. doi: 10.1038/nature09128. PMID: 20577214; PMCID: PMC2946785.

Avota E, Avots A, Niewiesk S, Kane LP, Bommhardt U, ter Meulen V, Schneider-Schaulies S. Disruption of Akt kinase activation is important for immunosuppression induced by measles virus. Nat Med. **2001** Jun;7(6):725-31. doi: 10.1038/89106. PMID: 11385511.

Avota E, Bodem J, Chithelen J, Mandasari P, Beyersdorf N, Schneider-Schaulies J. The Manifold Roles of Sphingolipids in Viral Infections. Front Physiol. 2021 Sep 29;12:715527. doi: 10.3389/fphys.**2021**.715527. PMID: 34658908; PMCID: PMC8511394.

Baczko, K., Lampe, J., Liebert, U. G., Brinckmann, U., ter Meulen, V., Pardowitz, I., Budka, H., Cosby, S. L., Isserte, S., & Rima, B. K. (**1993**). Clonal expansion of hypermutated measles virus in a SSPE brain. *Virology*, *197*(1), 188–195. https://doi.org/10.1006/viro.1993.1579

Barnette,n.d.Biorad-https://www.rndsystems.com/resources/protocols/flow-cytometry-protocol-analysis-cell-viability-using-propidium-iodide#:~:text=Propidium%20iodide%20(PI)%20is%20a,maximum%20wavelength%20of%20617%20nm

Bartke N, Hannun YA. Bioactive sphingolipids: metabolism and function. J Lipid Res. **2009** Apr;50 Suppl(Suppl):S91-6. doi: 10.1194/jlr.R800080-JLR200. Epub 2008 Nov 17. PMID: 19017611; PMCID: PMC2674734.

Bartz R, Brinckmann U, Dunster LM, Rima B, Ter Meulen V, Schneider-Schaulies J. Mapping amino acids of the measles virus hemagglutinin responsible for receptor (CD46) downregulation. Virology. 1996 Oct 1;224(1):334-7. doi: 10.1006/viro.1996.0538. PMID: 8862431.

Bartz R, Firsching R, Rima B, ter Meulen V, Schneider-Schaulies J. Differential receptor usage by measles virus strains. J Gen Virol. 1998 May;79 (Pt 5):1015-25. doi: 10.1099/0022-1317-79-5-1015. PMID: 9603316.

Batool, A., Majeed, S. T., Aashaq, S., Majeed, R., Bhat, N. N., & Andrabi, K. I. (**2020**). Eukaryotic initiation factor 4E is a novel effector of mTORC1 signaling pathway in cross talk with Mnk1. *Molecular and cellular biochemistry*, *465*(1-2), 13–26. https://doi.org/10.1007/s11010-019-03663-z

Beaty SM, Lee B. Constraints on the Genetic and Antigenic Variability of Measles Virus. Viruses. **2016**; 8(4):109. https://doi.org/10.3390/v8040109

Beaucourt, S., & Vignuzzi, M. (**2014**). Ribavirin: a drug active against many viruses with multiple effects on virus replication and propagation. Molecular basis of ribavirin resistance. *Current opinion in virology*, *8*, 10–15. https://doi.org/10.1016/j.coviro.2014.04.011

Biolegend v2 – a) https://www.biolegend.com/fr-lu/products/propidium-iodide-solution-2651

b) https://www.thermofisher.com/in/en/home/life-science/cellanalysis/fluorophores/propidium-iodide.html

Bio-sharing.org https://bio-sharing.org/pdfs/Leukoreduction.pdf

BJAB – a) https://www.accegen.com/product/bjab-abc-tc514s/

b) https://www.cellosaurus.org/CVCL_5711

Blondeau N, Lai Y, Tyndall S, Popolo M, Topalkara K, Pru JK, Zhang L, Kim H, Liao JK, Ding K, Waeber C. Distribution of sphingosine kinase activity and mRNA in rodent brain. J Neurochem. **2007** Oct;103(2):509-17. doi: 10.1111/j.1471-4159.2007.04755.x. Epub 2007 Jul 10. PMID: 17623044; PMCID: PMC2639651.

Bloyet LM, Welsch J, Enchery F, Mathieu C, de Breyne S, Horvat B, Grigorov B, Gerlier D. HSP90 Chaperoning in Addition to Phosphoprotein Required for Folding but Not for Supporting Enzymatic Activities of Measles and Nipah Virus L Polymerases. J Virol. **2016** Jul 11;90(15):6642-6656. doi: 10.1128/JVI.00602-16. PMID: 27170753; PMCID: PMC4944277.

Bodewes, R., Reijnen, L., Zwagemaker, F., Kohl, R., Kerkhof, J., Veldhuijzen, I. K., & van Binnendijk, R.. An efficient molecular approach to distinguish chains of measles virus transmission in the elimination phase. *Infection, genetics and evolution : journal of molecular epidemiology and evolutionary genetics in infectious diseases*, *91*, 104794. https://doi.org/10.1016/j.meegid.2021.104794

Burki TK. Lifting of COVID-19 restrictions in the UK and the Delta variant. Lancet Respir Med. **2021** Aug;9(8):e85. doi: 10.1016/S2213-2600(21)00328-3. Epub 2021 Jul 12. PMID: 34265238; PMCID: PMC8275031.

Cattaneo R. Four viruses, two bacteria, and one receptor: membrane cofactor protein (CD46) as pathogens' magnet. J Virol. **2004** May;78(9):4385-8. doi: 10.1128/jvi.78.9.4385-4388.2004. PMID: 15078919; PMCID: PMC387720.

CDC 2020 : https://www.cdc.gov/measles/hcp/index.html

Chan, J. P., & Sieburth, D. (**2012**). Localized sphingolipid signaling at presynaptic terminals is regulated by calcium influx and promotes recruitment of priming factors. *The Journal of neuroscience : the official journal of the Society for Neuroscience*, *32*(49), 17909–17920. https://doi.org/10.1523/JNEUROSCI.2808-12.2012

Chiu H, Jackson LV, Oh KI, Mai A, Ronai ZA, Ruggero D, Fruman DA. The mTORC1/4E-BP/eIF4E Axis Promotes Antibody Class Switching in B Lymphocytes. J Immunol. **2019** Jan 15;202(2):579-590. doi: 10.4049/jimmunol.1800602. Epub 2018 Dec 10. PMID: 30530594; PMCID: PMC6324996.

Cingolani F, Casasampere M, Sanllehí P, Casas J, Bujons J, Fabrias G. Inhibition of dihydroceramide desaturase activity by the sphingosine kinase inhibitor SKI II. J Lipid Res. **2014** Aug;55(8):1711-20. doi: 10.1194/jlr.M049759. Epub 2014 May 29. PMID: 24875537; PMCID: PMC4109765.

Cockman E, Anderson P, Ivanov P. TOP mRNPs: Molecular Mechanisms and Principles of Regulation. Biomolecules. **2020** Jun 27;10(7):969. doi: 10.3390/biom10070969. PMID: 32605040; PMCID: PMC7407576.

Corman A, Kanellis DC, Michalska P, Häggblad M, Lafarga V, Bartek J, Carreras-Puigvert J, Fernandez-Capetillo O. A chemical screen for modulators of mRNA translation identifies a distinct mechanism of toxicity for sphingosine kinase inhibitors. PLoS Biol. **2021** May 25;19(5):e3001263. PMID: 34033645; PMCID: PMC8183993. https://doi.org/10.1371/journal.pbio.3001263

Cox RM, Sourimant J, Govindarajan M, Natchus MG, Plemper RK. Therapeutic targeting of measles virus polymerase with ERDRP-0519 suppresses all RNA synthesis activity. PLoS Pathog. **2021** Feb 23;17(2):e1009371. doi: 10.1371/journal.ppat.1009371. PMID: 33621266; PMCID: PMC7935272.

de Vries RD, Lemon K, Ludlow M, McQuaid S, Yüksel S, van Amerongen G, Rennick LJ, Rima BK, Osterhaus AD, de Swart RL, Duprex WP. In vivo tropism of attenuated and pathogenic measles virus expressing green fluorescent protein in macaques. J Virol. 2010 May;84(9):4714-24. doi: 10.1128/JVI.02633-09. Epub **2010** Feb 24. PMID: 20181691; PMCID: PMC2863733.

de Vries RD, McQuaid S, van Amerongen G, Yüksel S, Verburgh RJ, Osterhaus AD, Duprex WP, de Swart RL. Measles immune suppression: lessons from the macaque model. PLoS Pathog. **2012**;8(8):e1002885. doi: 10.1371/journal.ppat.1002885. Epub 2012 Aug 30. PMID: 22952446; PMCID: PMC3431343.

de Witte L, de Vries RD, van der Vlist M, Yüksel S, Litjens M, de Swart RL, Geijtenbeek TB. DC-SIGN and CD150 have distinct roles in transmission of measles virus from dendritic cells to T-lymphocytes. PLoS Pathog. **2008** Apr 18;4(4):e1000049. doi: 10.1371/journal.ppat.1000049. PMID: 18421379; PMCID: PMC2277461.

Delpeut S, Noyce RS, Richardson CD. The tumor-associated marker, PVRL4 (nectin-4), is the epithelial receptor for morbilliviruses. Viruses. **2014** Jun 2;6(6):2268-86. doi: 10.3390/v6062268. PMID: 24892636; PMCID: PMC4074928.

Derakhshani S, Kurz A, Japtok L, Schumacher F, Pilgram L, Steinke M, Kleuser B, Sauer M, Schneider-Schaulies S, Avota E. Measles Virus Infection Fosters Dendritic Cell Motility in a 3D Environment to Enhance Transmission to Target Cells in the Respiratory Epithelium. Front Immunol. **2019** Jun 5;10:1294. doi: 10.3389/fimmu.2019.01294. PMID: 31231395; PMCID: PMC6560165.

Donohue, R. C., Pfaller, C. K., & Cattaneo, R. (**2019**). Cyclical adaptation of measles virus quasispecies to epithelial and lymphocytic cells: To V, or not to V. *PLoS pathogens*, *15*(2), e1007605. https://doi.org/10.1371/journal.ppat.1007605

Dörig RE, Marcil A, Chopra A, Richardson CD. The human CD46 molecule is a receptor for measles virus (Edmonston strain). Cell. **1993** Oct 22;75(2):295-305. doi: 10.1016/0092-8674(93)80071-l. PMID: 8402913.

Draper JM, Xia Z, Smith RA, Zhuang Y, Wang W, Smith CD. Discovery and evaluation of inhibitors of human ceramidase. Mol Cancer Ther. **2011** Nov;10(11):2052-61. doi: 10.1158/1535-7163.MCT-11-0365. Epub 2011 Sep 1. PMID: 21885864; PMCID: PMC3213284.

Duprex, W. P., Duffy, I., McQuaid, S., Hamill, L., Cosby, S. L., Billeter, M. A., Schneider-Schaulies, J., ter Meulen, V., & Rima, B. K. (**1999**). The H gene of rodent brain-adapted measles virus confers neurovirulence to the Edmonston vaccine strain. *Journal of virology*, *73*(8), 6916–6922. https://doi.org/10.1128/JVI.73.8.6916-6922.1999

Duprex, W. P., McQuaid, S., Hangartner, L., Billeter, M. A., & Rima, B. K. (**1999b**). Observation of measles virus cell-to-cell spread in astrocytoma cells by using a green fluorescent protein-expressing recombinant virus. *Journal of virology*, *73*(11), 9568–9575. https://doi.org/10.1128/JVI.73.11.9568-9575.1999

Düx, A., Lequime, S., Patrono, L. V., Vrancken, B., Boral, S., Gogarten, J. F., Hilbig, A., Horst, D., Merkel, K., Prepoint, B., Santibanez, S., Schlotterbeck, J., Suchard, M. A., Ulrich, M., Widulin, N., Mankertz, A., Leendertz, F. H., Harper, K., Schnalke, T., Lemey, P., … Calvignac-Spencer, S. **(2020)**. Measles virus and rinderpest virus divergence dated to the sixth century BCE. *Science (New York, N.Y.)*, *368*(6497), 1367–1370. https://doi.org/10.1126/science.aba9411

ECDC - https://www.ecdc.europa.eu/en/measles/facts

Edwards TG, Bloom DC. Lund Human Mesencephalic (LUHMES) Neuronal Cell Line Supports Herpes Simplex Virus 1 Latency *In Vitro*. J Virol. **2019** Mar 5;93(6):e02210-18. doi: 10.1128/JVI.02210-18. PMID: 30602607; PMCID: PMC6401467.

Erlenhoefer C, Wurzer WJ, Löffler S, Schneider-Schaulies S, ter Meulen V, Schneider-Schaulies J. CD150 (SLAM) is a receptor for measles virus but is not involved in viral contact-mediated proliferation inhibition. J Virol. **2001** May;75(10):4499-505. doi: 10.1128/JVI.75.10.4499-4505.2001. PMID: 11312320; PMCID: PMC114203.

Esolen, L. M., Ward, B. J., Moench, T. R., & Griffin, D. E. (1993). Infection of monocytes during measles. *The Journal of infectious diseases*, *168*(1), 47–52. https://doi.org/10.1093/infdis/168.1.47

Ferren M, Horvat B, Mathieu C. Measles Encephalitis: Towards New Therapeutics. Viruses. **2019** Nov 2;11(11):1017. doi: 10.3390/v11111017. PMID: 31684034; PMCID: PMC6893791.

French KJ, Upson JJ, Keller SN, Zhuang Y, Yun JK, Smith CD. Antitumor activity of sphingosine kinase inhibitors. J Pharmacol Exp Ther. 2006 Aug;318(2):596-603. doi: 10.1124/jpet.106.101345. Epub 2006 Apr 21. PMID: 16632640.

Furuta Y., Komeno, T., & Nakamura, T. (**2017**). Favipiravir (T-705), a broad spectrum inhibitor of viral RNA polymerase. *Proceedings of the Japan Academy. Series B, Physical and biological sciences*, *93*(7), 449–463. https://doi.org/10.2183/pjab.93.027

Gebai, A., Gorelik, A., Li, Z. *et al.* Structural basis for the activation of acid ceramidase. *Nat Commun* 9, 1621 (**2018**). https://doi.org/10.1038/s41467-018-03844-2

Geiger, N.; Kersting, L.; Schlegel, J.; Stelz, L.; Fähr, S.; Diesendorf, V.; Roll, V.; Sostmann, M.; König, E.-M.; Reinhard, S.; Brenner, D.; Schneider-Schaulies, S.; Sauer, M.; Seibel, J.; Bodem, J. The Acid Ceramidase Is a SARS-CoV-2 Host Factor. *Cells* **2022**, *11*, 2532. https://doi.org/10.3390/cells11162532

Generous AR, Harrison OJ, Troyanovsky RB, Mateo M, Navaratnarajah CK, Donohue RC, Pfaller CK, Alekhina O, Sergeeva AP, Indra I, Thornburg T, Kochetkova I, Billadeau DD, Taylor MP, Troyanovsky SM, Honig B, Shapiro L, Cattaneo R. *Trans*-endocytosis elicited by nectins transfers cytoplasmic cargo, including infectious material, between cells. J Cell Sci. **2019** Aug 23;132(16):jcs235507. doi: 10.1242/jcs.235507. PMID: 31331966; PMCID: PMC6737912.

Gingras, A. C., Raught, B., & Sonenberg, N. (**1999**). eIF4 initiation factors: effectors of mRNA recruitment to ribosomes and regulators of translation. *Annual review of biochemistry*, *68*, 913–963. https://doi.org/10.1146/annurev.biochem.68.1.913

Ginhoux, F., Jung, S. Monocytes and macrophages: developmental pathways and tissue homeostasis. *Nat Rev Immunol* 14, 392–404 (**2014**). https://doi.org/10.1038/nri3671

Grafen A, Schumacher F, Chithelen J, Kleuser B, Beyersdorf N, Schneider-Schaulies J. Use of Acid Ceramidase and Sphingosine Kinase Inhibitors as Antiviral Compounds Against Measles Virus Infection of Lymphocytes *in vitro*. Front Cell Dev Biol. **2019** Oct 1;7:218. doi: 10.3389/fcell.2019.00218. PMID: 31632969; PMCID: PMC6779704

Griffin DE. Measles virus persistence and its consequences. Curr Opin Virol. **2020** Apr;41:46-51. doi: 10.1016/j.coviro.2020.03.003. Epub 2020 May 5. PMID: 32387998; PMCID: PMC7492426.

Guseva S, Milles S, Blackledge M, Ruigrok RWH. The Nucleoprotein and Phosphoprotein of Measles Virus. Front Microbiol. **2019** Aug 21;10:1832. doi: 10.3389/fmicb.2019.01832. PMID: 31496998; PMCID: PMC6713020.

Hannun, Y., Obeid, L. Sphingolipids and their metabolism in physiology and disease. *Nat Rev Mol Cell Biol* 19, 175–191 (2018). https://doi.org/10.1038/nrm.2017.107

Hashiguchi, T., Maenaka, K., & Yanagi, Y. (**2011**). Measles virus hemagglutinin: structural insights into cell entry and measles vaccine. *Frontiers in microbiology*, *2*, 247. https://doi.org/10.3389/fmicb.2011.00247

Hashimoto K, Maeda H, Miyazaki K, Watanabe M, Norito S, Maeda R, Kume Y, Ono T, Chishiki M, Suyama K, Sato M, Hosoya M. Antiviral Effect of Favipiravir (T-705) against Measles and Subacute Sclerosing Panencephalitis Viruses. Jpn J Infect Dis. 2021 Mar 24;74(2):154-156. doi: 10.7883/yoken.JJID.2020.481. Epub **2020** Aug 31. PMID: 32863356.

Hashimoto K, Ono N, Tatsuo H, Minagawa H, Takeda M, Takeuchi K, Yanagi Y. SLAM (CD150)-independent measles virus entry as revealed by recombinant virus expressing green fluorescent protein. J Virol. **2002** Jul;76(13):6743-9. doi: 10.1128/jvi.76.13.6743-6749.2002. PMID: 12050387; PMCID: PMC136249.

Heath, E.I., Rosenberg, J.E. The biology and rationale of targeting nectin-4 in urothelial carcinoma. *Nat Rev Urol* 18, 93–103 (**2021**). https://doi.org/10.1038/s41585-020-00394-5

Helderman, T. A., Deurhof, L., Bertran, A., Richard, M., Kormelink, R., Prins, M., Joosten, M., & van den Burg, H. A. (**2022**). Members of the ribosomal protein S6 (RPS6) family act as pro-viral factor for tomato spotted wilt orthotospovirus infectivity in Nicotiana benthamiana. *Molecular plant pathology*, *23*(3), 431–446. https://doi.org/10.1111/mpp.13169

Hippee CE, Singh BK, Thurman AL, Cooney AL, Pezzulo AA, Cattaneo R, et al. (**2021**) Measles virus exits human airway epithelia within dislodged metabolically active infectious centers. PLoS Pathog 17(8): e1009458. https://doi.org/ 10.1371/journal.ppat.1009458

https://connects.catalyst.harvard.edu/Profiles/display/Concept/RNA%205'%20Terminal%20Oligopyrimidine%20Sequence

https://en.wikipedia.org/wiki/Bicinchoninic_acid_assay

https://en.wikipedia.org/wiki/SDS-PAGE

https://www.abcam.com/protocols/introduction-to-flow-cytometry

https://www.atcc.org/products/crl-2927 - LUHMES -
https://www.bio-rad-antibodies.com/blog/a-guide-to-gating-in-flow-cytometry.html
https://www.cdc.gov/measles/symptoms/complications.html
https://www.selleckchem.com/products/17-AAG(Geldanamycin).html
https://www.selleckchem.com/products/ski-ii.html
https://www.sigmaaldrich.com/DE/en/product/mm/219556
https://www.sinobiological.com/category/wb-semi-dry-transfer
https://www.**thermofisher**.com/order/catalog/product/**23225**

Ikegame, S., Hashiguchi, T., Hung, C. T., Dobrindt, K., Brennand, K. J., Takeda, M., & Lee, B. (**2021**). Fitness selection of hyperfusogenic measles virus F proteins associated with neuropathogenic phenotypes. *Proceedings of the National Academy of Sciences of the United States of America*, *118*(18), e2026027118. https://doi.org/10.1073/pnas.2026027118

Iwasaki, M., Takeda, M., Shirogane, Y., Nakatsu, Y., Nakamura, T., & Yanagi, Y**. (2009)**. The matrix protein of measles virus regulates viral RNA synthesis and assembly by interacting with the nucleocapsid protein. *Journal of virology*, *83*(20), 10374–10383. https://doi.org/10.1128/JVI.01056-09

Jefferies, H. B., Fumagalli, S., Dennis, P. B., Reinhard, C., Pearson, R. B., & Thomas, G. (**1997**). Rapamycin suppresses 5'TOP mRNA translation through inhibition of p70s6k. *The EMBO journal*, *16*(12), 3693–3704. https://doi.org/10.1093/emboj/16.12.3693

Jian-Jun Jia, Roni M Lahr, Michael T Solgaard, Bruno J Moraes, Roberta Pointet, An-Dao Yang, Giovanna Celucci, Tyson E Graber, Huy-Dung Hoang, Marius R Niklaus, Izabella A Pena, Anne K Hollensen, Ewan M Smith, Malik Chaker-Margot, Leonie Anton, Christopher Dajadian, Mark Livingstone, Jaclyn Hearnden, Xu-Dong Wang, Yonghao Yu, Timm Maier, Christian K Damgaard, Andrea J Berman, Tommy Alain, Bruno D Fonseca, mTORC1 promotes TOP mRNA translation through site-specific phosphorylation of LARP1, *Nucleic Acids Research*, Volume 49, Issue 6, 6 April **2021**, Pages 3461–3489, https://doi.org/10.1093/nar/gkaa1239

Kariko K, Buckstein M, Ni H, Weissman D. Suppression of RNA recognition by Toll-like receptors: the impact of nucleoside modification and the evolutionary origin of RNA. Immunity. **2005** Aug;23(2):165-75. doi: 10.1016/j.immuni.2005.06.008. PMID: 16111635.

Ke Z, Strauss JD, Hampton CM, Brindley MA, Dillard RS, Leon F, Lamb KM, Plemper RK, Wright ER. Promotion of virus assembly and organization by the measles virus matrix protein. Nat Commun. **2018** Apr 30;9(1):1736. doi: 10.1038/s41467-018-04058-2. PMID: 29712906; PMCID: PMC5928126.

Kemper C, Chan AC, Green JM, Brett KA, Murphy KM, Atkinson JP. Activation of human CD4+ cells with CD3 and CD46 induces a T-regulatory cell 1 phenotype. Nature. **2003** Jan 23;421(6921):388-92. doi: 10.1038/nature01315. PMID: 12540904.

Komune, N., Ichinohe, T., Ito, M., & Yanagi, Y. (**2011**). Measles virus V protein inhibits NLRP3 inflammasome-mediated interleukin-1β secretion. *Journal of virology*, *85*(24), 13019–13026. https://doi.org/10.1128/JVI.05942-11

Krumm, S. A., Yan, D., Hovingh, E. S., Evers, T. J., Enkirch, T., Reddy, G. P., Sun, A., Saindane, M. T., Arrendale, R. F., Painter, G., Liotta, D. C., Natchus, M. G., von Messling, V., & Plemper, R. K. (**2014**). An orally available, small-molecule polymerase inhibitor shows efficacy against a lethal morbillivirus infection in a large animal model. *Science translational medicine*, *6*(232), 232ra52. https://doi.org/10.1126/scitranslmed.3008517

Lai, M., Realini, N., La Ferla, M. *et al.* Complete Acid Ceramidase ablation prevents cancer-initiating cell formation in melanoma cells. *Sci Rep* 7, 7411 (**2017**). https://doi.org/10.1038/s41598-017-07606-w

Laksono, B.M.; De Vries, R.D.; McQuaid, S.; Duprex, W.P.; De Swart, R.L. Measles Virus Host Invasion and Pathogenesis. *Viruses* **2016**, *8*, 210. https://doi.org/10.3390/v8080210

Lang J, Bohn P, Bhat H, Jastrow H, Walkenfort B, Cansiz F, Fink J, Bauer M, Olszewski D, Ramos-Nascimento A, Duhan V, Friedrich SK, Becker KA, Krawczyk A, Edwards MJ, Burchert A, Huber M, Friebus-Kardash J, Göthert JR, Hardt C, Probst HC, Schumacher F, Köhrer K, Kleuser B, Babiychuk EB,

Sodeik B, Seibel J, Greber UF, Lang PA, Gulbins E, Lang KS. Acid ceramidase of macrophages traps herpes simplex virus in multivesicular bodies and protects from severe disease. Nat Commun. **2020** Mar 12;11(1):1338. doi: 10.1038/s41467-020-15072-8. PMID: 32165633; PMCID: PMC7067866.

Lawrence DM, Patterson CE, Gales TL, D'Orazio JL, Vaughn MM, Rall GF. Measles virus spread between neurons requires cell contact but not CD46 expression, syncytium formation, or extracellular virus production. J Virol. **2000** Feb;74(4):1908-18. doi: 10.1128/jvi.74.4.1908-1918.2000. PMID: 10644364; PMCID: PMC111669.

Lewis, N. D., Haxhinasto, S. A., Anderson, S. M., Stefanopoulos, D. E., Fogal, S. E., Adusumalli, P., Desai, S. N., Patnaude, L. A., Lukas, S. M., Ryan, K. R., Slavin, A. J., Brown, M. L., & Modis, L. K. (**2013**). Circulating monocytes are reduced by sphingosine-1-phosphate receptor modulators independently of S1P3. *Journal of immunology (Baltimore, Md. : 1950)*, *190*(7), 3533–3540. https://doi.org/10.4049/jimmunol.1201810

Li J, Kim SG, Blenis J. Rapamycin: one drug, many effects. Cell Metab. 2014 Mar 4;19(3):373-9. doi: 10.1016/j.cmet.2014.01.001. Epub **2014** Feb 6. PMID: 24508508; PMCID: PMC3972801.

Lin LT, Richardson CD. The Host Cell Receptors for Measles Virus and Their Interaction with the Viral Hemagglutinin (H) Protein. Viruses. **2016** Sep 20;8(9):250. doi: 10.3390/v8090250. PMID: 27657109; PMCID: PMC5035964.

Lin, W. H., Kouyos, R. D., Adams, R. J., Grenfell, B. T., & Griffin, D. E. (**2012**). Prolonged persistence of measles virus RNA is characteristic of primary infection dynamics. *Proceedings of the National Academy of Sciences of the United States of America*, *109*(37), 14989–14994. https://doi.org/10.1073/pnas.1211138109

Löffler P. Review: Vaccine Myth-Buster - Cleaning Up With Prejudices and Dangerous Misinformation. Front Immunol. **2021** Jun 10;12:663280. doi: 10.3389/fimmu.2021.663280. PMID: 34177902; PMCID: PMC8222972.

Ludlow, M., McQuaid, S., Cosby, S. L., Cattaneo, R., Rima, B. K., & Duprex, W. P. (**2005**). Measles virus superinfection immunity and receptor redistribution in persistently infected NT2 cells. *The Journal of general virology*, *86*(Pt 8), 2291–2303. https://doi.org/10.1099/vir.0.81052-0

Hektoen Ludvig, Experimental Measles, *The Journal of Infectious Diseases*, Volume 2, Issue 2, 1 March **1905**, Pages 238–255, https://doi.org/10.1093/infdis/2.2.238

Maceyka, M., Harikumar, K. B., Milstien, S., & Spiegel, S. **(2012**). Sphingosine-1-phosphate signaling and its role in disease. *Trends in cell biology*, *22*(1), 50–60. https://doi.org/10.1016/j.tcb.2011.09.003

Maceyka, M., Sankala, H., Hait, N. C., Le Stunff, H., Liu, H., Toman, R., Collier, C., Zhang, M., Satin, L. S., Merrill, A. H., Jr, Milstien, S., & Spiegel, S. (2005). SphK1 and SphK2, sphingosine kinase isoenzymes with opposing functions in sphingolipid metabolism. *The Journal of biological chemistry*, *280*(44), 37118–37129. https://doi.org/10.1074/jbc.M502207200

Maceyka, M., Spiegel, S. Sphingolipid metabolites in inflammatory disease. Nature 510, 58–67 **(2014).** https://doi.org/10.1038/nature13475

Maeurer C, Holland S, Pierre S, Potstada W, Scholich K. Sphingosine-1-phosphate induced mTOR-activation is mediated by the E3-ubiquitin ligase PAM. Cell Signal. **2009** Feb;21(2):293-300. doi: 10.1016/j.cellsig.2008.10.016. Epub 2008 Oct 30. PMID: 19000755.

Malinow R, Hayashi Y, Maletic-Savatic M, Zaman SH, Poncer JC, Shi SH, Esteban JA, Osten P, Seidenman K. Introduction of green fluorescent protein (GFP) into hippocampal neurons through viral infection. Cold Spring Harb Protoc**. 2010** Apr;2010(4):pdb.prot5406. doi: 10.1101/pdb.prot5406. PMID: 20360360; PMCID: PMC3923632.

McMahon J, Mackay IM, Lambert SB. Measles Vaccine Virus RNA in Children More Than 100 Days after Vaccination. *Viruses*. **2019**; 11(7):636. https://doi.org/10.3390/v11070636

McQuaid, S., Campbell, S., Wallace, I. J., Kirk, J., & Cosby, S. L. (**1998**). Measles virus infection and replication in undifferentiated and differentiated human neuronal cells in culture. *Journal of virology*, *72*(6), 5245–5250. https://doi.org/10.1128/JVI.72.6.5245-5250.1998

Memon, S. A., Afzal, S. S., Tukruna, A., Khan, A. T., Tebha, S. S., & Zaidi, Z. A. (**2021**). Trends and Treatment of Sub-Acute Sclerosing Panencephalitis: An Updated Review. *Global pediatric health*, *8*, 2333794X211065330. https://doi.org/10.1177/2333794X211065330

Mercado N, Kizawa Y, Ueda K, Xiong Y, Kimura G, Moses A, Curtis JM, Ito K, Barnes PJ. Activation of transcription factor Nrf2 signalling by the sphingosine kinase inhibitor SKI-II is mediated by the formation of Keap1 dimers. PLoS One. **2014** Feb 5;9(2):e88168. doi: 10.1371/journal.pone.0088168. Erratum in: PLoS One. 2014;9(5):e97208. PMID: 24505412; PMCID: PMC3914928

Mina, M. J., Kula, T., Leng, Y., Li, M., de Vries, R. D., Knip, M., Siljander, H., Rewers, M., Choy, D. F., Wilson, M. S., Larman, H. B., Nelson, A. N., Griffin, D. E., de Swart, R. L., & Elledge, S. J. (**2019**). Measles virus infection diminishes preexisting antibodies that offer protection from other pathogens. *Science (New York, N.Y.)*, *366*(6465), 599–606. https://doi.org/10.1126/science.aay6485

Minagawa, H., Tanaka, K., Ono, N., Tatsuo, H., & Yanagi, Y. (**2001**). Induction of the measles virus receptor SLAM (CD150) on monocytes. *The Journal of general virology*, *82*(Pt 12), 2913–2917. https://doi.org/10.1099/0022-1317-82-12-2913

Mühlebach MD, Mateo M, Sinn PL, Prüfer S, Uhlig KM, Leonard VH, Navaratnarajah CK, Frenzke M, Wong XX, Sawatsky B, Ramachandran S, McCray PB Jr, Cichutek K, von Messling V, Lopez M, Cattaneo R. Adherens junction protein nectin-4 is the epithelial receptor for measles virus. Nature. **2011** Nov 2;480(7378):530-3. doi: 10.1038/nature10639. PMID: 22048310; PMCID: PMC3245798.

Mushegian A. R. **(2020)**. Are There 10^{31} Virus Particles on Earth, or More, or Fewer?. *Journal of bacteriology*, *202*(9), e00052-20. https://doi.org/10.1128/JB.00052-20

Nandagopal N, Roux PP. Regulation of global and specific mRNA translation by the mTOR signaling pathway. Translation (Austin). **2015** Feb 2;3(1):e983402. doi: 10.4161/21690731.2014.983402. PMID: 26779414; PMCID: PMC4682803.

Naniche D, Varior-Krishnan G, Cervoni F, Wild TF, Rossi B, Rabourdin-Combe C, Gerlier D. Human membrane cofactor protein (CD46) acts as a cellular receptor for measles virus. J Virol. **1993** Oct;67(10):6025-32. doi: 10.1128/JVI.67.10.6025-6032.1993. PMID: 8371352; PMCID: PMC238023.tat

NCBI Library - 6505803

National Center for Biotechnology Information (2022). PubChem Compound Summary for CID 6505803, Tanespimycin. Retrieved August 30, 2022 from https://pubchem.ncbi.nlm.nih.gov/compound/Tanespimycin.

Ndungu, J. M., Krumm, S. A., Yan, D., Arrendale, R. F., Reddy, G. P., Evers, T., Howard, R., Natchus, M. G., Saindane, M. T., Liotta, D. C., Plemper, R. K., Snyder, J. P., & Sun, A. (**2012**). Non-nucleoside inhibitors of the measles virus RNA-dependent RNA polymerase: synthesis, structure-activity relationships, and pharmacokinetics. *Journal of medicinal chemistry*, *55*(9), 4220–4230. https://doi.org/10.1021/jm201699w

Neubauer H. A., Pham D. H., Zebol J. R., Moretti P. A.B., Peterson A. L., Leclercq T. M., Chan H., Powell J. A., Pitman M. R., Samuel M. S., Bonder C. S., Creek D. J., Gliddon B. L., et al An oncogenic role for sphingosine kinase 2. Oncotarget. **2016**; 7: 64886-64899. Retrieved from https://www.oncotarget.com/article/11714/text/

Noyce RS, Bondre DG, Ha MN, Lin L-T, Sisson G, et al. (**2011**) Tumor Cell Marker PVRL4 (Nectin 4) Is an Epithelial Cell Receptor for Measles Virus. PLoS Pathog 7(8): e1002240. doi:10.1371/journal.ppat.1002240

NT2 - https://www.dsmz.de/collection/catalogue/details/culture/ACC-527

Ogata A, Czub S, Ogata S, Cosby SL, McQuaid S, Budka H, ter Meulen V, Schneider-Schaulies J. Absence of measles virus receptor (CD46) in lesions of subacute sclerosing panencephalitis brains. Acta Neuropathol. **1997** Nov;94(5):444-9. doi: 10.1007/s004010050731. PMID: 9386776.

***Olsen BJ**, Markwell J **(2007)**. "Assays for the Determination of Protein Concentration" (PDF). Current Protocols in Protein Science: 14–17.*

Papetti, L., Amodeo, M. E., Sabatini, L., Baggieri, M., Capuano, A., Graziola, F., Marchi, A., Bucci, P., D'Ugo, E., Kojouri, M., Gioacchini, S., Marras, C. E., Nucci, C. G., Ursitti, F., Sforza, G., Ferilli, M., Monte, G., Moavero, R., Vigevano, F., Valeriani, M., … Magurano, F. (**2022**). Subacute Sclerosing Panencephalitis in Children: The Archetype of Non-Vaccination. *Viruses*, *14*(4), 733. https://doi.org/10.3390/v14040733

Paquet-Durand, F., Tan, S., & Bicker, G. (**2003**). Turning teratocarcinoma cells into neurons: rapid differentiation of NT-2 cells in floating spheres. *Brain research. Developmental brain research*, *142*(2), 161–167. https://doi.org/10.1016/s0165-3806(03)00065-8

Patterson JB, Thomas D, Lewicki H, Billeter MA, Oldstone MB. V and C proteins of measles virus function as virulence factors in vivo. Virology. **2000** Feb 1;267(1):80-9. doi: 10.1006/viro.1999.0118. PMID: 10648185.

Phan, M., Schapendonk, C., Oude Munnink, B. B., Koopmans, M., de Swart, R. L., & Cotten, M. **(2018**). Complete Genome Sequences of Six Measles Virus Strains. *Genome announcements*, *6*(13), e00184-18. https://doi.org/10.1128/genomeA.00184-18

Philippe L, Vasseur JJ, Debart F, Thoreen CC. La-related protein 1 (LARP1) repression of TOP mRNA translation is mediated through its cap-binding domain and controlled by an adjacent regulatory region. Nucleic Acids Res. **2018** Feb 16;46(3):1457-1469. doi: 10.1093/nar/gkx1237. Erratum in: Nucleic Acids Res. 2020 Jul 27;48(13):7604-7605. PMID: 29244122; PMCID: PMC5814973.

Pitson SM. Regulation of sphingosine kinase and sphingolipid signaling. Trends Biochem Sci. **2011** Feb;36(2):97-107. doi: 10.1016/j.tibs.2010.08.001. Epub 2010 Oct 1. PMID: 20870412.

Plattet P, Alves L, Herren M, Aguilar HC. Measles Virus Fusion Protein: Structure, Function and Inhibition. Viruses. **2016** Apr 21;8(4):112. doi: 10.3390/v8040112. PMID: 27110811; PMCID: PMC4848605.

Pleasure, S. J., and V. M. Lee. **1993**. NTera 2 cells: a human cell line which displays characteristics expected of a human committed neuronal progenitor cell. J. Neurosci. Res. 35:585–602.

Plemper RK, Hammond AL, Cattaneo R. Measles virus envelope glycoproteins hetero-oligomerize in the endoplasmic reticulum. J Biol Chem. **2001** Nov 23;276(47):44239-46. doi: 10.1074/jbc.M105967200. Epub 2001 Sep 4. PMID: 11535597.

Plumet, S., Duprex, W. P., & Gerlier, D. (**2005**). Dynamics of viral RNA synthesis during measles virus infection. *Journal of virology*, *79*(11), 6900–6908. https://doi.org/10.1128/JVI.79.11.6900-6908.2005

ProteinAtlas.Org - 2022

Karlsson M, Zhang C, Méar L, Zhong W, Digre A, Katona B, Sjöstedt E, Butler L, Odeberg J, Dusart P, Edfors F, Oksvold P, von Feilitzen K, Zwahlen M, Arif M, Altay O, Li X, Ozcan M, Mardinoglu A, Fagerberg L, Mulder J, Luo Y, Ponten F, Uhlén M, Lindskog C. A single-cell type transcriptomics map of human tissues. Sci Adv. 2021 Jul 28;7(31):eabh2169. doi: 10.1126/sciadv.abh2169. PMID: 34321199; PMCID: PMC8318366.

a) https://www.proteinatlas.org/ENSG00000063176-**SPHK2**
b) https://www.proteinatlas.org/ENSG00000104763-**ASAH1**
c) https://www.proteinatlas.org/ENSG00000117335-**CD46**
d) https://www.proteinatlas.org/ENSG00000117335-**CD46**/tissue
e) https://www.proteinatlas.org/ENSG00000143217-**NECTIN4**/tissue
f) https://www.proteinatlas.org/ENSG00000144395-C**CDC150**/tissue

g) https://www.proteinatlas.org/ENSG00000176170-**SPHK1**

Ramachandran A, Parisien JP, Horvath CM. STAT2 is a primary target for measles virus V protein-mediated alpha/beta interferon signaling inhibition. J Virol. **2008** Sep;82(17):8330-8. doi: 10.1128/JVI.00831-08. Epub 2008 Jun 25. PMID: 18579593; PMCID: PMC2519631.

Randall RE, Griffin DE. Within host RNA virus persistence: mechanisms and consequences. Curr Opin Virol. **2017** Apr;23:35-42. doi: 10.1016/j.coviro.2017.03.001. Epub 2017 Mar 17. PMID: 28319790; PMCID: PMC5474179.

Reid SP, Tritsch SR, Kota K, Chiang CY, Dong L, Kenny T, Brueggemann EE, Ward MD, Cazares LH, Bavari S. Sphingosine kinase 2 is a chikungunya virus host factor co-localized with the viral replication complex. Emerg Microbes Infect. **2015** Oct;4(10):e61. doi: 10.1038/emi.2015.61. Epub 2015 Oct 14. PMID: 26576339; PMCID: PMC4631929.

Reuter T, Weissbrich B, Schneider-Schaulies S, Schneider-Schaulies J. RNA interference with measles virus N, P, and L mRNAs efficiently prevents and with matrix protein mRNA enhances viral transcription. J Virol. **2006** Jun;80(12):5951-7. doi: 10.1128/JVI.02453-05. PMID: 16731933; PMCID: PMC1472597.

Reuter, D., Schneider-Schaulies, J. Measles virus infection of the CNS: human disease, animal models, and approaches to therapy. Med Microbiol Immunol 199, 261–271 (**2010**). https://doi.org/10.1007/s00430-010-0153-2

Richardson CD, Scheid A, Choppin PW. Specific inhibition of paramyxovirus and myxovirus replication by oligopeptides with amino acid sequences similar to those at the N-termini of the F1 or HA2 viral polypeptides. Virology. **1980** Aug;105(1):205-22. doi: 10.1016/0042-6822(80)90168-3. PMID: 7414950.

Riddell MA, Moss WJ, Hauer D, Monze M, Griffin DE. Slow clearance of measles virus RNA after acute infection. J Clin Virol. **2007** Aug;39(4):312-7. doi: 10.1016/j.jcv.2007.05.006. Epub 2007 Jul 10. PMID: 17625962.

Rik de Swart, R. L., Yüksel, S., & Osterhaus, A. D. **(2005)**. Relative contributions of measles virus hemagglutinin- and fusion protein-specific serum antibodies to virus neutralization. Journal of virology, 79(17), 11547–11551. https://doi.org/10.1128/JVI.79.17.11547-11551.2005

Rima BK, Duprex WP. New concepts in measles virus replication: getting in and out in vivo and modulating the host cell environment. Virus Res. **2011** Dec;162(1-2):47-62. doi: 10.1016/j.virusres.2011.09.021. Epub 2011 Oct 6. PMID: 22001568.

Rima BK, Duprex WP. The measles virus replication cycle. Curr Top Microbiol Immunol. **2009**;329:77-102. doi: 10.1007/978-3-540-70523-9_5. PMID: 19198563.

Rima, B., Balkema-Buschmann, A., Dundon, W. G., Duprex, P., Easton, A., Fouchier, R., Kurath, G., Lamb, R., Lee, B., Rota, P., Wang, L., & Ictv Report Consortium **(2019).** ICTV Virus Taxonomy Profile: *Paramyxoviridae*. *The Journal of general virology*, *100*(12), 1593–1594. https://doi.org/10.1099/jgv.0.001328

Roberts, 2020,a , https://media.nature.com/original/magazine-assets/d41586-020-01011-6/d41586-020-01011-6.pdf

Roberts, 2020,b, https://www.science.org/content/article/polio-measles-other-diseases-set-surge-covid-19-forces-suspension-vaccination-campaigns

Rota PA, Moss WJ, Takeda M, de Swart RL, Thompson KM, Goodson JL. Measles. Nat Rev Dis Primers. 2016 Jul 14;2:16049. doi: 10.1038/nrdp.**2016**.49. PMID: 27411684.

Roy Moulik N, Kumar A, Jain A, Jain P. Measles outbreak in a pediatric oncology unit and the role of ribavirin in prevention of complications and containment of the outbreak. Pediatr Blood Cancer. **2013** Oct;60(10):E122-4. doi: 10.1002/pbc.24575. Epub 2013 Apr 29. PMID: 23629813.

Ruvinsky, I., Sharon, N., Lerer, T., Cohen, H., Stolovich-Rain, M., Nir, T., Dor, Y., Zisman, P., & Meyuhas, O. (**2005**). Ribosomal protein S6 phosphorylation is a determinant of cell size and glucose homeostasis. *Genes & development*, *19*(18), 2199–2211. https://doi.org/10.1101/gad.351605

Sakamoto K, Satoh Y, Takahashi KI, Wakimoto H, Kitagawa Y, Gotoh B, Ayata M, Itoh M. Upregulation of viral RNA polymerase activity promotes adaptation of SSPE virus to neuronal cells. Virology. **2022** Aug;573:1-11. doi: 10.1016/j.virol.2022.05.006. Epub 2022 May 27. PMID: 35679629.

Sallie R. Permar, William J. Moss, Judith J. Ryon, Mwaka Monze, Felicity Cutts, Thomas C. Quinn, Diane E. Griffin, Prolonged Measles Virus Shedding in Human Immunodeficiency Virus—Infected Children, Detected by Reverse Transcriptase—Polymerase Chain Reaction, *The Journal of Infectious Diseases*, Volume 183, Issue 4, 15 February **2001**, Pages 532–538, https://doi.org/10.1086/318533

Sato, Y., Watanabe, S., Fukuda, Y., Hashiguchi, T., Yanagi, Y., & Ohno, S. (**2018**). Cell-to-Cell Measles Virus Spread between Human Neurons Is Dependent on Hemagglutinin and Hyperfusogenic Fusion Protein. *Journal of virology*, *92*(6), e02166-17. https://doi.org/10.1128/JVI.02166-17

Schmid, A., Spielhofer, P., Cattaneo, R., Baczko, K., ter Meulen, V., & Billeter, M. A. (**1992**). Subacute sclerosing panencephalitis is typically characterized by alterations in the fusion protein cytoplasmic domain of the persisting measles virus. *Virology*, *188*(2), 910–915. https://doi.org/10.1016/0042-6822(92)90552-z

Schmidt N, Lareau CA, Keshishian H, Ganskih S, Schneider C, Hennig T, Melanson R, Werner S, Wei Y, Zimmer M, Ade J, Kirschner L, Zielinski S, Dölken L, Lander ES, Caliskan N, Fischer U, Vogel J, Carr SA, Bodem J, Munschauer M. The SARS-CoV-2 RNA-protein interactome in infected human cells. Nat Microbiol. **2021** Mar;6(3):339-353. doi: 10.1038/s41564-020-00846-z. Epub 2020 Dec 21. PMID: 33349665; PMCID: PMC7906908.

Schneider-Schaulies J, Schnorr JJ, Brinckmann U, Dunster LM, Baczko K, Liebert UG, Schneider-Schaulies S, ter Meulen V. Receptor usage and differential downregulation of CD46 by measles virus wild-type and vaccine strains. Proc Natl Acad Sci U S A. **1995** Apr 25;92(9):3943-7. doi: 10.1073/pnas.92.9.3943. PMID: 7732009; PMCID: PMC42078.

Schneider-Schaulies, J., & Schneider-Schaulies, S. (**2015**). Sphingolipids in viral infection. *Biological chemistry*, *396*(6-7), 585–595. https://doi.org/10.1515/hsz-2014-0273

Schneider-Schaulies J., Niewiesk, S., Schneider-Schaulies, S., & ter Meulen, V. (**1999**). Measles virus in the CNS: the role of viral and host factors for the establishment and maintenance of a persistent infection. *Journal of neurovirology*, *5*(6), 613–622. https://doi.org/10.3109/13550289909021290

Schoelz, D., Pöltl, D., Genewsky, A., Weng, M., Waldmann, T., Schildknecht, S., & Leist, M. (**2011**). Rapid, complete and large-scale generation of post-mitotic neurons from the human LUHMES cell line. *Journal of neurochemistry*, *119*(5), 957–971. https://doi.org/10.1111/j.1471-4159.2011.07255.x

Selleckchem S7176 -https://www.selleckchem.com/products/ski-ii.html

Shirogane Y, Takemoto R, Suzuki T, Kameda T, Nakashima K, Hashiguchi T, Yanagi Y. CADM1 and CADM2 Trigger Neuropathogenic Measles Virus-Mediated Membrane Fusion by Acting in *cis*. J Virol. 2021 Jun 24;95(14):e0052821. doi: 10.1128/JVI.00528-21. Epub **2021** Jun 24. PMID: 33910952; PMCID: PMC8223924.

Shultz, 2015 https://www.science.org/content/article/what-does-measles-actually-do

Sidorenko SP, Clark EA. Characterization of a cell surface glycoprotein IPO-3, expressed on activated human B and T lymphocytes. J Immunol**. 1993** Nov 1;151(9):4614-24. PMID: 8409422.

Sidorenko, S., Clark, E. The dual-function CD150 receptor subfamily: the viral attraction. *Nat Immunol* 4, 19–24 (**2003**). https://doi.org/10.1038/ni0103-19

Signoretto, E., Zierle, J., Bhuyan, A. A., Castagna, M., & Lang, F. (**2016**). Ceranib-2-induced suicidal erythrocyte death. Cell biochemistry and function, 34(5), 359–366. https://doi.org/10.1002/cbf.3196

So L, Lee J, Palafox M, Mallya S, Woxland CG, Arguello M, Truitt ML, Sonenberg N, Ruggero D, Fruman DA. The 4E-BP-eIF4E axis promotes rapamycin-sensitive growth and proliferation in lymphocytes. Sci Signal**. 2016** May 31;9(430):ra57. doi: 10.1126/scisignal.aad8463. PMID: 27245614; PMCID: PMC4924540.

Sphingolipids. chapter UCD, 2021 (2021, March 28). https://phys.libretexts.org/@go/page/1977

Spiegel, S., & Milstien, S. (**2011**). The outs and the ins of sphingosine-1-phosphate in immunity. *Nature reviews. Immunology*, *11*(6), 403–415. https://doi.org/10.1038/nri2974

Tahara, M., Ohno, S., Sakai, K., Ito, Y., Fukuhara, H., Komase, K., Brindley, M. A., Rota, P. A., Plemper, R. K., Maenaka, K., & Takeda, M. (**2013**). The receptor-binding site of the measles virus hemagglutinin protein itself constitutes a conserved neutralizing epitope. *Journal of virology*, *87*(6), 3583–3586. https://doi.org/10.1128/JVI.03029-12

Tang H, Huang X, Pang S. Regulation of the lysosome by sphingolipids: Potential role in aging. J Biol Chem. **2022** Jul;298(7):102118. doi: 10.1016/j.jbc.2022.102118. Epub 2022 Jun 9. PMID: 35691340; PMCID: PMC9257404.

Tatsuo H, Ono N, Yanagi Y. Morbilliviruses use signaling lymphocyte activation molecules (CD150) as cellular receptors. J Virol. **2001** Jul;75(13):5842-50. doi: 10.1128/JVI.75.13.5842-5850.2001. PMID: 11390585; PMCID: PMC114299.

Tiwarekar V, Wohlfahrt J, Fehrholz M, Scholz CJ, Kneitz S, Schneider-Schaulies J. APOBEC3G-Regulated Host Factors Interfere with Measles Virus Replication: Role of REDD1 and Mammalian TORC1 Inhibition. J Virol. **2018** Aug 16;92(17):e00835-18. doi: 10.1128/JVI.00835-18. PMID: 29925665; PMCID: PMC6096796.

Trainic, M., Koren, I., Sharoni, S., Frada, M., Segev, L., Rudich, Y., & Vardi, A. **(2018).** Infection Dynamics of a Bloom-Forming Alga and Its Virus Determine Airborne Coccolith Emission from Seawater. *iScience*, *6*, 327–335. https://doi.org/10.1016/j.isci.2018.07.017

Uniprot.org. 2022. *UniProt*. - The UniProt Consortium **UniProt: the universal protein knowledgebase in 2021** Nucleic Acids Res. 49:D1 (2021)

a) L polymerase - https://www.uniprot.org/uniprotkb/P12576/entry
b) NECTIN4 - https://www.uniprot.org/uniprotkb/Q96NY8/entry

Uylangco CV, Beroy GJ, Santiago LT, Mercoleza VD, Mendoza SL. A double-blind, placebo-controlled evaluation of ribavirin in the treatment of acute measles. Clin Ther. **1981**;3(5):389-96. PMID: 7008941.

Vero – a) https://www.dsmz.de/collection/catalogue/details/culture/ACC-33
https://www.sigmaaldrich.com/IN/en/product/sigma/cb_04091501

Vethakanraj H. S., Sesurajan, B. P., Padmanaban, V. P., Jayaprakasam, M., Murali, S., & Sekar, A. K. (2018). Anticancer effect of acid ceramidase inhibitor ceranib-2 in human breast cancer cell lines MCF-7, MDA MB-231 by the activation of SAPK/JNK, p38 MAPK apoptotic pathways, inhibition of the Akt pathway, downregulation of ERα. *Anti-cancer drugs*, *29*(1), 50–60. https://doi.org/10.1097/CAD.0000000000000566

Vijayan M, Seo YJ, Pritzl CJ, Squires SA, Alexander S, Hahm B. Sphingosine kinase 1 regulates measles virus replication. Virology. **2014** Feb;450-451:55-63. Epub 2013 Dec 20. PMID: 24503067; PMCID: PMC3918136. https://doi.org/10.1016/j.virol.2013.11.039

Vijayan, Y., Lankadasari, M. B., & Harikumar, K. B. (**2019**). Acid Ceramidase: A Novel Therapeutic Target in Cancer. *Current topics in medicinal chemistry*, *19*(17), 1512–1520. https://doi.org/10.2174/1568026619666190227222930

Waldor, M. K., & Mekalanos, J. J. **(1996)**. Lysogenic conversion by a filamentous phage encoding cholera toxin. *Science (New York, N.Y.)*, *272*(5270), 1910–1914. https://doi.org/10.1126/science.272.5270.1910

Wang N, Morra M, Wu C, Gullo C, Howie D, Coyle T, Engel P, Terhorst C. CD150 is a member of a family of genes that encode glycoproteins on the surface of hematopoietic cells. Immunogenetics. **2001** Jul;53(5):382-94. doi: 10.1007/s002510100337. PMID: 11486275.

Watanabe, A., Yoneda, M., Ikeda, F., Terao-Muto, Y., Sato, H., & Kai, C. (**2010**). CD147/EMMPRIN acts as a functional entry receptor for measles virus on epithelial cells. *Journal of virology*, *84*(9), 4183–4193. https://doi.org/10.1128/JVI.02168-09

White, L. K., Yoon, J. J., Lee, J. K., Sun, A., Du, Y., Fu, H., Snyder, J. P., & Plemper, R. K. (**2007**). Nonnucleoside inhibitor of measles virus RNA-dependent RNA polymerase complex

activity. *Antimicrobial agents and chemotherapy*, *51*(7), 2293–2303. https://doi.org/10.1128/AAC.00289-07

WHO Resources

a) MMR surveillance lab network **Manual Chapter 7, 2018** pdf-https://cdn.who.int/media/docs/default-source/immunization/vpd_surveillance/lab_networks/measles_rubella/manual/chapter-7.pdf?sfvrsn=8ac65ea0_2&download=true
b) **Fact sheet 2019** https://www.who.int/news-room/fact-sheets/detail/measles
c) **Press 2022**, https://www.who.int/news/item/27-04-2022-unicef-and-who-warn-of--perfect-storm--of-conditions-for-measles-outbreaks--affecting-children
d) **Measles Vaccines**, https://www.who.int/teams/health-product-policy-and-standards/standards-and-specifications/vaccine-standardization/measles#:~:text=Measles%20vaccines&text=Many%20of%20the%20attenuated%20strains,(Ji%2D191)%20strains.

Wittwer K, Anderson DE, Pfeffermann K, Cox RM, Wolf JD, Santibanez S, Mankertz A, Plesker R, Sticher ZM, Kolkykhalov AA, Natchus MG, Pfaller CK, Plemper RK, von Messling V. Small-molecule polymerase inhibitor protects non-human primates from measles and reduces shedding. Nat Commun. **2021** Sep 2;12(1):5233. doi: 10.1038/s41467-021-25497-4. PMID: 34475387; PMCID: PMC8413292.

Wombwell, E., Fangman, M.T., Yoder, A.K. *et al.* Religious Barriers to Measles Vaccination. *J Community Health* 40, 597–604 (**2015**). https://doi.org/10.1007/s10900-014-9956-1

Yoshikawa, Y., Mizumoto, K., & Yamanouchi, K. (**1986**). Characterization of messenger RNAs of measles virus. *The Journal of general virology*, *67 (Pt 12)*, 2807–2812. https://doi.org/10.1099/0022-1317-67-12-2807

Yu FPS, Amintas S, Levade T, Medin JA. Acid ceramidase deficiency: Farber disease and SMA-PME. Orphanet J Rare Dis. 2018 Jul 20;13(1):121. doi: 10.1186/s13023-018-0845-z. PMID: 30029679; PMCID: PMC6053731.

Zhang Y, Wang Y, Wan Z, Liu S, Cao Y, Zeng Z (**2014**) Sphingosine Kinase 1 and Cancer: A Systematic Review and Meta-Analysis. PLoS ONE 9(2): e90362. https://doi.org/10.1371/journal.pone.0090362

Zhdanov, V. Integration of viral genomes. *Nature* 256, 471–473 (1975). https://doi.org/10.1038/256471a0

Zinke M, Kendl S, Singethan K, Fehrholz M, Reuter D, Rennick L, Herold MJ, Schneider-Schaulies J. Clearance of measles virus from persistently infected cells by short hairpin RNA. J Virol. **2009** Sep;83(18):9423-31. Epub 2009 Jul 8. PMID: 19587038; PMCID: PMC2738273. https://doi.org/10.1128/JVI.00846-09

Acknowledgements

‘Feeling gratitude and not expressing it, is like wrapping a present and not giving it’

- William A Ward

Firstly, I thank Deutscher Akademischer Austausch Dienst (DAAD) for providing me the opportunity and funding to carry out interesting research here in Germany. I am very grateful to my supervisor Prof. Dr. Jürgen Schneider-Schaulies who agreed to be my supervisor and support my DAAD application and was also always patient with my slow pace of practical lab work. Right from my very first week in the lab by donning a lab-coat and teaching us how to handle the large western blot machine, till almost the very end of my doctoral lab work - still calmly answering my numerous academic and technical queries and even tips for further research ahead, it was always a valuable learning experience under your guidance.

I also would like to thank my thesis committee members PD. Dr: Niklas Beyersdorf and Dr. Martin Fraunholz for sharing their knowledge and expertise during the meetings so that I could improve and have a broader perspective of the experimental data and its interpretation. Also, I owe thanks to the Graduate School of Life Sciences (GSLS) for having a very pro-active role in encouraging us doctoral students to be aware of and participate in numerous courses and events, and also exposing us to various social aspects of research in academia as well as industry.

Further, I extend my sincere gratitude to Prof. Dr. Sibylle Schneider-Schaulies and Prof. Dr. med. Lars Dölken for their insightful comments, challenging questions and sharing their valuable expertise during the weekly seminars that helped in troubleshooting and improving for planning future experiments and also for sharing their lab resources. During the weekly journal clubs, I’d also like to thank Prof. Sibylle for sharing informal science facts that made them interesting to look forward to. My special thanks to Dr. Elita Avota whom I could approach whenever I had any big or small professional or personal query and she always helped with a smile. The ‘Immunomodulation’ sessions conducted by Dr. Friederike Berberich-Siebelt also influenced me to think out of the box as well as thanks to the research group SphingoFOR 2123 and SphingoInf GRK2581 for including me in their collaborative retreats which was really beneficial.

I immensely thank all my lab colleagues – Hannah, Nora, Claudia, Julia and Agnes for various aspects of the lab experimental and routine work. Besides thank you very much for so enthusiastically introducing me to various local German food, culture, traditions, jokes, stories and trivia that helped to adapt faster especially after the initial few difficult months since I arrived. I also

thank the ‘neighbouring lab’ right from Charlene, to Anna, Nicole and Annika – lunch sessions with regular supply of coffee and sweets from all made the day better. Both working in the lab all as well as lunch sessions were fun and memorable with you all.

I may also mention my seniors and peers – Vini, Maria, Khushi, Sherry, Lara, Manivel, Nada, Daud, Rebecca, Marie, Trushnal, Teresa, Christine, Andrea, Mohinder, Vishakha and Putri – discussions, get togethers and complaints with them made it easier to sail through tough days. I’d also like to thank Arhnild for helping with trouble shooting few experiments and Thomas from Dölken lab group, for sharing their knowledge. I also thank the numerous people who may have directly or indirectly helped/influenced me and I really apologize if I forgot to specifically mention anyone.

A special and warm thank you to my family like friends –, Shubhankar, Aman, Khushboo, Siddesh, Anam, Sarangi, Sumi, Virta and Parul who were amazing friends and constant source of entertainment. I cannot miss to thank my mentors from India Prof. Vikram Ghole and Dr. Varsha Potdar who encouraged and supported to apply for this fellowship. Finally, I am indebted to my family for their love an trust – firstly my parents Leena and Joseph, my sister Jillianne, aunt Theresa, Ammama, uncle Capt. Jacob, Queenie, Lally aunty and Rocky uncle who have been a solid support during my tough, rough and even best phases.

Lastly in deep gratitude I thank God

Curriculum Vitae